UNIVERSITÀ DEGLI STUDI DI MILANO

Scuola di Dottorato in
SCIENZE E TECNOLOGIE CHIMICHE

Dottorato di Ricerca in
CHIMICA DEL FARMACO - XXVII ciclo

Dipartimento di
SCIENZE FARMACEUTICHE "PIETRO PRATESI"

Tesi di Dottorato di Ricerca

DEVELOPMENT OF NOVEL HIGH PERFORMANCE PROTEIN MICROARRAYS FOR DIAGNOSTIC APPLICATIONS

CHIM/08

Paola GAGNI
Matricola N. R09804

Tutor: Prof. Carlo DE MICHELI
Co-Tutor: Dr. Marcella CHIARI

Anno Accademico 2013-2014

To my parents,

Isa and Lino

TABLE OF CONTENTS

Chapter 1 – GENERAL OVERVIEW

The present PhD thesis will present the develompent of high sensitivity and specificity protein microarrays for molecular diagnostics using both fluorescence-based and label-free detection platforms. The *Chapter 2 - Introduction on Microarrays* will illustrate the principles of this technique in protein analyses, while the following *Chapter 3* will focus on the *Optical Detection Methods* used: both fluorescence-based and label-free detection platforms are described at the state-of-the-art.

Advantages and limitations of the microarray technology will be depicted in *Chapter 5*. The first studies investigated on innovative approaches to improve immunoassay performances on solid supports, using surface immobilized hydrogels as versatile reagent reservoir.

Further investigation moved towards the exploitation of fluorescent-based and label-free microarray detection platforms in diagnostic application for early detection of Neurodegenerative Disorders (NDs) biomarkers. First, in *Chapter 6*, a high sensitivity immunoassay developed for Amyloid-β peptides detection on a silicon microarray platform is presented. Afterwards, as described in *Chapter 7*, the microarray platforms have been applied to detect whole extra-cellular nanosized vesicles, i.e. exosomes, as carriers of biomarkers of NDs or as biomarkers themselves. Exosomes were characterized according to their dimensions and physical properties using label-free detection and, at the same time, they were phenotyped based on protein expression on their surface using the fluorescence detection platform.

The present PhD research was carried out at the *Istituto di Chimica del Riconoscimento Molecolare– CNR*, Milan, under the supervision of Dr. Marcella Chiari.

Label-free Single Particle-IRIS experiments described in *Chapter 7* were conducted at the *Electrical and Computer Engineering department at Boston University* (MA, USA), in collaboration with Prof. S. Unlu.

Chapter 2 - INTRODUCTION ON MICROARRAYS

2.1 - MICROARRAY TECHNOLOGY

This dissertation focuses on the development of biosensing platforms based on protein microarray technology. In particular, the attention is focused on the development of novel diagnostic tools for the diagnosis of Neurodegenerative Disorders with high sensitivity and specificity. Microarray assays were developed on silicon/silicon oxide surfaces, coated with a polymeric film; surface binding interactions were then analysed with both fluorescent-based and label-free detection methods.

2.1.1 – Protein Microarrays

Microarray analyses were developed at first for DNA investigation, but in the last years they also gained increasing interest in proteomic studies. Over the past decade, the combination of two-dimensional gel electrophoresis/mass spectrometry (MS) has been the major tool in comprehensive proteomic studies; in this technique, the proteome is resolved and each spot is analyzed by MS or MS/MS. The resolution of this method is good enough to separate protein isoforms that are modified by post-translational processes (for example, phosphorylation [Kaufmann et al., 2001], glycosylation [Taniguchi et al., 2001], and deamination [Sarioglu et al., 2000]). However, this technique has some limitations, such as lack of automation of the processes involved, poor detection of low abundant proteins, low reproducibility, cumbersome protocols and difficulties in the separation of hydrophobic membrane proteins and basic or high-molecular-mass proteins [Santoni et al., 2000; Molloy et al., 2002; Patton et al., 1999]. Another current approach in proteomics is the liquid chromatography (LC)/MS

method, in which ion-exchange, reversed-phase and affinity-based separations can be combined to improve the resolution of each protein species. Although these two technologies theoretically offer a complete coverage of the proteome, they still lack of parallelization and miniaturization, features that are required for high-throughput screening of proteins. In order to comply with these characteristics, protein microarray technology has emerged in last ten years [Kambhampati, 2003;Fung, 2004]. Microarrays can be accounted as an evolution of conventional Enzyme Linked ImmunoSorbent Assays (ELISA) moved toward a miniaturized scale where each well is turned into a single spot. The general scheme of a typical microarray experimentis reported in **Figure 2.1** and it requires the patterning of a large set of capture ligands (DNA, protein or peptide probes) on a solid functionalized support using a robot (spotter) able to spot nano-litres of probe solutions. The probes are required to bind the surface and to remain stable during washing and blocking of surface unreacted sites. The array is then probed with a sample containing (among a variety of unrelated molecules) the counterparts (target) of the molecular recognition event under study. Usually, protein microarrays study the interaction between proteins or peptides and their specific antibodies. The high affinity interaction between probes and target molecules is monitored by another component, the *transducer*, which converts the molecular complex into a quantifiable physic signal, which often is fluorescence.

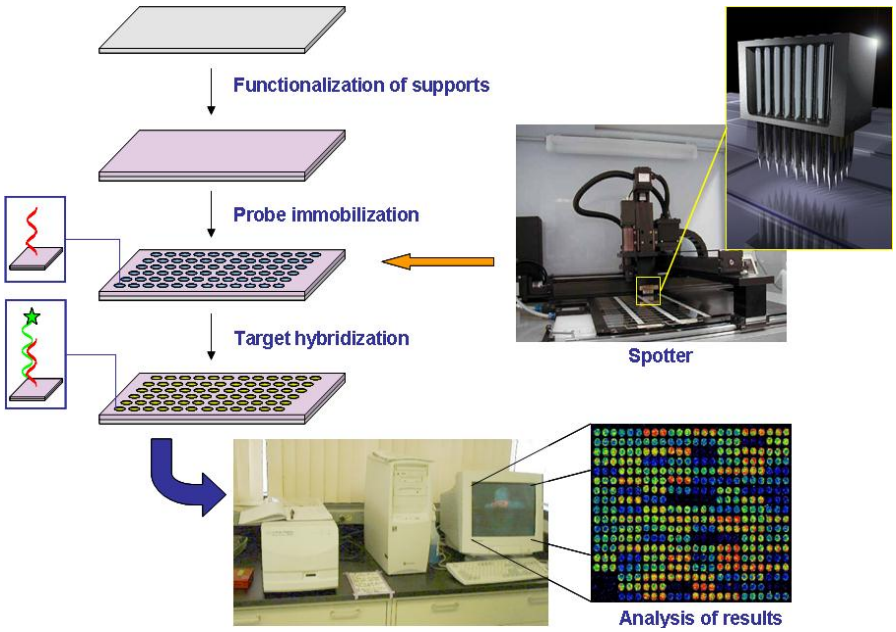

Fugure 2. 1 - General scheme of a typical microarray experiment.

By using this approach, both multiplexing and miniaturization are achieved relative to ELISA, thus dramatically increasing the amount of data that can be obtained per volume of biological sample. Moreover, on each microarray support many different sub-arrays can be printed (**Figure 2.2**).

Two different type of analyses can be performed with protein microarrays, depending on the purpose of the analisis. One consists of determining the abundance of proteins of interest in complex protein mixtures with highly specific capture agents, one for each target protein, for example, by antigen–antibody interactions.

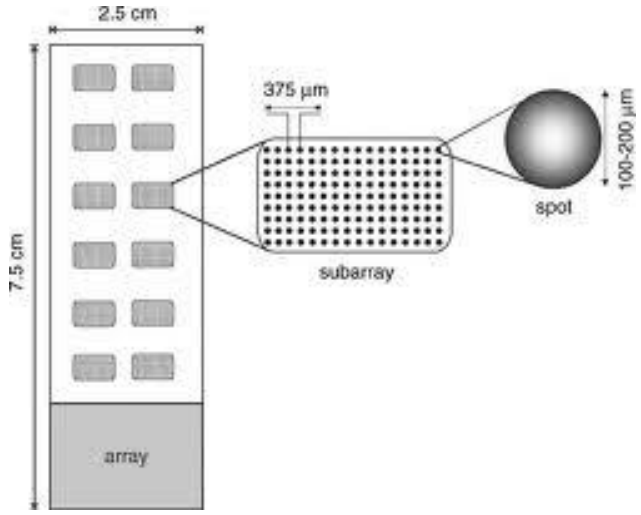

Fugure 2. 2 - Traditional microarray format. Many subarrays can be printed on a conventional microscope slide. Each subarray can be constituted of many replicate spots patterned on specific positions.

The other possibility is to find out the functions of proteins of interest, including protein–protein interactions, receptor–ligand interactions, enzymatic activities etc. Hence, protein arrays generally fall in one of these categories [Cretich et al., 2006]: (i) *detection arrays* (or analytical arrays) and (ii) *function arrays*.

In *protein detection microarrays*, an array of affinity reagents (antigens or antibodies) is immobilized on a support and used to determine the presence and the abundance of the target protein in a complex matrix such as plasma or serum. Analytical arrays can be used to assay antibodies, for example for diagnosis of allergy [Cretich et al., 2009] or autoimmune diseases [Robinson et al., 2003; Balboni et al., 2006] or to monitor protein expression on a large scale [Phizicky et al., 2003; Zhu et al., 2003].

In *protein function microarrays* (which are generally aimed at discovering protein function in fundamental research) a large set of purified proteins or peptides or even an entire proteome is spotted and immobilized. The array is then used for parallel

screening of a range of biochemical interactions. Protein function arrays [Blackburn et al., 2005] can be used to study the effect of substrates or inhibitors on enzyme activities [Zhu Q. et al., 2003], protein-drug or hormone effector interactions [Kim et al., 2005] or in epitope mapping studies [Chiari et al., 2005]. In an another kind of protein function arrays, usually referred as *reverse phase microarrays* [Zhu H. et al., 2003], tissues, cell lysates or serum samples are spotted on a surface and probed with one antibody per analyte for a multiplex readout.

2.2 – MICROARRAYS and BIOSENSORS

Microarray technology falls in the bigger field of biosensors, which were defined by IUPAC in 1992 as "devices that use specific biochemical reactions mediated by isolated enzymes, immune systems, tissues, organelles or whole cells to detect chemical compounds usually by electrical, thermal or optical signals" [Brandenburg et al., 2009]. By this definition classical biosensors are made of three components:

1) a biological recognition component that sensitively and specifically recognizes the analyte;

2) the transducer element that transforms the event of physiochemical interaction into another quantifiable signal;

3) electronics and a user interface that outputs the results in an easy and user-friendly way.

From this point of view, biomarkers are all kinds of quantitative parameters that can be obtained from a patient and that correlate to a particular disease [Bier et al., 2013], in a way making them key components of the biosensor tools.

2.2.1 - Biomarkers

A biological marker, or biomarker [Frey et al., 2005; Henley et al., 2005; Sprott, 2010; Cedazo-Minguez et al., 2010; Ho et al., 2010], is objectively measured and evaluated as an indicator of normal biological processes, pathogenic processes or pharmacological responses to a therapeutic intervention. A biomarker can serve as an indicator of health (i.e. biomarker of ageing) and disease. The sensitivity, specificity and ease-of-use are the most important factors that ultimately define the diagnostic utility of a biomarker. Some biomarkers are more reasonably viewed as risk factors rather than true disease markers. In order for a diagnostic biomarker to be useful, specific criteria for the given status must be contemporary statisfied [Hampel et al., 2010; Desai et al., 2005; Sjogren et al., 2003; Zetterberg et al., 2003].

Biomarkers can be discovered from different human tissues or liquids, such as blood, urine and saliva. Plasma/serum measurements are the gold standard in clinics, because they are minimally invasive, as compared with cerebrospinal fluid (CSF), and therefore easily collected and processed [Humpel, 2011]. A major advantage of blood samples is that patients can be followed up and screened over several years. The collection of other fluids (e.g. saliva, urine, fibroblasts or eye secretions) is fast, cheap and non-invasive; however, the use of these fluids requires very sensitive methods to detect low-level of proteins and a well-known correlation to specific pathologies. Also CSF is a very useful fluid for some diagnosis (e.g. neurodegenerative pathologies), because it reflects metabolic processes in the brain owing to direct contact between the brain and CSF itself, but its diagnostic use is only limited because of invasive collection by lumbar puncture [Humpel, 2011].

2.3 - MICROARRAY SUPPORTS

Microarrays aim to study the molecular interactions occurring between two partners: one contained in a liquid sample (target molecule) and one immobilized on a solid support (probe). The chemistry used for the immobilization of probe molecules on the substrate plays a significant role in the success of any experiment [Sola, 2012]. This is particularly true with protein arrays, as polypeptides tend to bind to surfaces in a nonspecific manner, sometimes affecting their biological activity [Chiari et al., 2005]. The key requirements of protein microarray surfaces are [Sola, 2012]:

(1) provision of an optimal binding capacity of capture ligands (probes);

(2) retaining of biological activity of probes (proteins tend to unfold when immobilized onto a support, in order to allow internal hydrophobic side chains to form hydrophobic bonds with the solid surface);

(3) accessibility of the ligand to the interaction partner (protein–surface interactions reduce the accessibility of the target, possibly leading to false negative results). This issue is particularly important for peptide microarrays due to the small molecular mass of capture ligands;

(4) low degree of non-specific interaction (the achievement of a low degree of non-specific binding is extremely difficult when the sample is a complex mixture of thousands of molecules such as serum).

These requirements are of outstanding importance as the abundance of many proteins in animal and human plasma can be even lower than 1 pg/mL making their detection very problematic. Therefore the surface chemistry of the supports plays a key role in the development of tools compatible with a broad set of biomolecules while maintaining their integrity, native conformation and biological function.

2.3.1 - Characteristics of the Supports

The final performance of a microarray biochip strongly depends on parameters related to the immobilization process itself, which include [Sola, 2012]:

(a) the chemical and physical properties of the surface, as they influence both specific and non-specific binding of target and non-target biomolecules;
(b) the density of the probes on the surface, which determines the sensitivity of the chip and the limit of detection, defining the distance between the immobilized probes and the chip surface;
(c) the orientation of the immobilized proteins, which might impair binding, especially to large analytes such as proteins.

The selection of the solid surface employed for generating microarray chip depends on the intended application. For example, gold surfaces are often used for the development of biosensors with electrochemical and surface plasmon resonance (SPR) read-out [Lee et al., 2005] because of their outstanding electrical conductivity and convenient functionalization by means of thiol chemisorption. In contrast, glass or silicon [Cretich et al., 2009b] is typically preferred for optical sensors because of their low intrinsic fluorescence and, in the case of glass, transparency. In general, these surfaces are characterized by their chemical homogeneity and stability, their controllable surface properties (such as polarity and wettability), their reactivity towards a wide range of chemical functionalities and the reproducibility of surface modification [Sola, 2012].

2.3.2 - Polymer Coating

The reactivity of a chip surface is determined by the functional groups it displays. The density of the reactive groups is one important factor controlling the amount of protein that can be immobilized on a specific surface area and thus consequently influences the limit of detection attainable with the particular chip. Proteins offer many functional groups, mainly in the amino acid side chains, that are suitable for

immobilization purposes. Such functional groups can be used to covalently couple proteins to surfaces by a range of different reactions. To this end, more complex three-dimensional structure that moves away from the surface and exposes the functional groups have been developed in M. Chiari's laboratory at the *Institute of Chemistry of Molecular Recognition* of the *National Council of the Research* in Milan (ICRM-CNR) [Sola, 2012].

In an attempt to obtain a suitable polymer coating with high capacity for probes immobilization offering a homogeneous "natural" aqueous environment, an hydrophilic copolymer made by *N,N*-dimethylacrylamide (DMA), *N*-acryloyloxysuccinimide (NAS), and 3-(trimethoxysilyl)propyl methacrylate (MAPS) (poly(DMA-NAS-MAPS)) firstly reported for the preparation of low-density DNA microarrays on glass surfaces was developed (**Figure 2.3**) [Pirri et al., 2004]. This poly(DMA-NAS-MAPS) is a ter-copolymer whose silanizing properties are due to the presence of the 3-(trimethoxysilyl)propyl methacrylate, that allows the stable binding of the polymer itself on glass or silicon surfaces. On the other side, the *N*-acryloyloxysuccinimide behaves as a monomer reactive towards nucloephilic groups (i.e., amines) on probe biomolecules.

Moreover, the innovative aspect of this approach relies on the fact that the polymer self-adsorbs onto the glass (or silicon) surface very quickly, simply by immersing glass slides in a diluted aqueous solution of the polymer and without time consuming glass pre-treatments. Therefore, the coating procedure provides a simple, fast and inexpensive method for producing a hydrophilic functional nanometric film surface bearing active esters, able to react with amino groups of modified DNA, proteins and peptides.

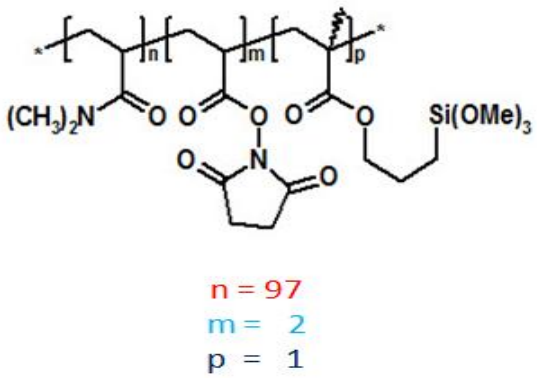

Fugure 2. 3 – Structure of poly(DMA-NAS-MAPS): the polymer used to coat silicon chips for the microarray applications described in the following studies. The composition of thethree monomers in the final copolymer is different: 97% of DMA, 2% of NAS and 1% of MAPS.

The quality of a microarray assay is not only determined by the desired binding events between the target and the probe biomolecules but also, to a large extent, by the suppression of undesired, nonspecific binding of analytes and other components within the biological sample [Sola, 2012]. Such non-specific binding can give rise to background signals and thus to low *signal-to-noise* ratios and higher limits of detection. Although many elaborate approaches have proven to be effective for minimizing nonspecific adsorption, it must be clearly stated that the old fashioned blocking of reactive surface sites by the addition of blocking agents such as the protein bovine serum albumin (BSA), skim milk powder, or other reagents and the presence of surfactants such as Tween-20 and sodium dodecyl sulfate (SDS) are usually indispensable to the suppression of non-specific protein adsorption [Crowther, 1995]. In case of poly(DMA-NAS-MAPS) coating, before any sample incubations, silicon chips are blocked either with ethanolamine or BSA, to inactivate unreacted sites on the polymer chains, leading to a very low background.

2.3.3 - Silicon Surfaces for Microarrays

The present research focused on the development of microarray tools based on optical detection methods, among which fluorescent-based and Interferometric Reflectance Imaging Sensor (IRIS) platforms.

One of the easiest way to enhance fluorescent signals is based on optic interference, which takes advantage of layered materials with different refractive index to increase the photosorption of the fluorochromes in proximity of the surfaces thus resulting in a constructive interference of the reflected light onto the detector. The condition of constructive interference is satisfied with many kind of glass slides coated with very complex dielectric or metallic layers [Fouqué et al., 2005]. Glass slides are the favoured surfaces for microarrays thanks to their availability, cost, flatness, rigidity, transparency, amenability of the surface to chemical modification and non-porosity [Holloway et al., 2002].

However in last years, Cretich and colleagues introduced innovative materials for microarray supports, such as silicon/silicon oxide [Cretich et al., 2009b] and alluminium [Cretich et al., 2014]. It has been demonstrated thatthe optimized 100 nm layer of thermally grown silicon oxide (SiO_2) with low roughness and low fluorescence background, provides fluorescence intensification due to the constructive interference between the incident and reflected waves of the fluorescence radiation [Cretich et al., 2009b]. Polymeric coatings, such as the poly(DMA-NAS-MAPS), with nanometric thickness, does not appreciably alter the optical properties of the silicon oxide, conferring to the surfaces optimal binding specificity, thus leading to a high signal-to-noise ratio. [Cretich et al., 2009b]. Moreover, the techniques chosen for both substrate production and surface modification are simple, inexpensive, and amenable to mass production. The novel Si/SiO_2 surfacecoated with poly(DMA-NAS-MAPS) provided a 5- to 10-fold enhancement of the fluorescence signals in comparison to commercial glass slides, thus providing higher sensitivity in analytes detection (**Figure 2.4**) [Cretich et al., 2009b].

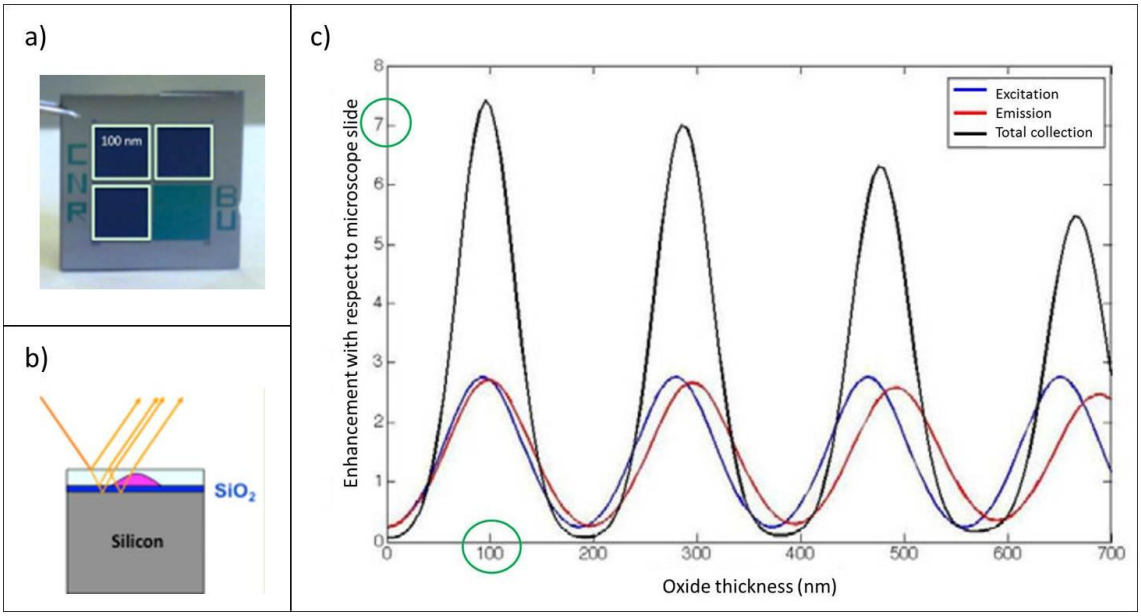

Fugure 2.4 - The silicon chips with a top layer of 100 nm oxide provided a 5 to 10-fold enhancement of the fluorescence signals in comparison to commercial glass slides, thus providing higher sensitivity in analytes detection. **a)** Silicon chip used for fluorescence detection: white square evidence the 100 nm silicon oxide layer thickness. **b)** Layers of well defined thickness act as interference layers and reflect, towards the detector, the light that would be otherwise absorbed by the substrate. **c)** Fluorescence enhancement on reflecting substrates at normal incidence of excitation and collection. The simulations for excitation (blu line), emission (red line) and total collected intensity enhancement (black line), via utilization of the layered reflecting substrate for varying thickness of the top transparent oxide layer are shown. Monochromatic excitation at 543nm, and collection in the 550-600nm range are assumed [Yalcin et al., 2009].

By varying the thickness of the SiO_2 layer, it is possible to enhance the emission of any fluorophore of choice by constructive interference with significant improvements in detection sensitivity [Cretich et al., 2011] and to employ the Interferometric Reflectance Imaging Sensor (IRIS), a platform amenable to high-throughput screening for label-free multiplexed detection [Monroe et al., 2011]. Respectively, 100 nm silicon oxide thickness is optimal for fluorescence-labelling detection, while a thickness of 500

nm is required for the label-free IRIS one. Thankfully, silicon technology and tuned modulation of the oxide layer facilitate dual detection of label-based and label-free detection schemes on a single chip. The possibility to detect changes in a spot on a single chip using two complementary detection approaches is of immense utility during the assay development process, providing information which is generally not available in glass microarray technology but crucial for determining the consistency and quality of the spotted array, quantifying the amount of immobilised probes and detecting the fluorescence of bioassays.

Chapter 3 - OPTICAL DETECTION METHODS

The detection of protein in microarray technology is mainly based on optical measurements. Available methods can be divided in two categories: the label-based and the label-free detection platforms.

3.1 – Label-based detection methods

Detection methods based on labeled-probes have been developed and adapted from immunoassay protocols and require the use of fluorescently labeled, chromogenic or chemiluminescent molecules in order to detect analytes bound to the surface. As described in Cretich et al., 2006*,* microarrays can be classified into two categories: (i) *function arrays* and (ii) *detection arrays* (or analytical arrays). Function arrays use a *direct* detection method (**Figure 3.1, *a***), where a protein mixture is immobilized on a proper surface and then detected by labelled specific antibodies. Analytical arrays can be further classified according totheassay protocol used as indirect and sandwich detections (**Figure 3.1**, respectively ***b*** and ***c***). In both cases capture biomolecules are immobilized on a proper surface and subsequently incubated with the sample. *Indirect* detection requires the straight labeling of the target biomolecules, while *sandwich* assays necessitate a secondary labeled antibody which interacts with a different epitope on the same target protein [Espina et al., 2004]. In this latter case, the combination of two binding events for the detection of a single analyte increases the specificity of the analysis. However, this approach might be less sensitive because of increasing working steps.

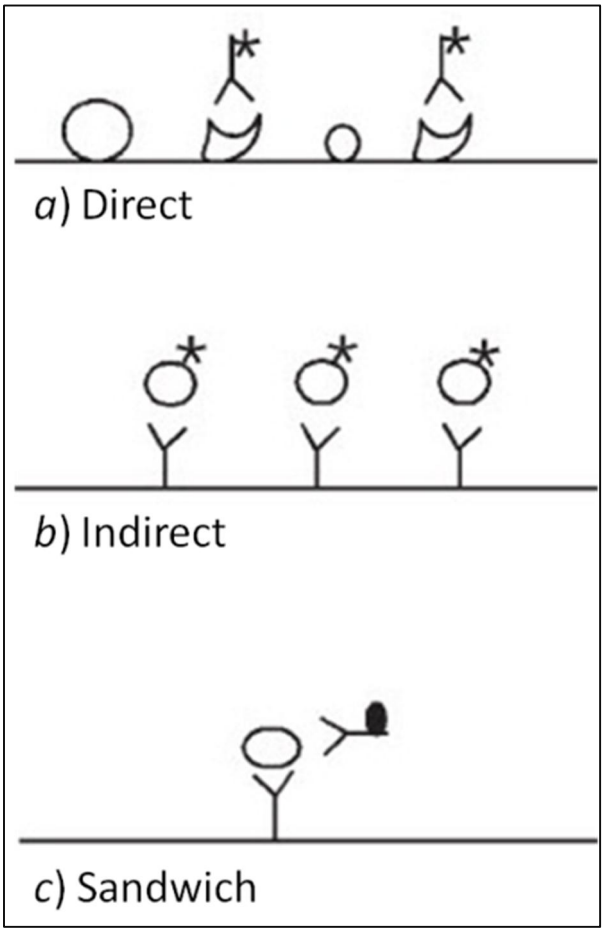

Fugure 3.1 - Label-based microarray detection methods [Espina et al., 2004]. ***a***) *Direct* detection: the analyte is printed on the surface and probed with labeled targets; ***b***) *Indirect* detection: the labeled analyte is captured by probes arrayed on the surface; ***c***) *Sandwich* assay: the analyte is first captured by probes bound to the surface and then detected by labeled secondary antibodies against a different epitope on the same protein.

3.1.1 – Chromogenic Labels

Chromogens are compounds that can be converted to a dye or a pigment through an enzymatic reaction (e.g. oxidation). In microarray technologies, they are employed as substrate of enzymes covalently bound to detection antibodies. The most commonly

used enzymes are the horseradish peroxidase (HRP) and the alkaline phosphatase (AP), both able to act on many kinds of substrates. Depending on the chromogen employed, the signal intensity might be different. However, in all cases the coloured product precipitates in correspondence of the spot and is often visible by naked eye. The higher the colour intensity, the higher concentration of target biomolecule in the sample.

3.1.2 - Chemiluminescent Labels

Microarrays detection methods based on chemiluminescence reactions are adapted from *Western blotting* protocols. Also in this case, detection antibodies are covalently bounded to enzymes (e.g. HRP or AP), but the oxidation of a different substrate such as luminol, elicits a prolonged light emission. Emitted photons can be captured by X-ray films, phosphorous plates or more commonly by a CCD camera. Non-specific signals are prevented thanks to opportune buffer solutions, usually containing diluted bovine serum albumin (BSA) or casein. Although very sensitive, chemiluminescence has low resolution due to small spot size and limited dymanic range [Schweitzer et al., 2003].

3.1.3 - Fluorescent Labels

Nowadays, the fluorescent label method has become the gold standard for microarray detection. A lot of fluorochromes have been developed in order to enhance brightness and stability. Many molecules are available on the market, such as fluorescein, Cyanine, AlexaFluor, rodamine, acridine, ficobiliproteins and Bodipy. These molecules, characterized by stability in a large range of pH values, have narrow peaks of excitation/emission spectra, whose tunability provides multicolour assay schemes [Angenendt et al., 2005]. The fluorescent molecules are chosen based on the sample properties, spectra emission and type of support used. In fact, not all surfaces or

supports are compatible with fluorescence detection, due to auto-fluorescence phenomena. Moreover, the sample itself may contain molecules which interferes with the signal emission, as it happens in the case of flavoproteins whose emitted light has the same wavelengths range of fluorescein dye.

Cyanine-3 (Cy3) and Cyanine-5 (Cy5) are the most wide-spread used fluorochromes as they can be used to screen simultaneously for two different targets without any overlapping in emission spectra. In fact, Cy3 absorbs green light at 550 nm wavelength and emits at 570 nm, while Cy5 absorbs and emits red light, respectively at 649 and 670 nm. The *N*-hydroxysuccinimide (NHS) esters of these dyes react with covalently bound primary amines on arginine and lysine residues on proteins or peptides, rendering them fluorescent. Moreover, the high interest for these molecules is also due to the very low photobleaching, which means that fluorescence performance does not decrease after prolonged exposure to a light source. In the following studies described in this PhD thesis, label-based microarray detection was always based on the use of Cyanine fluorescent dyes, whose signals were revealed through a confocal laser scanner.

3.2 – Label-free detection methods

For every label-based detection approach, the production and selection of specific antibodies (or ligand biomolecules) as well as their labelling is still a major problem. Moreover, miniaturized technologies, such as microarrays, designed to detect low sample concentrations, required the development of *ad-hoc* protocols for signals amplification in order to increase sensitivity and signal-to-noise ratios. The added value of label-free detection techniques lies on the prevention of any kind of interference in the signal due to the presence of the dye itself. However, label-free platforms require sophisticated and expensive equipments, which are limited to

laboratory applications and are not always available in clinical settings. Moreover, up to now, the sensibility of these methods is still lower than label-based detection devices.

The most popular label-free detection methods for proteins are: mass spectrometry (MS), surface plasmonic resonance imaging (SPR) and atomic force microscopy (AFM). However, all these approaches share the limit of not being applicable to detect signals from microarray tools. To overcome this problem, a label-free imaging technique using photonic crystals for both qualitative and quantitative spot analysis was developed [Ozkumur et al., 2008] by S. Unlu laboratory at the Boston University (MA, USA) and successfully applied to both DNA and protein microarrays without altering standard microarray protocols. In this simple interferometric method, the optical phase-shift resulting from the surface accumulation of biological mass at different binding sites is monitored to investigate molecular interactions [Ozkumur et al., 2008]. The so called Interferometric Reflectance Imaging Sensor (IRIS) is an innovative label-free platform which provides high sensitivity, even up to single particle detection. Moreover, it is amenable to high-throughput screening for label-free multiplexed detection [Monroe et al., 2011]. According to the amplitude of optical magnification two application can be achieved: measurement of biomaterial massed on the surface as consequence of binding events (conventional IRIS) or detection of nanostructures such as single particles (SP-IRIS).

3.2.1 - Interferometric Reflectance Imaging Sensor (IRIS)

IRIS is a platform technology for the high-throughput screening of biomolecular interactions on a solid surface, that aims to measure total biomass gathered on each spot operating on the base of optical interference. IRIS platform requires a silicon support with a thermally grown 500 nm silicon oxide layer on top of which probe molecules are spotted in an array format. The detectionprinciple is based on

quantifying the shifts in the spectral reflectance signature to calculate the added biomass by sampling it at specific wavelengths and measuring the characteristic reflection intensities using a CCD camera (Retiga 2000R from QImaging) [Cretich et al., 2011b]. The sensor surface is sequentially illuminated using an ACULED VHL surface-mount LED package (Perkin-Elmer), which has four independently driven LEDs with peak emission wavelengths of 455, 518, 598 and 635 nm. When light incident to a layered surface reflects off the interfaces, it undergoes interference due to the refractive index variation of various layers and acquires a spectral signature. In IRIS, the principle of detection for total biomass is based on quantifying the shifts in the spectral reflectance curve due to accumulation of biomass on the chip (**Figure 3.2**). After acquiring images of the substrate for each of the four wavelengths, each pixel of the CCD represents an individual measurement of the reflective interference intensity at each wavelength, forming a 3-dimensional array of data (pixel, wavelength, intensity) for the entire sensor. The data points for each pixel are fitted to a curve derived using Fresnel equations, which govern the behaviour of reflection from a semi-transparent bi-layered substrate [Daaboul et al., 2010; Cretich et al., 2011b].

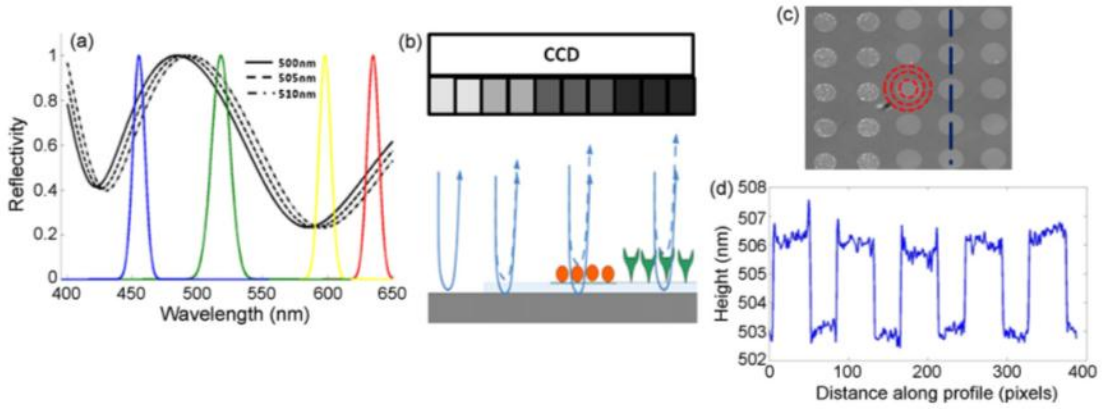

Fugure 3.2 - IRIS detection method [Daaboul et al., 2010]. Panel (**a**) displays the shift of the reflectivity curve due to 5nm step increases in thickness on the surface. The colored Gaussians represent the 4 LEDs used to sample the curve. Picture (**b**) outlines the sensor's imaging path, illustrating biomass accumulation dependent grayscale intensity changes. Image (**c**) shows an example of the sensor'ssurface with an array of protein spots. Theheight profile along the blu dashed line in across spots is then shown in panel (**d**).

To maintain the simplicity of the system without sacrificing sensivity, an on-chip reference is utilized [Vedula et al., 2010]. The reference is created by including a non-interfering region, such as a region etched to the bare silicon, within the field of view (**Figure 3.3**).

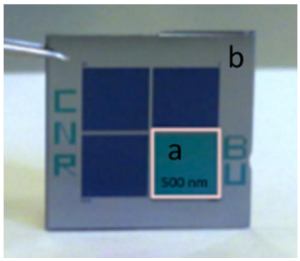

Fugure 3.3 – Silicon chip used for IRIS detection:
a) region of 500 nm silicon oxide layer thickness;
b) non-interfering reference region.

Information related to every pixel in each image are at first fitted using a custom-made algorithm written in MATLAB software, then the surface topography of the sensor's surface is presented in a grey scale image where brighter regions indicate greater thickness on the surface (see **Figure 3.2**, panel **c**). To determine optical spot heights, the average value from pixels in an annular region outside of the spot (background) is subtracted from the average value of pixels inside the spot. By using previously determined calibration factors, this information can be converted to mass densities at each spot location on the chip to determine the binding [Özkumur et al., 2009]. Özkumur et al. proved that this technique is quantitative by directly relating the measured optical thickness of the biolayers to the absolute amount of molecules on the surface. They demonstrated that 1 nm of optical thickness correlates to an absorbed mass conversion factor of 1.21 ng/mm^2 for BSA, 1.28 ng/mm^2 for IgG and 0.8 ng/mm^2 for DNA [Özkumur et al., 2009].

Moreover, the silicon technology and the tuned modulation of the oxide layer allow the fabrication of supports with areas bearing both 100 and 500 nm silicon oxide layers, thus providing the possibility of dual detection of label-based and label-free detection schemes on a single chip [Cretich et al., 2012]. The possibility to detect both, mass and fluorescence, changes in a spot on the samesupport is of immense benefit

during the assay development process to characterise the quality and the quantity of spotted reagents. This information, which is generally not available in glass microarray technology, is crucial for determining the consistency and quality of the spotted array. By knowing the amount of immobilised probes it is possible to correlate the fluorescence detected to the actual mass on the surface which, due to the minute amounts of probe spotted, varies considerably from one experiment to another [Gagni et al., 2013].

3.2.2 - Single Particle-IRIS (SP-IRIS)

Single Particle-IRIS (SP-IRIS) is the latest evolution of the conventional IRIS platform, developed to enable digital detection of nanoparticles (NP) on surface with unique orthogonal verification via size/shape discrimination and minimal sample preparation. By increasing the magnitude of the numerical aperture of the same IRIS optical lenses, SP-IRIS is amenable to detect and characterize NPin the single particle limit [Yurt et al., 2012]. This opportunity is useful to understand NP behaviour and to develop devices for diagnostic applications. Despite the significant progress in the last decade in the development of novel methods for single NP detection, their characterization still remains a challenge for most practical applications. For istance, the analysis of nanoparticles with different shape, size or chemical composition in heterogeneous solutions requires specific detection principles to classify the NP of interest in a complex population. Recent techniques for label-free detection and characterization of individual nanoparticles are based on electrical, mechanical, optical and microscopic principles, which include surface plasmon resonance (SPR) and interferometric microscopy [Yurt et al., 2012].

Interferometric microscopy applied to the study of nanoparticles is based on the illumination of NP with a coherent or incoherent visible light source and probing the light scattered or absorbed by the nanoparticles using free-space optical elements

such as objective lenses and array/single-element detectors [Yurt et al., 2012]. For a small spherical nanoparticle, the scattered intensity at a detector, at a given wavelength of light, depends on the dielectric index of both NP and surrounding medium as well as on the radius of the NP themselves [van de Hulst, 1981]. The strong dependence of the scattered intensity on the particle size makes smaller nanoparticles difficult to detect. One approach useful to overcome this issue relies on mixing the weak scattered field with a stronger reference field [Yurt et al., 2012]. In this way,the phase angle difference between reference and scattered fields gains a very important role [Plakhotnik et al., 2001; Ignatovich et al., 2006]. Furthermore, the strong reference field contributes as a constant background intensity, while the weak scattered field usually vanishes for small NP because of its dependence on the sixth power of the particle radius. By combining all together these three data, the dominant optical response of the nanoparticle is given [Yurt et al., 2012].

Interferometric techniques were initially applied to the characterization of single plasmonic metallic nanoparticles [Boyer et al., 2002; Lindfors et al., 2004] as well as dielectric synthetic and natural ones. The optical properties of dielectric nanoparticles differ from the metallic ones [Yurt et al., 2012] because dielectric NP do not exhibit distinct spectral resonances in the visible spectral region and, moreover, they provide a low index contrast to the background which makes the detection more difficult. More recently, the interferometric detection was demonstrated for gold nanoparticles (Au-NP) fixed on a glass substrate, reaching a detection down to 5 nm in diameter [Lindfors et al., 2004; Jacobsen et al., 2006; Zuchner et al., 2008; Failla et al., 2006]. In other studies, higher order laser beams have been utilized to differentiate nanospheres and nanorods for which the orientation was also accurately determined [Zuchner et al., 2008; Failla et al., 2006]. Despite the increased sensitivity, the dimension-based analysis of the nanoparticles was limited due to the double valued optical response curve of the nanoparticles as a function of dimension [Lindfors et al., 2004; Zuchner et al., 2008]. Using the SP-IRIS platform, Daaboul and colleagues

circumvented this ambiguity in sizing due to non-unique optical response by using a layered reflective substrate [Daaboul et al., 2010]. The principle of detection for SP-IRIS is based on the enhanced contrast in the scattering signal from particles on 100 nm silicon oxide layer, thermally grown on silicon supports. To detect and size NPs, IRIS shines a single green light beam (518 nm) from visible LED sources (using the same ACULED VHL surface-mount LED package, Perkin-Elmer, adopted for conventional IRIS measurements) on NPs bound to the sensor surface. Scattered beams are collected by a CCD camera. Acquired images are processed and fitted by a custom-made algorithm on MATLAB software which provides the total number of count nanoparticles per diameter range. Interference of light reflected from the sensor surface is modified by the presence of particles producing a distinct signal that reveals the size of the particle itself. In this approach the dielectric layered structure acts as an optical antenna optimizing the elastic scattering characteristics of NPs for sensitive detection and analysis. The instrument is set for low-index dielectric particles with diameters of 60 to 200 nm and metallic (Au and Ag) NPs with diameters ranging from 20 to 100 nm [Yurt et al., 2012]. At Boston University, the group of Prof. Unlu demonstrated the identification of virus particles in complex samples for replication-competent wild-type vesicular stomatitis virus (VSV), defective VSV, and Ebola- and Marburg-pseudotyped VSV. Size discrimination of the imaged NPs (virions) allows differentiation between modified viruses having different genome lengths and facilitates a reduction in the counting of non-specifically bound particles to achieve a limit-of-detection (LOD) of 5E+03 pfu/mL (< 10 atto-molar of viable virus) for the Ebola and Marburg VSV pseudo-types. In that approach, they have demonstrated the simultaneous detection of multiple viruses in serum or whole blood as well as in samples contaminated with high levels of bacteria [Daaboul et al., 2014]. By employing affinity-based capture, size discrimination, and a “digital” detection scheme to count single virus particles, they showed that a robust and sensitive virus/NP sensing assay could be established for targets in complex samples.

Chapter 4 – AIM OF THE WORK

Several application of protein microarray technology in diagnostics have been published and a limited number of protein microarrays is currently available on the *In Vitro Diagnostics* (IVD) market. Albeit several advantages, related to the miniaturization, the multiplexing capability and the possibility of integrating the immunoassays in biosensing devices, microarrays may still lack of specificity or sensitivity. To overcome these limitations and expand the use of protein microarray platform in diagnostics, the present PhD research aimed at developing innovative approaches to increase the assay specificity and sensitivity, reaching very low detection limits, that are compatible with the use of the proposed devices in diagnostics. Furthermore, the use of protein microarrays has been applied to the characterization of emerging biomarkers: exosomes.

First of all, surface immobilized hydrogels have been investigated as reagent reservoir for microarray reagents. They have been demonstrated to store reagents in a dry form, stable over days, in a format easy to transport and to preserve. Moreover, they also acted as chambers able to physically separate analytes or reagents which may cross-react with proteins on the printed arrays. In this way the solution was prevented from spreading over the surface and the assays provided sentitive performances, comparable to standard static incubations.

In further studies, the complementarity of information provided by fluorescence-based, label-free IRIS and SP-IRIS microarray platforms has been applied to develop immunoassays useful in the diagnostics of Neurodegenerative Disorders. Specifically, two different assay formats have been exploited. The first part of the work focused on

the development of a classical sandwich immunoassay able to detect physiological concentrations of Amyloid-beta peptides, biomarkers for Alzheimer's disease, in both artificial cerebrospinal fluid and real human samples.

The second study was aimed at extending the concept of protein microarrays to extracellular vesicles (i.e., exosomes) detection through surface antigen-antibodies recognition. In this innovative application, the nanoparticles were detected with label-free IRIS (total biomass measurements) and SP-IRIS (particle counting and size distribution). In addition, individual particles were incubated with gold-labeled antibodies to identify biomarkers expressed on their surface.

Chapter 5 – Innovative Approaches to Improve Protein Microarray Performances: Surface Immobilized Hydrogels as Versatile Reagent Reservoir for Microarrays

In the last decade, protein microarrays have been adopted to investigate protein expression patterns and the function of the entire proteome [Kung et al., 2009], to identify biomarkers in serum [Bohm et al., 2011] and to predict evolution of cancer disease [Carlsson et al., 2011]. Despite their huge potential, protein microarrays still have not revolutioned routinary human diagnostics because many technical and operational challenges hinder their application in clinical settings [Ellington et al., 2010]. The major obstacle in the development of protein microarrays is due to the complexity of protein-based interactions. Unlike the predictable sequence-specific hybridization chemistry of DNA arrays, proteins exhibit an extraordinary wide range of structures and mutual affinities [Gaster et al., 2011].

Among all, protein microarrays based on immunoassay format gain higher specificity in binding events, thanks to the antigen-antibody interaction. However, in many cases, this high specificity implicates the ability of other molecules with structural similarity or identical epitopes to bind to the same antibody. This competition is known as as *cross-reactivity* and mainly takes place when polyclonal antibodies (pAbs) are used to capture or detect target antigens in a given sample. pAbs are an etherogeneous mixture of immunoglobulines (usually belonging to the IgG family) against many epitopes on the same protein antigen. Examples of several non-specific interactions that take place during microarray assays are depicted in **Figure 5.1**.

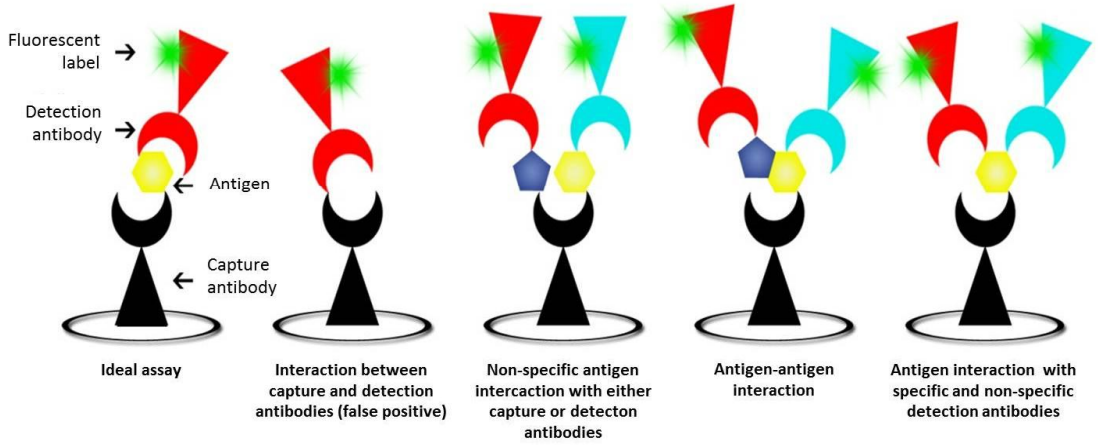

Figure 5.1 –Several interactions that may take place during immunoassays. The first picture on the left represents the ideal test, when specific interactions happen between the antigen and both capture as well as detection antibodies. In other cases, depicted on the right, false positive signals can be revealed, due to non-specific binding events which may occour between capture and detection antibodies, non-specific antigen with the probe, different antigens in the same sample solution or the antigen and another detection antibody.

A way to prevent cross-reactivity is by using monoclonal antibodies (mAbs), which are a homogeneous pool of IgGs all able to recognize the same single epitope on the target antigen. Moreover, this trick can be combined with the more specific approach of two-site (or sandwich) assay that requires two distinct epitopes on the antigen to be recognized, greatly decreasing cross-reactivity even though sometimes it is not enough to fully eliminate this kind of interference [Diamandis et al., 1996]. The Enzyme Linked ImmunoSorbent Assay (ELISA) immunoassay is the gold standard for protein profiling, as the contemporary binding of the target analytes to both capture and detection antibodies yields greater specificity than using a direct detection approach.However, in most of microarray based multiplex assays the detection antibodies are used in mixture, leading to cross-reactivity events between non-matched pairs of antibodies. This effect increases background noise, thus affecting sensitivity and causing false

positive results [Ellington et al., 2010]. The accuracy of microarray-based immunoassays depends on the elimination or, at least, the minimization of antibody cross-reactivity, but the development of multiplex immunoassays on a planar microarray format usually requires extensive validation and a complex development processes [Gonzalez et al., 2008]. Moreover, when dealing with multiplex sandwich assays, the number of required antibody pairs increases with the number of analytes, making unfeasible to increase the number of assays. Whenever cross-reactivity happens, assay components need to be physically separated. For instance, Schneiderhan-Marra and colleagues proposed a multiple bead-based assay [Schneiderhan-Marra et al., 2010] to separate microarray reagents. Otherwise, Pla-Roca and colleagues took advantage from a different assay set-up which let them co-localize both capture and detection antibodies trough two sequential spotting sessions on precise spot coordinates. This precise localization of antibodies allowed to deliver detection antibodies specifically to the locations of the matched capture antibodies [Pla-Roca et al., 2012]. However, up to now, multiplex sandwich assays have only been used simultaneously for tens of targets [Pla-Roca et al., 2012; Djoba Siawaya et al., 2008]. Recently, the SnapChip method, introduced by Li and colleagues, was demonstrated to solve the problem of cross-reactivity in multiplex immunoassay [Li et al., 2012], using detection antibodies, spotted on a “transfer slide”, that are transferred at once by snapping on an “assay slide” with capture antibodies and antigens. Though interesting, this approach is limited by the spot volume in the amount of material to be transferred.

To overcome the problem of detection antibodies cross-reactivity, the use of hydrogels as a versatile method to create compartments for parallel analysis in microarrays was investigated. The hydrogels were polymerized using a 4% w/v N,N-dimethylacrylamide and 3% w/v bisacrylamide solution, thus generating large pore sizes to allow the facile transfer of intact, functional biomolecules. The hydrogel microenvironments were desiccated and rehydrated with solutions containing the microarray reagents [Sola et

al., 2013]. During the incubation step, hydrogel plugs were placed on the corresponding subarray printed on the microarray support to allow entrapped reagents to face the capture biomolecules (**Figure 5.2**).

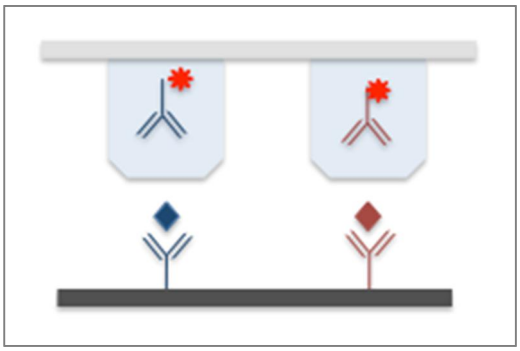

Figure 5.2 – Example of immunoassay using hydrogel plugs to confine microarray reagents. The plugs, rehydrated with detection antibodies, are faced to the corresponding capture biomolecules arrayed on the silicon support.

Hydrogel compartments are versatile reservoirs that can be used to avoid cross-reactivity by separating single detection antibodies. For example, the detection of Staphylococcus aureus enterotoxins A and B was used to demonstrate how hydrogel plugs prevent cross-reactivity. In fact,the detection antibodies selected in this work are a good example of cross-reacting reagents.

Furthermore, it has been found that there are other advantages on the use of hydrogel plugs, besides overcoming cross-reactivity. The versatility of hydrogel plugs makes them useful microarray reagent reservoirs. For istance, the hybridization with gel plugs rehydration requires few microliters of sample. This is advantageous when low

incubation volumes are available.Embedding the analyte solution in the plug and contacting the surface allows to use lower volumes. In particular, an immunoassay for the HIV p24 antigen detection has been chosen to demonstrate the equivalence in sensitivity when using either hydrogel plugs or standard incubation conditions.Due to the low limits of detection required by clinical assays for infectious disease diagnostics, sensitivity is of paramount importance in this assay [Sola et al., 2013]. Another interesting application lies on the use hydrogel plugs as containers of the calibration standards required for accurate quantifications or for long-term reagent storage in dry conditions (**Figure 5.3**). For example, interleukin 10 detection has been selected to demonstrate accuracy in quantification when using an integrated calibration curve since evaluation of cytokine expression levels is a critical step in biomarker discovery and development process [Sola et al., 2013].

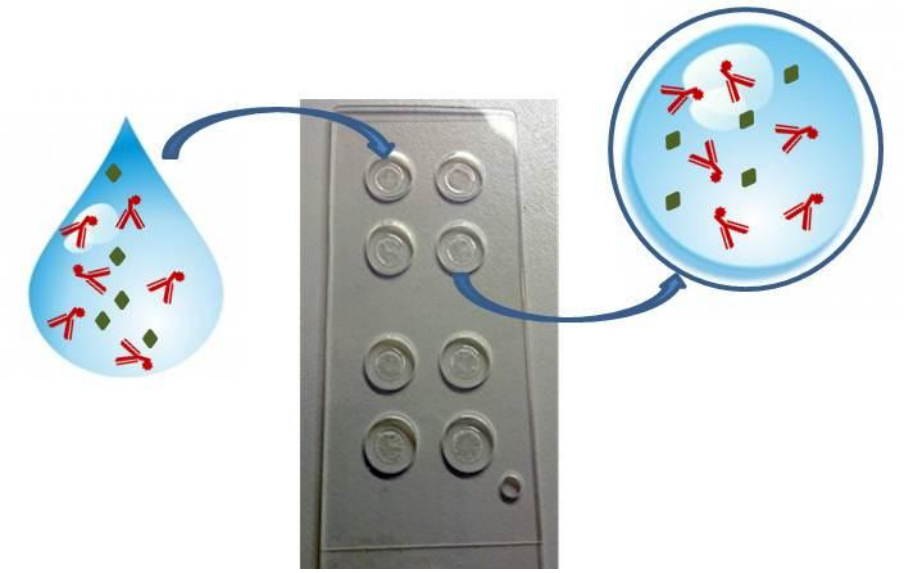

Figure 5.3 - Hydrogel plugs used as containers of calibration standards required for accurate quantifications. Gels are rehydrated with a solution containing desired microarray reagents; plugs are then desiccated for long-term reagent storage in dry conditions.

5.1 - MATERIALS AND METHODS

5.1.1 - Materials

Phosphate saline buffer (PBS), Trizma base (Tris), HCl, ethanolamine, NaCl, Tween-20, ammonium sulfate, N,N-dimethylacrylamide (DMA), 3-(trimethoxysilyl)-propylmethacrylate (MAPS), ammonium persulfate (APS), tetramethylethylenediamine (TEMED) and N,N'-methylenebisacrylamide (Bis), *Staphylococcus aureus* enterotoxins A and B (SEA and SEB) and their respective capture rabbit polyclonal antibodies were purchased from Sigma-Aldrich (St. Louis, MO, USA).

Cyanine-3 labelled Streptavidin (SA-Cy3), goat anti rabbit IgG labelled with Cy3 (anti-Rabbit IgG Cy3) and rabbit IgG were obtained from Jackson Immunoresearch (West Grove, PA, USA). Mouse monoclonal antibodies respectively against SEA and SEB were purchaised from HyTest (Turku, Finland), while labelling kit with fluorophores Cy3 and Cy5 was obtained from GE Healthcare (Buckinghamshire, UK).

Both capture and biotin-labeled mouse monoclonal antibodies against HIV-p24 antigen as well as the peptide itself were a gift from DiaPro s.r.l. (Milan, Italy).

Interleukin 6 (IL-6) and interleukin 10 (IL-10) ELISA kits were from BioLegend (SanDiego, CA). The kits provided respectively standards of IL-6 or IL-10 together with the corresponding capture and biotin-labeled detection antibodies against the interested protein.

Silicon oxide slides were bought from Silicon Valley Microelectronics (Santa Clara, CA, USA). Multiwell cell culture slides were purchased from Grace Bio-labs (Redmond, OR).

5.1.2 - Coating of microarray slides with poly(DMA-NAS-MAPS)

Poly(DMA-NAS-MAPS)-coated silicon microarrays were simply fabricated by immersing the silicon supports for 30 min in a poly(DMA-NAS-MAPS) solution (1% w/v in 0.9 M $(NH_4)_2SO_4$). The chips were then rinsed with deionized (DI) water, dried with nitrogen and finally cured for 15 min under vacuum at 80 °C [Cretich et al., 2009b].

5.1.3 - Fabrication of hydrogel plugs

Multiwell cell culture system slides were used to compartmentalize eight hydrogel plugs onto the same slide (**Figure 5.4**). Each slide was pre-treated with oxygen plasma for 10 min, then the silanization solution was prepared by dissolving MAPS in toluene at a final concentration of 10% v/v and aliquots (30 µL) of this solution were added to each well. Slides were stored in a chamber saturated with toluene vapor for 30 min, washed with acetone, dried with nitrogen and cured in a vacuum oven at 80 °C for 30 min. A DMA-Bis solution (4% T, 3% C) was prepared by diluting a stock solution (20% T, 3% C) in DI water, where:

$\%\ T = [grams_{(acrylamide + methylenebisacrylamide)}/total\ volume] \times 100;$

$\%\ C = [grams_{(methylenebisacrylamide)}/grams_{(acrylamide + bis\text{-}acrylamide)}] \times 100.$

Moreover, 40% w/v APS and TEMED were added to give a final concentration of 5 µL/mL for both components. The monomer solution (30 µL) was immediately loaded into each well and polymerized for 30 min at room temperature. After polymerization the slides were washed twice with DI water (10 min each) and with a solution of 1% v/v glycerol in DI water for 10 min on a shaker. The excess water was removed by evaporation with nitrogen, and the hydrogel plugs were finally dried in a vacuum oven at room temperature. The dry hydrogel plugs were rehydrated simply by filling the wells with a volume of solution containing the protein of interest [Sola et al., 2013].

Figure 5.4 - Picture of the multiwell system used to compartmentalize eight hydrogel plugs. The hydrogels are made of a DMA-Bis solution (4% T, 3% C) that can be dessiccated and rehydrated in 60 min by adding 30 uL of desired slution [Sola et al., 2013].

5.1.4 - Microarray experiments: compartmentalization of secondary antibodies

Rabbit polyclonal antibodies against *Staphylococcus aureus* enterotoxin A (SEA) and enterotoxin B (SEB), together with streptavidin labeled with Cyanine 3 (SA-Cy3) as a reference were patterned on each silicon chip using a SciFlexArrayer S5 spotter from Scienion (Berlin, Germany) according to the scheme reported in Figure 2.3. The printed chips were placed in a humid chamber and incubated overnight at room temperature. The chips were then blocked with **50 mM ethanolamine in 1 M Tris/HCl (pH 9)** for 1 h, washed with DI water and dried with nitrogen. Then, the chips were incubated for 2 h with a protein solution made of a mixture of 100 ng/mL SEA and 10 ng/mL SEB. The chips were washed with the **washing buffer (50 mM Tris/HCl (pH 9), 0.25 M NaCl, 0.05% v/v Tween 20)** for 10 min while stirring and next rinsed with DI water.

The standard incubation protocol required an incubation step with a drop of target solution on the array followed by an incubation with a mixture of labeled secondary monoclonal antibodies at 1 μg/mL each in the **incubation buffer (50 mM Tris–HCl, 150 mM NaCl and 0.02% Tween 20)** for 1 h. The mouse monoclonal antibody against SEA was labeled with Cy5, whereas the mouse monoclonal antibody against SEB was labeled with Cy3.

Differently, the hydrogel-mediated incubations required the rehydration of plugs with 20 μL of a single labeled antibody at 1 μg/mL in the incubation buffer. In this way the antibodies were compartmentalized in separate plugs, as shown in **Figure 5.5**. Each plug was placed in contact for 1 h with the corresponding sub-array patterned on the chip. After removal of the plugs, the chips were washed with PBS (10 min) and DI water (10 min).

Fluorescence imaging was performed by a ProScanArray scanner from Perkin Elmer (Boston, MA); the silicon slides were analyzed using 90% photomultiplier (PMT) gain and laser power. The fluorescence intensities of 12 replicated spots were averaged.

5.1.5 - Microarray experiments: HIV-p24 assay

Four arrays of the capture antibody against HIV-p24 and SA-Cy3 as a reference were spotted on each chip. The printed chips were placed in a humid chamber and incubated at room temperature overnight. The chips were then blocked with 50 mM ethanolamine in 1 M Tris/HCl (pH 9) for 1 h, washed with DI water and dried with nitrogen.

DMA hydrogel plugs were rehydrated for 1 h with 20 or 10 μL of the HIV-p24 antigen solutions at 0, 1, 2, and 5 ng/mL in the incubation buffer. Each array on the silicon chips was incubated for 2 h, by contacting the corresponding hydrogel plug with the printed array. At the same time, the control chips were incubated according to the conventional static protocol, with 20 μL of the HIV-p24 antigen solutions at at the

same concentrations for 2 h. The chips were then washed with the washing buffer for 10 min while stirring, rinsed with DI water, and incubated with 100 µL of 1 µg/mL biotinylated secondary antibody against HIV-p24 in incubation buffer for 1 h in static conditions. The chips were washed with PBS (10 min) and DI water (10 min) and incubated with 100 µL of 1 µg/mL SA-Cy3 in PBS for 1 h. The chips were washed again with PBS (10 min) and DI water (10 min).

Fluorescence signals were detected using a ProScanArray scanner from Perkin Elmer (Boston, MA); the silicon chips were analysed using 90% photomultiplier (PMT) gain and laser power. A calibration curve was created using the fluorescent intensities obtained and the limit of detection (LOD) was extrapolated from the fluorescent value of blank samples plus three standard deviations (3σ). Three replicates of each experiment were performed.

5.1.6 - Microarray experiments: calibration curve

Eight arrays of the capture antibody against interleukin 10 (IL-10) and SA-Cy3 as a reference were patterned on a silicon slide using a SciFlexArrayer S5 spotter according to the scheme reported in **Figure 5.8**. The printed slide was placed in a humid chamber and incubated overnight at room temperature. The slide was then blocked with 50 mM ethanolamine in 1 M Tris/HCl (pH 9) for 1 h, washed with DI water and dried with nitrogen.

Six of the eight hydrogel plugs were hydrated with 20 µL of the incubation buffer containing 1 µg/mL of the biotinylated detection antibody against IL-10 together with 0, 2, 5, 10, 20 or 40 ng/mL of IL-10 (BioLegend, San Diego, CA) to obtain the calibration curve. The dried plugs were stored at 4 °C. Upon use, the two remaining plugs were rehydrated with sample solutions of 3 and 10 ng/mL of freshly prepared IL-10 with 1 µg/mL of biotinylated detection antibody in incubation buffer. Simultaneously, the six plugs, already containing the detection reagents, were simply rehydrated by adding DI

water for 1 h. The silicon-arrayed slide was incubated for 2 h at room temperature on the corresponding rehydrated hydrogel plugs. The slide was then washed with the washing buffer for 10 min while stirring, rinsed with DI water and incubated with 1 μg/mL Cy3-streptavidin in the incubation buffer for 1 h. The slide was then washed with PBS (10 min) and DI water (10 min). Fluorescence visualization was performed by a ProScanArray scanner; the slide was analyzed using 90% photomultiplier (PMT) gain and laser power. The fluorescence intensities of nine replicated spots were averaged.

Multiwell cell culture system slides with fifty wells were used for the fifty-plug format. The assay was performed according to the same protocol described above, now using IL-6 ELISA kit. Calibration mixtures were composed of 0, 2, 5, 10, 50 ng/mL IL-6 with 1 μg/mL biotinylated detection antibody. Fluorescence detection was performed by a ProScanArray scanner; the slides were analyzed using 70% photomultiplier (PMT) gain and laser power. The fluorescence intensities of 8 spots from 50 or 10 replicated gel plugs were averaged.

5.2 - RESULTS AND DISCUSSION

5.2.1 - Compartments for secondary antibodies

The cross-reactivity between capture and detection antibodies is one of the most critical issues when developing multiplex sandwich immunoassays. To prove how hydrogel-plugs can prevent antibody cross-reactivity, the detection of *S. aureus* enterotoxins A and B (SEA and SEB) was investigated using a fluorescence-based analytical microarray platform.

According to the standard microarray incubation protocol, the sample contacts a slide on which two polyclonal capture antibodies have been arrayed. Then, the analytes, in the present case the SEA and SEBtoxins, are detected with a mixture of their fluorescently-labeled monoclonal antibodies. The specificity of the detection antibodies selected in this work is poor. In fact, the SEA detection antibody cross-reacts with SEB and its capture antibody, whereas the SEB detection antibody slightly interacts with SEA and its capture probe.

To overcome this issue, hydrogel plugs to confine the detection antibodies were exploited. **Figure 5.5** outlines the scheme of the assay using hydrogel-plugs under study. In particular, the capture antibodies for SEA and SEB were spotted on the same slide in two separate sub-arrays. The entire slide was then incubated with the sample containing either SEA, SEB or both of them, and afterwards the toxins were revealed using the two detection antibodies confined in the different hydrogels. Printed sub-arrays of each capture antibody were aligned with the corresponding hydrogel plugs, which were in turn rehydrated either with the anti-SEA antibody labeled with Cy5 or with the anti-SEB antibody labeled with Cy3 in the incubation buffer.

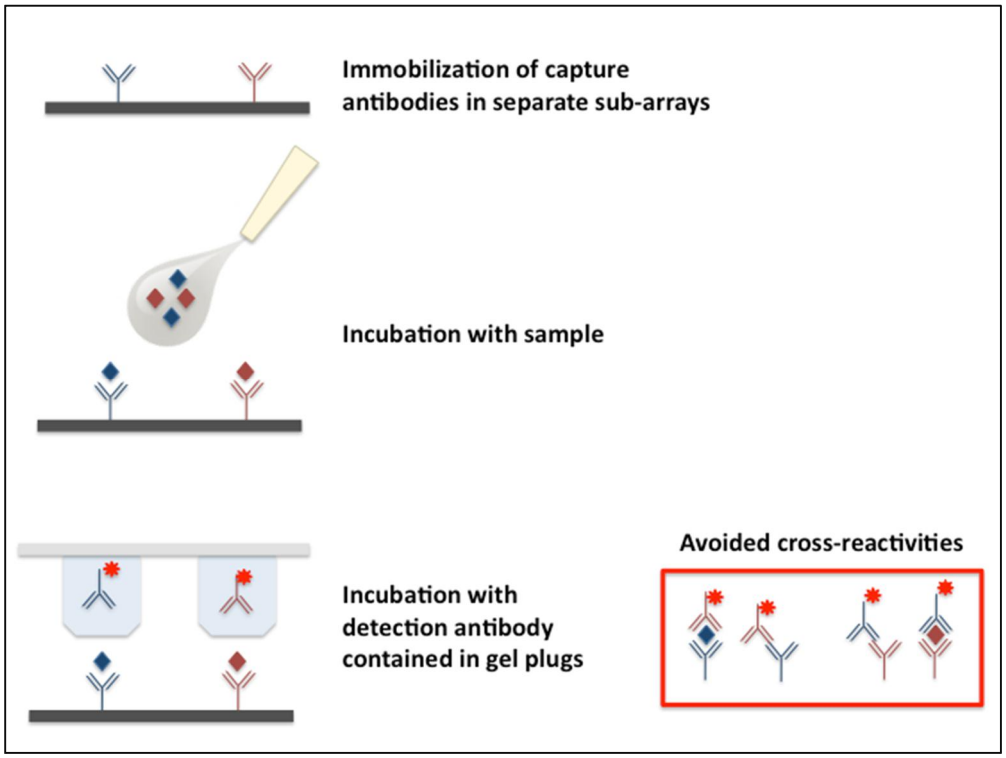

Figure 5.5 - Scheme of the *Staphylococcus aureus* enterotoxins A and B (SEA and SEB) detection assay. The sample was incubated on a microarray spotted with two polyclonal capture antibodies. The toxins were then detected with a mixture of the two monoclonal detection antibodies. To overcomecross-reactivities, the capture antibodies for SEA and SEB were spotted in two separate sub-arrays. The entire area of the microarray slide was then incubated with the sample, and toxins were revealed using the two detection antibodies confined in different hydrogel plugs [Sola et al., 2013].

The spotting scheme and the fluorescence results are reported in **Figure 5.6**. In panel ***a***, the fluorescence of the reference standard assay, using a mixture of the SEA and SEB detection antibodies, is shown. The array was first incubated with a solution containing a mixture of SEA (100 ng/mL) and SEB (10 ng/mL), as previously described, and then with a mixture of the two monoclonal detection antibodies in the incubation buffer at 1 µg/mL. The Anti-SEA antibody was labeled with Cy5, and the anti-SEB antibody was labeled with Cy3. The specific signals originating from the capture and detection

antibody sandwiches are clearly visible on the left sub-array of the Cy5 channel for SEA and on the right sub-array of the Cy3 channel for SEB. The cross-reacting antibody signals, Cy3 anti-SEA on anti-SEB and Cy5 anti-SEB on anti-SEA, are also visible on the left sub-array of the Cy3 channel and right sub-array of the Cy5 channel, respectively. When the antibodies are labeled with the same fluorophore (as in most assays), it is not possible to distinguish this type of non-specific binding from a real toxin detection event, leading to false positive results [Sola et al., 2013].

On the contrary, **Figure 5.6**, panel ***b*** displays the fluorescence detection results, using the hydrogels to confine the detection antibodies, as described above. Because the toxins on the surface were contacted only by their specific detection antibodies, only the signals from those detection antibodies were observed, and the non-specific, cross-reactivity fluorescence was prevented.

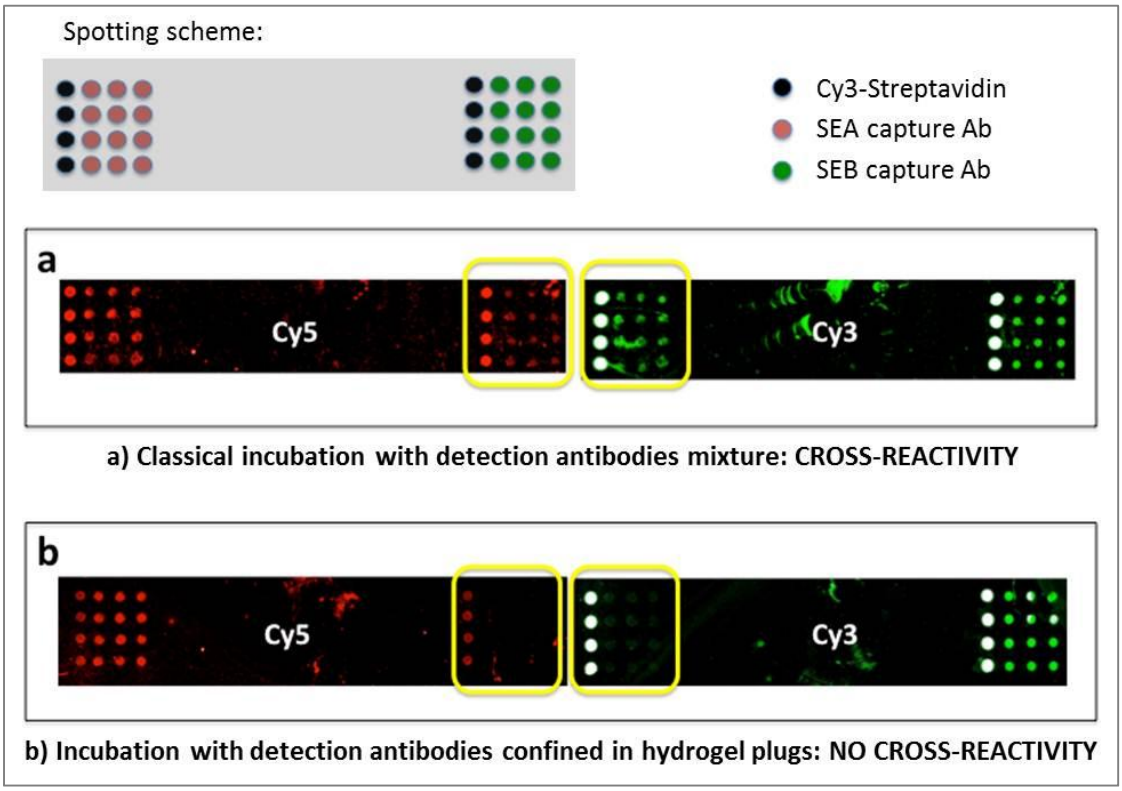

Figure 5.6 - Spotting scheme and dual channel detection of SEA and SEB. ***a***) Fluorescence detection of the assay performed using a mixture of the SEA and SEB detection antibodies. The specific signals originating from the perfect match between capture and detection antibodies mediated by the toxin are clearly visible on the left sub-array of the Cy5 channel for SEA and on the right sub-array of the Cy3 channel for SEB. However, the cross-reacting antibody signals, are visible as well for each sub-array on the same chip, as highlighted in the rectangle. ***b)*** Fluorescence detection of the assay performed using hydrogel-plugs to confine the detection antibodies: in this case, the labeled detection antibodies were entrapped in hydrogel plugs facing the corresponding sub-arrays on the slide. Specific toxin signals are clearly visible on the left sub-array of the Cy5 channel for SEA and on the right sub-array of the Cy3 channel for SEB, whereas nonspecific fluorescence, originating from antibody cross-reactivities, is not detectable (as highlighted in the rectangle) [Sola et al., 2013].

5.2.2 - Compartments for samples

The hydrogel plugs prevent liquid spreading on the microarray surfaces. By rehydrating the hydrogel with the target solution, the liquid is entrapped into the gel fibers. Gel plugs of defined shape provides a way to increase its local concentration, resulting in

improved signal intensities.In a standard microarray experiment, the target solution covers the entire surface, including unspotted areas. Concentrating the sample in a specific zone of the slide reduces the volume consumption and thus the cost per experiment [Sola et al., 2013]. Moreover, multi-well formats are commercially available for parallel analysis of multiple samples; however, they rely on the use of hydrophobic patterning, adhesive silicon chambers or microplates to be used in combination with multiple wells. Differently, hydrogel compartments can be used to incubate calibration standards together with the unknown sample at the same time on a single device, leading to higher quantitation accuracy [Sola et al., 2013]. In order to achieve this goal, to demonstrate the concept, hydrogel compartments were applied to a sandwich immunoassay for the HIV-p24 antigen detection. It was shown that using a conventional incubation method with the target in solution provided results that were identical to those obtained with the desiccated hydrogel-plaques rehydrated with the sample solution right before the incubation [Sola et al., 2013].

The assay was performed using poly(DMA-NAS-MAPS)-coated silicon slides on which capture anti-p24 monoclonal antibodies (1 mg/mL) were patterned. The slides were incubated for 2 h with 20 µL of HIV-p24 antigen dissolved in the incubation buffer either in standard static incubation (drop on the entire chip surface) or with rehydrated hydrogel-plugs. In this case the analyte was embedded in gel plugs, while to detect the captured antigen, a conventional incubation method with the detection antibody was performed in both cases. Several antigen concentrations were assayed from 0 to 5 ng/mL, and calibration curves (reported in **Figure 5.7**) were built to extrapolate the limits of detection (LODs). The LOD values provided by both incubation protocols, were 37 pg/mL with the conventional incubation method and 45 pg/mL with hydrogel-plugs. These values were similar, thus demonstrating that both tests provide similar sensitivity. Moreover, it was noticed that when using 6 mm diameter hydrogel plugs, a reduction of rehydration volume from 30 to 10 µL did notaffect the sensitivity of the assay, allowing the use of a reduced sample volume.

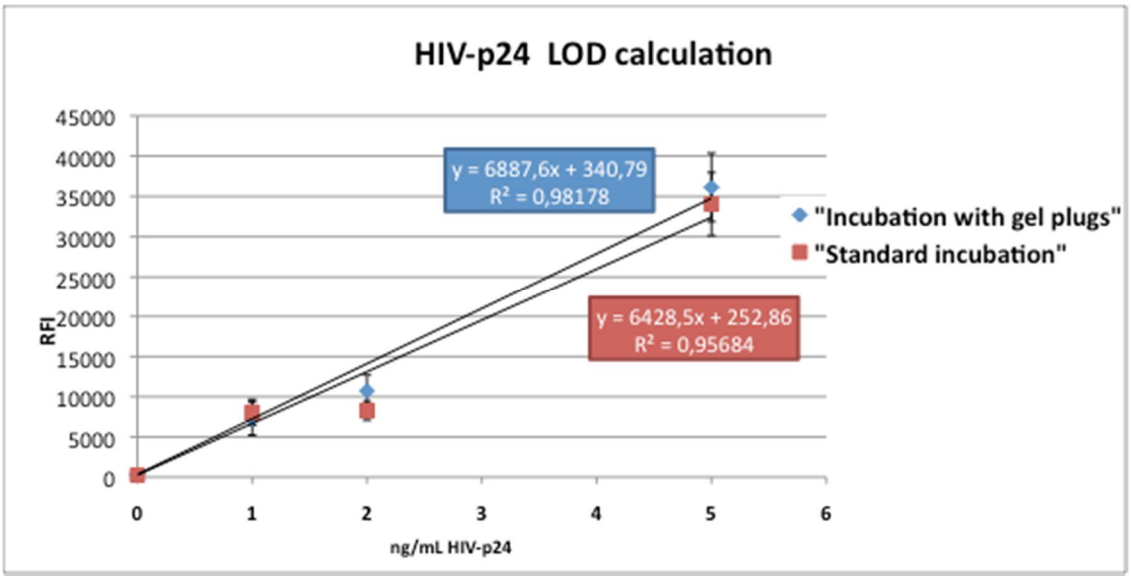

Figure 5.7 - Calibration curves used to calculate the limits of detection (LODs) for HIV-p24 antigen when using either standard incubation (red dots) or hydrogel plugs (blue diamonds). Curves led to LOD of 37 pg/mL for standard incubation and 45 pg/mL for incubation with gel plugs.

5.2.3 - Integrated calibration curves

Another interesting application of hydrogel-plugs consists of using them as reservoirs of calibrations standards and reagents [Sola et al., 2013]. Indeed, storing reagents in dry-form represents a useful way to maintain their stability without using refrigeration.This simplifies assay automation, thus improving repeatability. It also reduces training requirements and facilitates integration into lab-on-chip devices [Stevens et al., 2008]. In order to prepare the storage hydrogels, the reagents solutions at required concentrations were used to rehydrate dry plugs, which were then desiccated and stored. Immediately before usage, the hydrogels were rehydrated simply with DI water and used in the assay.

To demonstrate the feasibility of the method, a sandwich immunoassay for interleukin 10 (IL-10) detection with an integrated calibration curve was carried out. A picture of

the hydrogel compartments and the spotting scheme is reported in **Figure 5.8**. In this experiment, an eight-plug format was empolyed. Six of the eight hydrogels (from *a* to *f*) contained the standard mix for the calibration curve (0, 2, 5, 10, 20 or 40 ng/mL IL-10 and 1 µg/mL biotinylated detection antibody), while the remaining two plugs (*g* and *h*) were rehydrated with samples of unknown concentration immediately defore the assay. The slide bearing the hydrogels was stored in dry form. Before use, the calibration hydrogels were rehydrated with water while the empty hydrogels were rehydrated with two samples to be assayed (plug *g* and *h*, respectively at 10 and 3 ng/mL) together with the biotin-labeled detection antibodyboth dissolved in the incubation buffer. The IL-10 capture antibody was spotted in 8 replicate sub-arrays on a coated silicon slide, placed in contact with the hydrogel compartments for 1 h. Washing steps and incubation with Cy3-labeled streptavidin were carried out as described in previous assays. The fluorescence results obtained for the calibration standards and the two testing samples are shown on the right side of **Figure 5.8**.

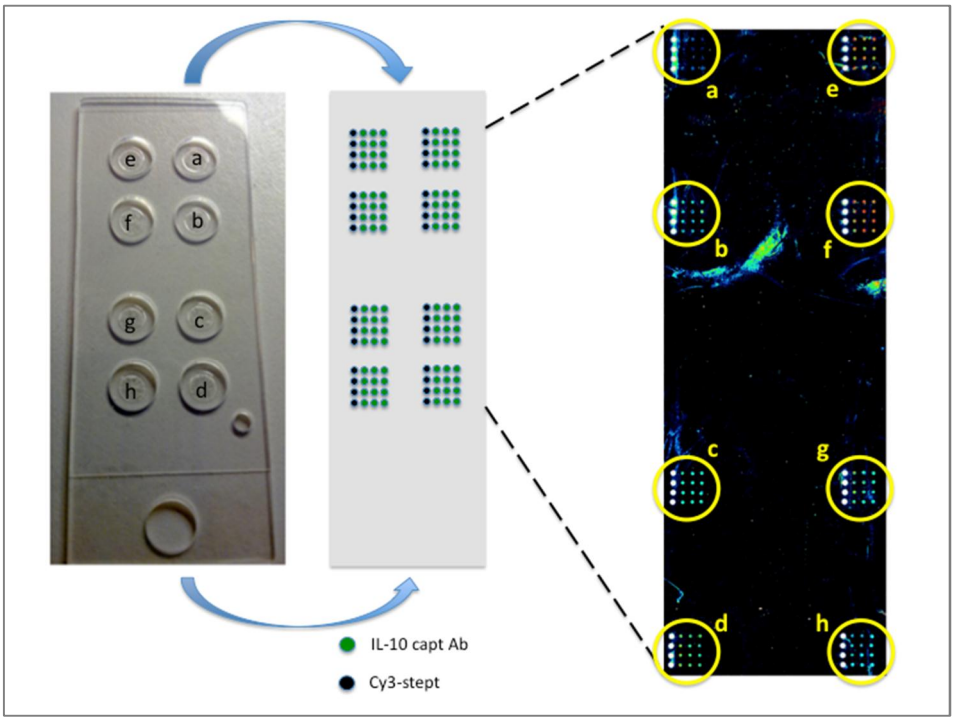

Figure 5.8 - Picture of the hydrogel plugs and spotting scheme. Six of the eight hydrogel plugs (from *a* to *f*) contained a standard mix for a calibration curve (IL-10 and the biotinylated detection antibody) while the hydrogel plugs *g* and *h* were used to assay unknown samples. The IL-10 capture antibody was spotted in eight replicated sub-arrays that were placed in contact with the hydrogel plugs. The right panel reports the resulting fluorescence signals.

The calibration curve reported in **Figure 5.9** was obtained by incubating the arrays with the calibrating hydrogel plugs (blue dots). The mean fluorescence signals of the samples *g* (10 ng/mL IL-10) and *h* (3 ng/mL IL-10) were found to be 8524 Relative Fluorescence Intensity (RFI) (standard deviation, SD = 1773) and 3849 RFI (SD = 682) (red dashes). According to the calibration curve generated using the concentrations from 0 to 20 ng/mL, the signals were quantified as 11.14 ng/mL and 2.27 ng/mL, respectively.

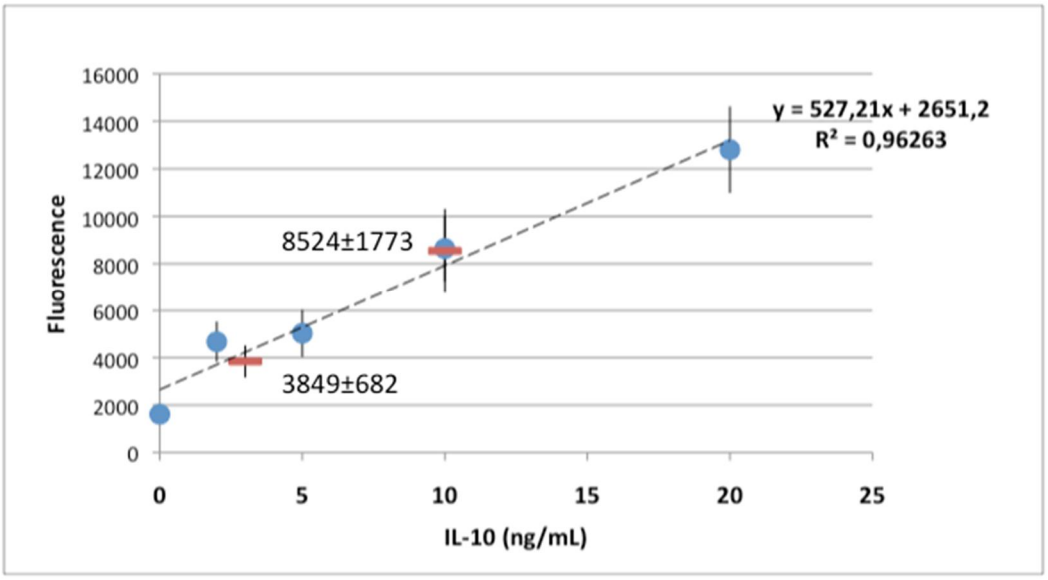

Figure 5.9 - Calibration curve based on fluorescent signals obtained on arrays from *a* to *e* (blue dots). The fluorescence of array *f* was not included because it was out of the linear range. Samples in arrays *g* and *h* (red dashes) provided fluorescence signals equal to 8524 ± 1773 RFI and 3849 ± 682 RFI. According to the calibration curve, these signals were quantified as 11.14 ng/mL and 2.27 ng/mL, respectively.

Moreover, the scalability of this approach was also tested using a fifty-hydrogel plugs format to demonstrate its usefulness in high-density microarray technology. **Figure 5.10** (panel ***a***) shows a picture of a 50-multiwell cell culture system where the 50 gel plugs were re-hydrated with a Bromophenol Blue solution [Sola et al., 2013].

To demonstrate the feasibility of this format, a sandwich immunoassay for interleukin 6 (IL-6) detection was carried out. **Figure 5.10** (panel ***b***) reports the fluorescence results of a slide where each of the 50 gel plugs was re-hydrated with 7 µL of 50 ng/mL IL-6 solution. The fluorescence value from the 8 spots on 50 arrays was evaluated using 70% laser power and PMT gain. The resulting overall average intensity was 29582 ± 3589 RFI, thus revealing a good reproducibility of the device.

Moreover, using the same 50-gel plugs format, ten calibration curves for interleukin 6 (IL-6) were perfomed simoultaneously. The assay was carried out in a fashion similar to te one described above, but in this case the gel plugs were re-hydrated with 7 uL of the standard mixutres for the calibration curve (0, 2, 5, 10, 50 ng/mL IL-6 and 1 μg/mL biotinylated detection antibody). Ten gel per each condition were tested. The fluorescence signals from the 8 spots assayed in the same condition (corresponding to 10 gel replicates) were evaluated and averaged. The resulting calibration curve, shown in **Figure 5.10** (panel ***c***), displays a good degree of linearity corroborating the stability of this assay format.

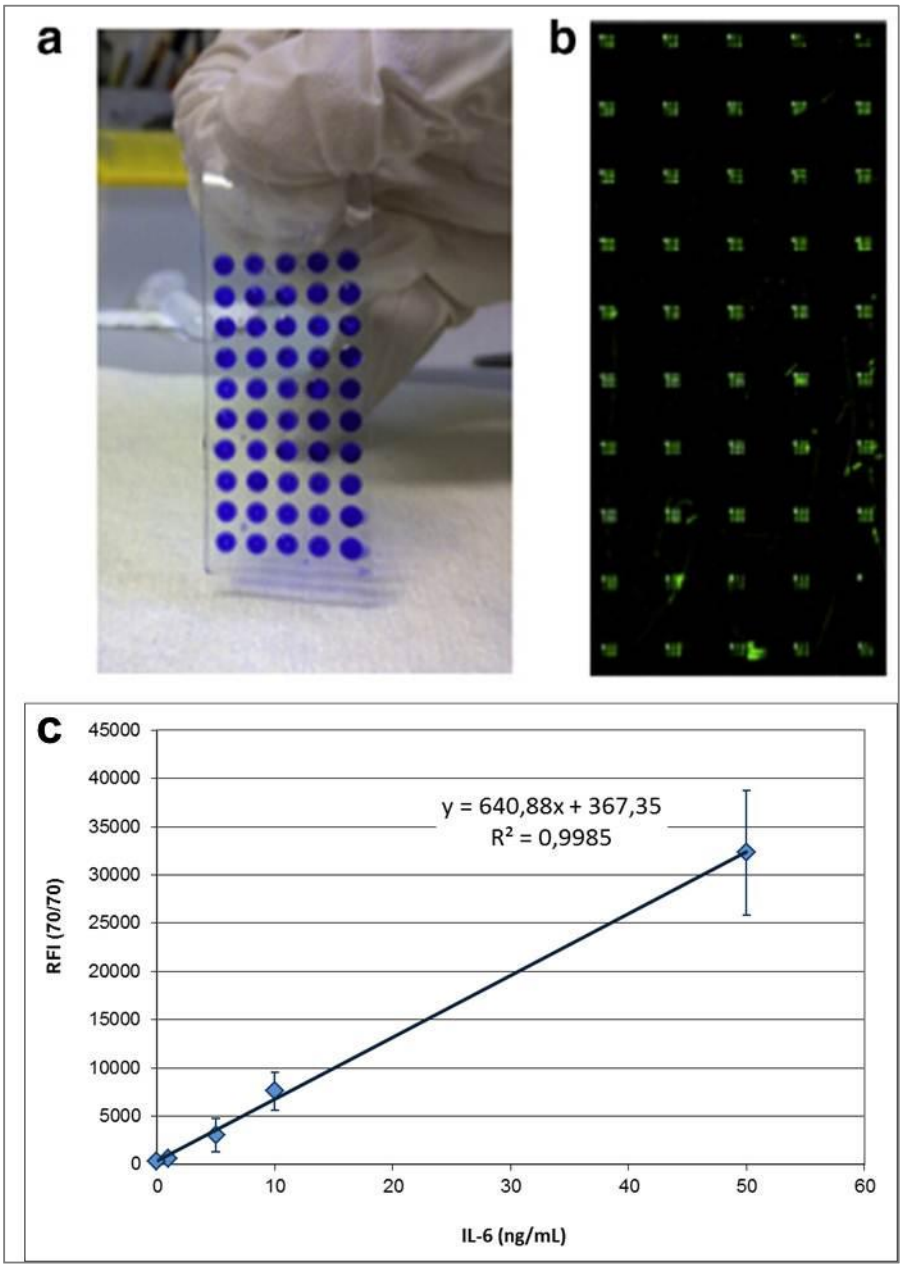

Figure 5.10 – Multiplexing of the system and calibration curve. *a*) Picture of the multiwell system used to compartmentalize fifty hydrogel plugs re-hydrated with a Bromophenol Blue solution. *b*) Fluorescence results obtained with a slide in contact with the calibration plugs in which IL-6 was spiked at concentrations of 50 ng/mL. *c*) Calibration curve based on fluorescent signals obtained from 10 replicates of each calibration mixtures (0, 2, 5, 10, 50 ng/mL IL-6 and the biotinylated detection antibody at 0.001 mg/mL).

5.3 - CONCLUSIONS

In this work, the role of antibody-based microarrays specificity and selectivity was investigated. The specificity of binding events depends on eliminating or at least minimizing cross-reactivity events that take place whenever capture or detection antibodies bind to epitopes with similar structures aberrantly. To overcome this issue, compartments for detection antibodies and soluble microarray reagents were developed. The containers are made of hydrogels immobilized on a silicon slide or chip facing the corresponding sub-array on the printed surface. Moreover, these hydrogels were used as reagents reservoir as in each plug proteins can be stored and transported in a dry form, but not irreversibly trapped due to the gel porosity [Sola et al., 2013]. Hydrogels define a highly aqueous environment because they are about 97% water.Within the array, they are physically compartmentalized and fully functional. According to Holmes and Stellwagen [Holmes et al., 1991], the pore size of a polyacrylamide hydrogel strongly depends on the concentration of the acrylamide monomer (%T) and of the bisacrylamide cross-linker (%C). At a fixed concentration of cross-linker, the apparent pore radius decreases from 140 to 20 nm while % T is increased from 3 to 10%. In this work, the hydrogels were made of DMA (4% T) cross-linked with Bis (3% C). The low monomer concentration was used to facilitate the protein diffusion and to increase the transfer efficiency. DMA was chosen thanks to its greater stability compared to polyacrylamide in order to create round hydrogels with a diameter of 6 mm, covalently attached to a glass slide to facilitate their handling [Sola et al., 2013]. Surface attached hydrogels can therefore be used as a versatile tool for the compartmentalization, storage and transport of soluble microarray reagents, providing performances comparable to standard incubation protocols.

Chapter 6 - High Sensitivity Immunoassay for Amyloid-beta Detectionon on a Silicon Microarray platform

In the second study presented in this thesis, a high sensitive immunoassay for the detection of the Alzheimer's disease (AD) biomarker Amyloid-β 1-42 (Aβ(1-42) or Aβ42) using both fluorescence-based and label-free IRIS microarray platforms was developed [Gagni et al., 2013].

Alzheimer's disease (AD) is a widespread pathology associated with aging and classified in the major group of Neurodegenerative disorders (ND), which includes also vascular dementia (VD), Parkinson's disease (PD), frontotemporal lobar degeneration (FTLD), Lewy body dementia (LBD) and amyotrophic lateral sclerosis (ALS). These disorders are characterized by a progressive loss of function of specific groups of neurons in different regions of the brain and they are variably associated with dementia, personality changes, language abnormalities or progressive muscle weakness [Cretich et al., 2013]. Although strategies to prevent or delay the accumulation of the protein aggregates associated with these diseases have been proposed, at present, there is no perspective cure or preventive treatment for brain damage [Klafki et al., 2006]. In fact, NDs processes are initiated long before the clinical symptoms become obvious and proceed for years in a slow and irreversible manner. Therefore, the early diagnosis of NDs and the efficient discrimination between disorders is of paramount importance in order to provide effective treatments.

Alzheimer's disease is a progressive and fatal neurodegeneration process, clinically characterized by progressive cognitive decline, for which currently there are no

available treatments to prevent or slow down the pathology evolution [Cretich et al., 2013]. The treatment of AD is significantly hampered by the lack of easily accessible biomarkers that can detect the presence of the disease reliably. At present, biomarkers in collected fluids (such as blood/plasma or cerebrospinal fluid) from patients only provide indications of the disease stage because they are not robust predictors of disease progression or treatment response [Henriksen et al., 2014]. Definitive diagnosis requires both clinical assessment of the disease and post-mortem verification of the AD pathology (plaques and tangles). A probable diagnosis of AD can be established with more than 90% confidence, based on the combination and integration of several clinical criteria, including medical history, physical examination, laboratory tests, neuroimaging and neuropsychological evaluation. An accurate early diagnosis of AD is still difficult because early symptoms are shared by a variety of disorders, which reflects common neuropathological features. An ideal biomarker would distinguish AD from other types of dementia, such as mild cognitive impairment (MCI), or mixed forms of dementia, such as vascular dementia (VD), frontotemporal lobe dementia (FTLD), or Lewy body dementia (LBD) [Humpel, 2011]. Concerning this topic, Shneider and colleagues compared the accuracy of traditional biomarkers from CSF with neuroimaging in terms of both early and selective diagnosis of AD and other NDs, demonstrating the similarity of the obtained results in ranking patients [Schneider et al., 2009].

Figure 6.1 – Aminoacidic sequence of the Amyloid-β (1-42) peptide.

Abnormal extracellular accumulation of Amyloid peptides observed in the brains of AD patients consists predominantly of the Aβ(1-42) (**Figure 6.1**), that is a peptide derived from the proteolytic cleavage of a larger Amyloid Precursor Protein (β-APP). **Figure 6.2** shows the pathways of APP processing. The activity of α and β-secretase release the soluble fractions of APP, respectively $sAPP_{\alpha}$ and $sAPP_{\beta}$, accordin to a physiological mechanism. Whenever APP is cleaved by γ-secretase, the Amyloid-β peptide is released in the extracellular medium.In healthy individuals, Aβ is found in CSF and plasma as a soluble monomer at sub-nanomolar concentrations.

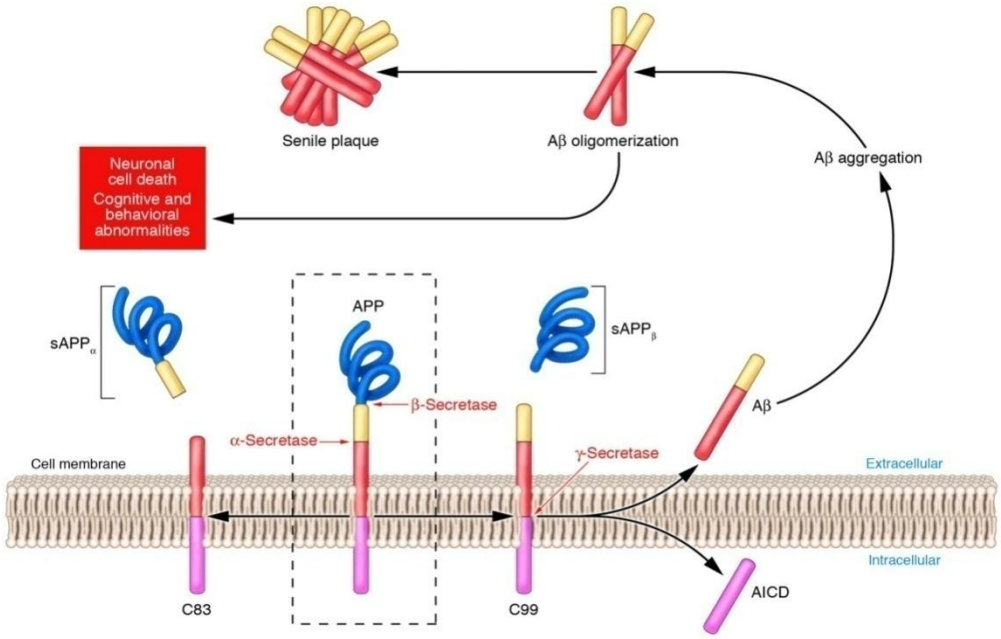

Figure 6.2 – APP processing release of Amyloid-β peptides [www.jci.org].

However, Amyoid peptides exist in several isoforms that differ at the amino or carboxy terminus, whose heterogeneity is particularly interesting. *In vitro*, the longer peptide

Aβ(1–42) aggregates magnitudes of order faster than the short forms Aβ(1–40) and Aβ(1–39) [Seilheimer et al., 1997]. Aβ(1–42) has a high propensity to form oligomers even*in vitro*, which decreases its detection efficiency and makes accurate evaluation of the Limit of Detection (LOD) very difficult. Aβ42 is a difficult peptide to work with, in the sense that its aggregation properties are highly sensitive to sequence, purity and preparation conditions. The actual monomeric peptide concentrations in the commercial samples are largely unknown [Ammar et al., 2013].

The identification and validation of biomarkers for early and specific diagnosis of AD is of huge importance. The measurement of a single biomarker widely varies between studies [Fagan et al., 2012], but the evaluation of a panel of biomarkers increases the diagnostic accuracy [Cretich et al., 2013]. The main source of AD biomarkers is the cerebrospinal fluid (CSF), as it directly reflects brain metabolic processes. However, lumbar puncture is an invasive and delicate procedure, restricted to patients with significant symptoms and is not applicable for widespread screening [de Almeida et al., 2011; Schneider et al., 2009]. For this reason, many researches are moving towards the discovery and validation of novel biomarkers in easily collectible samples, such as plasma/serum [Cretich et al., 2013]. Biomarker signatures are under study through the use of proteomics, metabolomics, and gene expression studies. However, their reproducibility across different cohorts of patients is lacking [Snyder et al., 2014]. Many studies focused on novel biomarkers in plasma proteomics and lipidomics, in trascriptome, microRNA, autoantibodies and blood-derived genetic markers to discriminate AD from other NDs, but a large scale validation is still required [Henriksen et al., 2014].

At state-of-the-art, established and well-characterized biomarkers of AD from CSF are only Amyloid-β 1-42 peptide (Aβ1–42), total tau protein, and hyperphosphorylated tau protein [Cummings, 2011; Blennow et al., 2010]. To date, the combined ELISA measurement of the given three biomarkers in CSF is the most advanced and accepted

method to diagnose probable AD with high specificity and sensitivity [Blennow et al., 2010; Hampel et al., 2007]. In addition, these biomarkers have also shown prognostic potential because they were able to separate subjects with mild cognitive impairment (MCI) who progressed to AD from those who did not [Hampel et al., 2007; Mattsson et al., 2009].

More specifically, CSF levels of Aβ(1-42) are lower in AD patients than in normal controls, reflecting amyloid precipitation. Specifically, low CSF Aβ(1-42) levels are detected in preclinical disease stages and predict future cognitive decline and neurodegeneration [Blennow et al., 2010; Buchhave et al., 2012; Ringman et al., 2012]. An Aβ(1-42) concentration of less than 500 pg/mL (0.1 nM) is indicative that this peptide is accumulating in the plaques and no more soluble in the CSF (**Table 6.1T**) [Humpel, 2011]. Changes of Aβ-levels in CSF differ based on the disease (**Table 6.2T**) [Zetterberg et al., 2010; Stefani et al., 2005; Noguchi et al., 2005]. For example, decreased Aβ(1–38) levels correlate with FTLD, while low Aβ(1–37) levels are associated with LBD [Cedazo-Minguez et al., 2010].

Table 6.1T - Established biomarkers in CSF used to diagnose AD[a] [Humpel, 2011].

Biomarker	Controls (pg/mL)	AD (pg/mL)
Aβ(1-42)	794 ± 20	< 500*
Total tau	136 ± 89 (21-50 years) 243 ± 127 (51-70 years) 341 ± 171 (> 71 years)	[b] > 450 > 600*
Phospho-tau-181	23 ± 2	> 60*

[a] *Data obtained using the Innogenetics single 96-well ELISA kits.*
[b] *Not relevant for sporadic AD*
* $p < 0.001$

Table 6.2T - Changes in the level ofestablished CSF biomarkers in different central nervous system diseases (-, no change; ↑, increase; ↓, decrease) [Humpel, 2011].

Disease	Aβ(1-42)	Total tau	Phospho-tau-181
Acute stroke	-	↑(↑)	-
Alcohol dementia	-	-	-
AD	**↓**	**↑**	**↑**
CJD	↓↓	↑↑↑	-
Depression	-	-	-
FTLD	↓	↑	-
LBD	↓	↑	↑
Neuroinflammation	↓	-	-
Normal aging	-	-	-
Parkinson's disease	-	-	-
VaD	↓(↓)	↑	-

Interestingly, CSF levels of shorter Aβ(1–40) form are unchanged or increased in AD. Sunderland and Schoonenboom have therefore suggested that the Aβ(1-42)/Aβ(1-40) ratio can improve AD diagnosis, but others have not found such changes [Sunderland et al., 2004; Schoonenboom et al., 2005]. A meta-analysis by Koyama and colleagues, examined plasma levels of Aβ(1-42) and the ratio of Aβ(1-42)/Aβ(1-40) as predictors of dementia and AD. They argued that a decrease of the Aβ(1-42)/Aβ(1-40) ratio in plasma is a statistically significant and clinically meaningful predictor of subsequent cognitive decline [Koyama et al., 2012]. Also Lewczuk et al. measured cerebrospinal fluid (CSF) concentrations of amyloid Aβ(1-40) and Aβ(1-42) peptides, and total tau (tTau) protein by ELISA in order to compare their accuracy in discriminating patients with Alzheimer's disease (AD), non-Alzheimer dementia (nAD) and control subjects (CON). As compared to the other groups, the concentrations of Aβ(1-42) and tTau

were, respectively, decreased and increased in AD, while Aβ(1-40) did not differ significantly among the groups. According to all compared groups the peptides ratio Aβ(1-42)/Aβ(1-40) classified more patients correctly, as compared to the concentration of Aβ(1-42) alone. Moreover, the percentage of correctly classified patients was further improved when the Aβ ratio was combined with the analysis of the tTau concentration [Lewczuk et al., 2004]. Conversely Perez and colleagues suggested the use of other Aβ species, particularly Aβ(1-17), for the diagnosis of AD. In particular, they demonstrated that the ratio of free to cell-bound Aβ(1-17) in blood was able to discriminate between healthy individuals from patients with MCI or mild AD, with high sensitivity and specificity [Perez et al., 2012].

To date, most of the Aβ(1-42) assays rely on immunochemical detection [Cullen et al., 2012] such as the conventional ELISAs, electrochemiluminescence-based ELISAs or the bead-based methods [Kang et al., 2012]. One of the most widely used assays for Aβ(1-42) is the INNOTESTs ELISA from Innogenetics NV. It has been cited in numerous publications and has been recently validated and optimised leading to a lower limit of quantitation of 375 pg/mL [Cullen et al., 2012]. However, it is well known that ELISA tests lack multiplexing capability, whereas the best way to distinguish AD from other NDs is by using a combination of the three overmentioned biomarkers. To this end, an xMAP-Luminex platform that utilises the Innogenetics AlzBio3 immunoassay reagents, was developed to analyse AD biomarkers in CSF using 150 μL of sample, 10 handling steps and a total analysis time of 19 h for three targets [Kang et al., 2012]. Recently, an immuno-sensing platform for Aβ(1-42) based on a silane-modified silicon wafer and fluorescence microscopy set-up has been developed with a limit of detection (LOD) of 300 ng/mL [Ammar et al., 2013]. Signal enhancement in antibody microarrays using quantum dots for the screening of the potential AD biomarker Apolipoprotein E (ApoE) has been demonstrated with LODs up to 62 pg/mL [Morales-Narvaez et al., 2012].

In this context, because of the multiplexing capability, low volume sample consumption and sample-to-result time, microarrays are ideal tools, provided they have high sensitivity and specificity. However, no high-sensitivity microarray-based methods for Aβ(1-42) detection have been developed as yet. To fill this gap, the present research aimed to develop a highly sensitive immunoassay based on a microarray platform that utilize silicon/silicon oxide (Si/SiO_2) substrates for the detection of the AD biomarkers Aβ(1-40) and Aβ(1-42) in artificial cerebrospinal fluid (ACSF) and real human samples [Gagni et al., 2013]. Prior to immunoassay development, the Aβ(1-42) aggregation status was evaluated by circular dichroism (CD) and an optimal antibody pair was selected based on the specificity of recognition of the 1-42 aminoacid Aβ monomers and the optimal binding yield of the capture antibody on the coated silicon surface. Finally, incubation conditions were optimised to achieve the lowest Aβ(1-42) limit of detection (LOD) using an artificial CSF sample [Gagni et al., 2013]. In the same conditions the LOD for Aβ(1-40) was evaluated. Moreover, this tool has been applied to detect both the Aβ peptides in real human CSF samples.

6.1 - MATERIALS AND METHODS

6.1.1 - Materials

Phosphate buffered saline (PBS), Trizma base (Tris) , HCl, ethanolamine, NaCl, KCl, $CaCl_2$,$MgCl_2$ ° $6H_2O$, Sodium bicarbonate, Sodium phosphate, Glucose, Human serum albumin (HSA), Tween 20, ammonium sulphate, N,N-dimethylacrylamide (DMA), 3-(trimethoxysilyl)propylmethacrylate (MAPS), ammonium persulfate (APS), tetramethylethylenediamine (TEMED) and N,N'-methylenebisacrylamide (Bis) were purchased from Sigma-Aldrich (St. Louis, MO, USA).

Amyloid-β (1–42) and Amyloid-β (1-40) were bought from Anaspec (Fremont, CA , USA). Amyloid-β (1–39) was a kind gift from Prof. Annalise E. Barron (Stanford University, CA , USA).

Mouse monoclonal antibodies to full-length Amyloid-β (clone 12F4), to amino acids 1–16 (clone 6E1) and to amino acids 17–24 (clone 4G8) were purchased from Covance (Princeton, NJ, USA). Mouse monoclonal antibodies to the Amyloid-β A4 N-terminus (clone 1E8 and clone 11H3) and C-terminus (clone 8G7) were bought from Nanotools (Teningen, Germany). Goat polyclonal antibody to the Amyloid-β C-terminus (clone D-17) was bought from Santa Cruz Biotechnology (Santa Cruz, CA , USA). Mouse monoclonal antibodies to Amyloid-β amino acids 1–42 (clone G2-13 and clone W0-2) were purchased from Millipore (Temecula, CA , USA). Rabbit polyclonal Amyloid-β anti-oligomer antibody (clone A11) was bought from Invitrogen (Frederick , MD, USA). Mouse monoclonal antibody to the Aβ(1-40) carboxy terminus clone G2-10 was bought from Millipore (Temecula, CA , USA), while the clones 29-6 and 11A50-B10 against the same epitope were purchaised from Covance (Princeton, NJ, USA).

Goat anti-Rabbit IgG, Cyanine 3-labeled streptavidin (SA-Cy3) and Cyanine 3-labeled Rabbit anti-Mouse IgG were obtained from Jackson Immunoresearch (West Grove, PA , USA).

Real human samples of CSF were kindly provided by Prof. Markus Otto (University of Ulm, Germany) and by Dr. Roberta Ghidoni (IRCCS Fatebenefratelli of Brescia, Italy).

Silicon oxide chips with a 100 nm thermal oxide layer were bought from Silicon Valley Microelectronics (Santa Clara, CA , USA) and IRIS chips with a 500 nm thermal oxide layer were a kind gift from Prof. Selim M. Unlu from Boston University, MA (USA).

6.1.2 - Amyloid-β solutions in artificial cerebrospinal fluid (ACSF)

The Aβ(1–42) and Aβ(1–39) lyophilised peptides were dissolved in 40 µL of 1M Ammonia, sonicated for one minute, diluted with 20mM sodium phosphate buffer (pH 7.4) to a final concentration of 200 mM (1 mg/mL) and divided into small aliquots, stored at -80° C.

Artificial cerebrospinal fluid (ACSF) was used in microarray assays in order to mimic physiologic conditions. ACSF is an acqueous buffer at pH 7.3 containing 120 mM NaCl, 25 mM $NaHCO_3$, 2.5 mM KCl, 1 mM NaH_2PO_4, 2.5 mM $CaCl_2$, 1 mM $MgCl_2$ ° 6 H_2O and 20 mM glucose. Human serum albumin (HSA) was added before use at a mean concentration of 0.4 mg/mL.

6.1.3 - Coating of microarray slides with poly(DMA-NAS-MAPS)

Poly(DMA-NAS-MAPS)-coated silicon microarrays were fabricated according to the protocol described in ***paragraph 5.1.2***. Briefly, silicon chips were immersed in a poly(DMA-NAS-MAPS) solution (1% w/v in 0.9 M $(NH_4)_2SO_4$) for 30 min. The chips were then rinsed with water, dried under nitrogen and cured for 15 min under vacuum at 80° C [Cretich et al., 2009b].

6.1.4 - Aggregation status of Aβ(1-42) and Aβ(1-39) by circular dichroism spectroscopy

Far-UV circular dichroism (CD) spectra were recorded with a Jasco 600 spectro-polarimeter over the 190–250 nm range at 25° C, using an optical path of 0.1 cm. The peptide concentration used was 50 mM. The spectrum of the blank sample was subtracted from all sample spectra, which were then baseline corrected and smoothed using Spectra Analysis JASCO software. Aβ(1–42) and Aβ(1–39) frozen stocks were thawed and diluted in ACSF (HSA-free) to a final concentration of 50 mM. HSA was

intentionally removed from the ACSF as it would prevent Aβ(1–42) detection [Gagni et al., 2013].

6.1.5 - Microarray experiments with Aβ(1-42)

For the label-free IRIS imaging, antibodies against Aβ(1–42) (mouse monoclonal antibodies from Covance: clones 4G8, 12F4 and Biotin-labeled 6E10; mouse monoclonal antibodies from Nanotools: clones 1E8, 11H3 and 8G7; goat polyclonal antibody from Santa Cruz: clone D-17; mouse monoclonal antibodies from Millipore: clone G2-13 and W0-2; rabbit polyclonal anti-oligomer antibody from Invitrogen: clone A11) were patterned on IRIS chips using a SciFlexArrayer S5 spotter from Scienion (Berlin, Germany). Each protein was spotted in PBS in one array corresponding to one area on the chip. In the experimental conditions used, the volume of the spotted drops was 400 pL. Printed chips were placed in a humid chamber and incubated overnight at room temperature. The chips were then blocked with 50 mM ethanolamine solution in 1 M TRIS/HCl pH 9 for 1 h, washed with water and dried under a stream of nitrogen. IRIS images were acquired and fitted with Zoiray Acquire software. For each protein, signals from 35 replicate spots were averaged [Gagni et al., 2013].

For the fluorescence detection of Aβ(1–42) and Aβ(1–39), capture antibodies against Amyloid-β (clone D-17 from Santa Cruz; clone 11H3 and 8G7 from Nanotools; clone 12F4 and 4G8 from Covance) and Cyanine 3-labeled with streptavidin (reference) were patterned on silicon chips using a SciFlexArrayer S5 spotter from Scienion (Berlin, Germany). The capture antibodies were spotted in PBS in 12 replicates on each chip. The volume of the spotted drops was 400 pL. Printed chips were placed in a humid chamber and incubated overnight at room temperature. The chips were then blocked with 50 mM ethanolamine solution in 1 M TRIS/HCl pH 9 for 1 h, washed with water and dried under a stream of nitrogen. The chips were then incubated with Aβ(1–42) or Aβ(1–39) diluted in ACSF. Chips were then washed with **washing buffer (0.05 M**

Tris/HCl pH 9, 0.25 M NaCl, 0.05% v/v Tween-20) for 10 min with stirring, rinsed with water, and incubated with the biotin-labeled secondary antibody (mouse monoclonal antibody to Amyloid-β amino acids 1–16, clone 6E10, from Covance) at 1 mg/mL in PBS for 1 h. Chips were then washed with PBS and water for 10 min each and then incubated for 1 h with Cy3-streptavidin (Jackson Immunoresearch) at 2 mg/mL in PBS. Chips were washed again with PBS and water for 10 min each. Fluorescence was measured by a ProScanArray scanner (PerkinElmer, Boston, MA), and silicon chips were analysed using 80% or 90 % Photomultiplier (PMT) gain and laser power. The fluorescence intensities of 12 replicate spots were averaged.

For detection limit experiments, 9 chips were incubated for 2 h in either dynamic or static conditions with Amyloid-β at 100, 50, 20, 5, 2, 1, 0.5, 0.1 and 0 ng/mL in ACSF. For overnight experiments, chips were incubated for 18 h under static conditions, washed with washing buffer for 10 min with stirring, rinsed with water, and incubated with the Biotin-labeled secondary antibody (mouse monoclonal antibody clone 6E10, from Covance) at 1 mg/ml in PBS for 1 h. The chips were washed with PBS and water for 10 min each and then incubated for 1 h with Cyanine 3 labeled with streptavidin (Jackson Immunoresearch) at 2 mg/mL in PBS. Chips were washed again with PBS and water (10 min each). Fluorescence intensities of 36 replicate spots were averaged. Calibration curves (dose–response curves) were generated using a three-parameter equation in the OriginLab software. The detection limit (LOD) was defined as the analyte concentration corresponding to a signal of three times the standard deviation (3σ) above the background signal as calculated from the linear range of the calibration curves [Gagni et al., 2013].

Moreover, the capture antibodies clone D-17 from Santa Cruz and clone 12F4 from Covance and Cy3 labeled with streptavidin (as reference) were patterned on silicon chips according to the same spotting protocol previously described. Printed chips were placed in a humid chamber and incubated overnight at room temperature and then

blocked with 50 mM ethanolamine solution in 1 M TRIS/HCl pH 9 for 1 h, washed with water and dried under a stream of nitrogen. The chips were incubated with real human samples of CSF, kindly provided by Prof. Marcus Otto (University of Ulm, Germany), in both static and dynamic conditions, each for 2 h or overnight. Fluorescence detection was performed using the Cov-6E10 biotin-labeled antibody coupled with Cy3-labeled streptavidin, and then resulting signals were measured by a ProScanArray scanner (PerkinElmer, Boston, MA), and silicon chips were analysed using 80% or 90 % Photomultiplier (PMT) gain and laser power. The signal-to-noise ratios of 9 replicate spots were eavaluated.

6.1.6 - Detection of Aβ(1-40) in ACSF

For the fluorescence detection of Aβ(1–40), capture antibodies against both Amyloid-β peptides (1-40) and (1-42) (as control of specific binding) together with SA-Cy3 (as reference) were patterned on poly(DMA-NAS-MAPS)-coated silicon chips using a SciFlexArrayer S5 spotter from Scienion (Berlin, Germany). The capture antibodies were spotted in PBS in 18 replicates on each chip. The volume of the spotted drops was 400 pL. Printed chips were placed in a humid chamber and incubated overnight at room temperature. The chips were then blocked with 50 mM ethanolamine solution in 1 M TRIS/HCl pH 9 for 1 h, washed with water and dried under a stream of nitrogen. The chips were then incubated for 2 hours either in static or dynamic conditions, with 50 ng/mL Aβ(1–40) or Aβ(1–42) diluted in ACSF otherwise with blank samples. Chips were then washed with washing buffer for 10 min with stirring, rinsed with water, and incubated with the biotin-labeled secondary antibody (mouse monoclonal antibody to Amyloid-β amino acids 1–16, clone 6E10, from Covance) at 1 mg/mL in PBS for 1 h. Chips were then washed with PBS and water for 10 min each and then incubated for 1 h with Cy3-streptavidin at 2 mg/mL in PBS. Chips were washed again with PBS and water for 10 min each. Fluorescence was measured by a ProScanArray scanner

(PerkinElmer, Boston, MA), and silicon chips were analysed using 90% Photomultiplier (PMT) gain and laser power. The fluorescence intensities of 18 replicate spots were averaged.

According to this protocol, several concentration of Aβ(1-40) were tested with both static and dynamic conditions in order to define calibration curves from which to extrapolate limits of detection, according to the same statistics applied for Aβ(1-42) calculations.

6.1.7 - Contemporary detection of Aβ(1-40) and Aβ(1-42) in human CSF

In order to contemporary detect both peptides Aβ(1–40) and Aβ(1–42), two capture antibodies against their C-termini were patterned on poly(DMA-NAS-MAPS)-coated silicon chips. Thus, antibodies from Covance, repsectively Cov11A50-B10 and Cov-12F4, and Cy3-labeled streptavidin (as reference) were spotted on four chips according to the same printing protocol described above. Chips were then placed in a humid chamber and incubated overnight at room temperature. Subsequently they were blocked with 50 mM ethanolamine solution in 1 M TRIS/HCl pH 9 for 1 h, washed with water and dried under a stream of nitrogen. Each chip was then incubated for 2 hours in static conditions with human CSF samples, kindly provided by Dr. Ghidoni, from IRCSS Fatebenefratelli (Brescia, Italy). Chips were then washed with washing buffer for 10 min with stirring, rinsed with water, and incubated with the biotin-labeled secondary antibody (mouse monoclonal antibody to Amyloid-β amino acids 1–16, clone 6E10, from Covance) at 1 mg/mL in PBS for 1 h. Chips were washed with PBS and water for 10 min each and then incubated for 1 h with Cy3-streptavidin at 2 mg/mL in PBS. Chips were washed again with PBS and water for 10 min each. Fluorescence was measured by a ProScanArray scanner (PerkinElmer, Boston, MA), and silicon chips were analysed using 90% Photomultiplier (PMT) gain and laser power.

6.2 - RESULTS AND DISCUSSION

6.2.1 - Control of Aβ(1-42) and Aβ(1-39) aggregation status

As mentioned in the introductive session of the present chapter, several isoforms of the Amyloid-β peptide exist, which mainly differ at the carboxy terminus. Aβ(1-42) is a difficult peptide to work with, in the sense that its aggregation properties are highly sensitive to sequence, purity and preparation conditions.*In vitro*, the longer form Aβ(1–42) aggregates faster than the short forms Aβ(1–40) and Aβ(1–39) [Seilheimer et al. 1997]. Indeed, this high propensity to form oligomers decreases Aβ(1–42) detection efficiency, making accurate evaluation of the detection limit very difficult. The actual monomeric peptide concentrations in the commercial samples are largely unknown [Ammar et al. 2013]. In this work, the aggregation status of Aβ(1-42) standards used was assessed by circular dichroism (CD) spectroscopy. In particular, solubility, storage conditions and stability of the aggregates during the assay of the longer form Aβ(1–42) were compared with that of the shorter form Aβ(1–39). The CD spectra suggest that Aβ(1–42) in ACSF (**Figure 6.3**) maintains a stable structure for at least 2 h, which is the time used for microarray incubations in most experiments performed in this study. After 24 hours incubations in ACSF, a cloudy precipitate, most likely composed of insoluble oligomers, was observed. This is consistent with a random coil structure, as determined by CD. In contrast, the shorter form Aβ(1–39) did not show any conformational change (**Figure 6.4**), corroborating the greater stability of this peptide compared with Aβ(1–42) [Gagni et al., 2013].

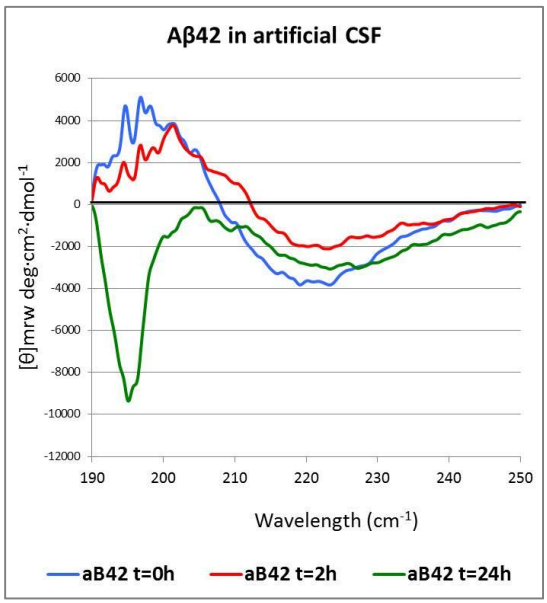

Figure 6.3 - CD specta of Aβ(1-42) in ACSF at different times. A fresh Aβ(1-42) sample shows a random coil structure (t=0h) which rapidly evolves into a β-sheet conformation within 2 h.

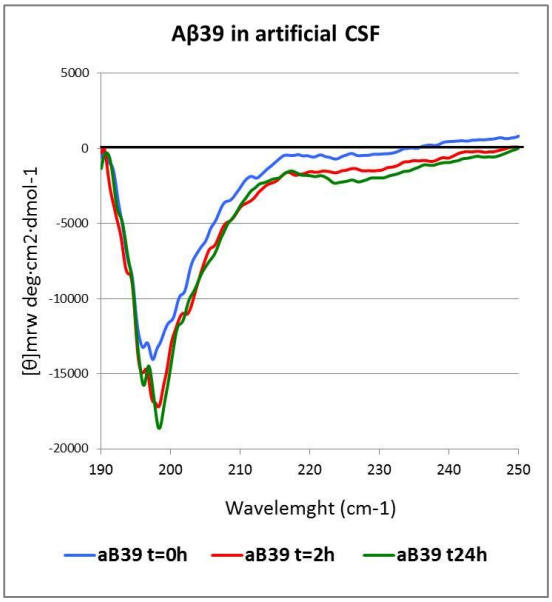

Figure 6.4 - CD spectra of Aβ(1-39) in ACSF at different times. The shorter peptide Aβ(1-39) does not show any aggregation propensity: the random coil structure of the fresh sample (t=0h) is maintained over 24 h, thus suggesting the greater stability of this peptide.

6.2.2 - Matched pair antibody selection for Aβ(1-42) in ACSF

The binding yield and spot morphology chips of several commercial antibodies against different epitopes on the Aβ(1-42) peptide immobilized on poly(DMA-NAS-MAPS)-coated silicon were evaluated by label-free IRIS. **Table 6.3T** reports for each antibody evaluated in this study: epitope specificity, concentration of the spotted solution and amount of antibody bound to the surface (ng/mm^2). A typical image of the spot morphology is also shown.

Table 6.3T - Deteails for antibodies used in this study. The epitope specificity, spotted solution concentration and image showing the typical spot morphology and the antibody binding yeld on the surface (ng/mm^2) when analysed by LowMag-IRIS are presented.

Antibody	Epitope	Concentration	IRIS image	Binding yield (ng/mm^2)
Santa Cruz D17 (Goat pAb)	C-term	0.2 mg/mL (Dyalized vs PBS)		2.895±0.22
Millipore W0-2 (Mouse mAb)	AA 4-10	1 mg/mL (Dyalized vs PBS)		0.562±0.12
Millipore G2-13 (Mouse mAb)	C-term	1 mg/mL (Dyalized vs PBS)		0.681±0.32
Invitrogen A11 (Rabbit pAb)	Soluble oligomers	1 mg/mL		3.644±0.25
Nanotools 1E8 (Mouse mAb)	N-term	0.1 mg/mL		1.930±0.24
Nanotools 11H3 (Mouse mAb)	N-term	0.2 mg/mL		1.043±0.12
Nanotools 8G7 (Mouse mAb)	C-term	0.2 mg/mL		0.776±0.09
Covance 4G8 (Mouse mAb)	AA 17-24	1 mg/mL		5.062±0.42
Covance 12F4 (Mouse mAb)	C-term	0.5 mg/mL		1.515±0.16
Covance 6E10 (Mouse mAb)	AA 1-16	1 mg/mL		2.81±0.

Among the ten antibodies analysed, six were selected for subsequent functional tests: SC-D17, NT-11H3, NT-8G7, Cov-4G8, Cov-12F4 and Cov-6E10. Both antibodies from Millipore, clones W0-2 and G2-13, were kept out due to their low binding on the support (0.56 and 0.68 ng/mm^2, respectively). Similarly, the NT1E8 antibody was also left out for its poor spot morphology while A11 for being specific for soluble oligomers.

The antibodies SC-D17, NT-11H3, NT-8G7, Cov-4G8 and Cov12F4 were tested further as Aβ(1-42) and Aβ(1-39) capturing antibodies, using the biotin-labeled Cov-6E10 for the detection, followed by incubation with Cy3 labeled streptavidin (SA-Cy3). The assay scheme is outlined in **Figure 6.5**. This experiment aimed to select the best capture antibody in terms of signal intensity and specificity for the Aβ(1-42) peptide.

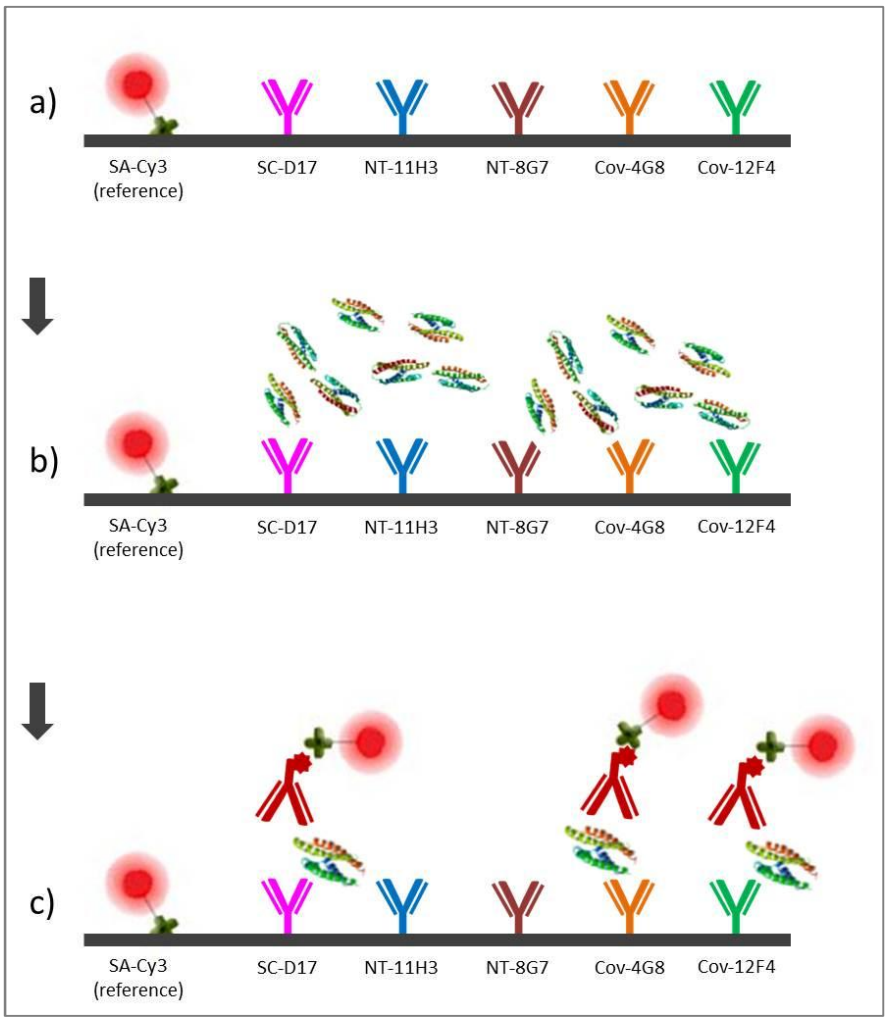

Figure 6.5 – Assay scheme for the selection of matched antibody pair for Aβ(1-42) in ACSF. The antibodies SC-D17 (pink), NT-11H3 (blu), NT-8G7 (brown), Cov-4G8 (orange) and Cov12F4 (green) were arrayed on the same silicon chip (step ***a***) and tested further as Aβ(1-42) and Aβ(1-39) capturing antibodies (step ***b***). The biotin-labeled Cov-6E10 (red) uas used for the detection, followed by incubation with Cy3 labeled streptavidin (SA-Cy3) (step **c**).

Fluorescence images from the analysis of 100 ng/mL of Aβ(1-42), 100 ng/mL Aβ(1-39) and a blank sample, with a similar fluorescence value at 80% laser and PMT gain, are shown in **Figure 6.6**. The antibodies SC-D17 and Cov-12F4 resulted in higher signal intensity and specificity for Aβ(1-42) as indicated by the absence of any fluorescence

for Aβ(1-39). On the contrary, antibodies NT-11H3 and NT-8G7 did not provide any signal either for Aβ(1-42) and Aβ(1-39). Capture antibody Cov-4G8 gave intense signals when incubating with both Aβ(1-42) and Aβ(1-39), thus lacking in specificity for the interested peptide.

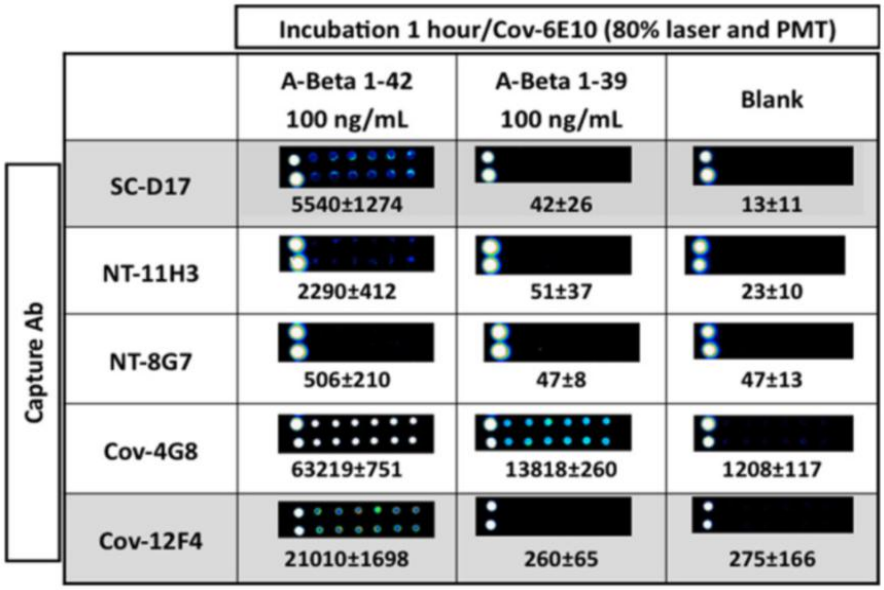

Figure 6.6 - Fluorescence images and intensities values (mean and SD using 80% laser power and PMTgain) for the detection of Aβ(1-42), Aβ(1-39) and a blank using SC-D17, NT-11H3, NT-8G7, Cov-4G8 and Cov-12F4 antibodies as capture reagents and biotinilated Cov-6E10 as the detection antibody. In addition to optimal specificity for Aβ(1–42), the antibody matched pair SC-D17/Cov-6E10 and Cov12F4/Cov-6E10 resulted in absence of fluorescence for the blank samples and were therefore chosen as the optimal matched reagents for Aβ(1-42) detection in this study.

Although sandwich immunoassay is the gold standard for protein profiling, antibody cross-reactivity is often observed in this method. This effect produces background noise, which affects sensitivity and causes false positive results [Ellington et al. 2010]. In addition to the intensity of fluorescence, when detecting the target analyte, it is of high importance to check for signal absence from the blank sample at high laser power and PMT gain. In fact, the sensitivity of microarray-based immunoassays depends on the elimination or at least the minimisation of cross-reactivity between the capture and detection antibodies. In addition to being most specific for Aβ(1–42), these two matched antibody pairs (SC-D17/Cov-6E10 and Cov-12F4/Cov-6E10) resulted in the absence of fluorescence for the blank samples and, therefore, were chosen as the optimal matched reagents for Aβ(1-42) detection in this study [Gagni et al., 2013].

6.2.3 - Limits of detection for Aβ(1-42) in ACSF

The antibodies SC-D17 and Cov-12F4 were immobilised on poly(DMA-NAS-MAPS) coated silicon slides as previously described. The chips were incubated with several concentrations of Aβ(1-42) dissolved in artificial cerebrospinal fluid (ACSF), in order to mimic the composition of endogenous CSF, in static (using a cover slip) and dynamic (in a petri dish on a horizontal shaker at 50 rpm) conditions, followed by incubation with Cov-6E10 biotin-labeled detection antibody and Cy3-labeled streptavidin (SA-Cy3). Fuorescence intensities obtained upon incubation with Aβ(1-42) in the ng/mL range provided data that were fitted to the three-parameter logistic equation in order to determin the calibration curves reported in **Figure 6.7**. Curves were obtained with both capture antibodies, respectively Cov-12F4 on the left and SC-D17 on the right column, for the three different incubation protocols: 2 h dynamic (first line), 2 h static (second line) and overnight static conditions (third line).

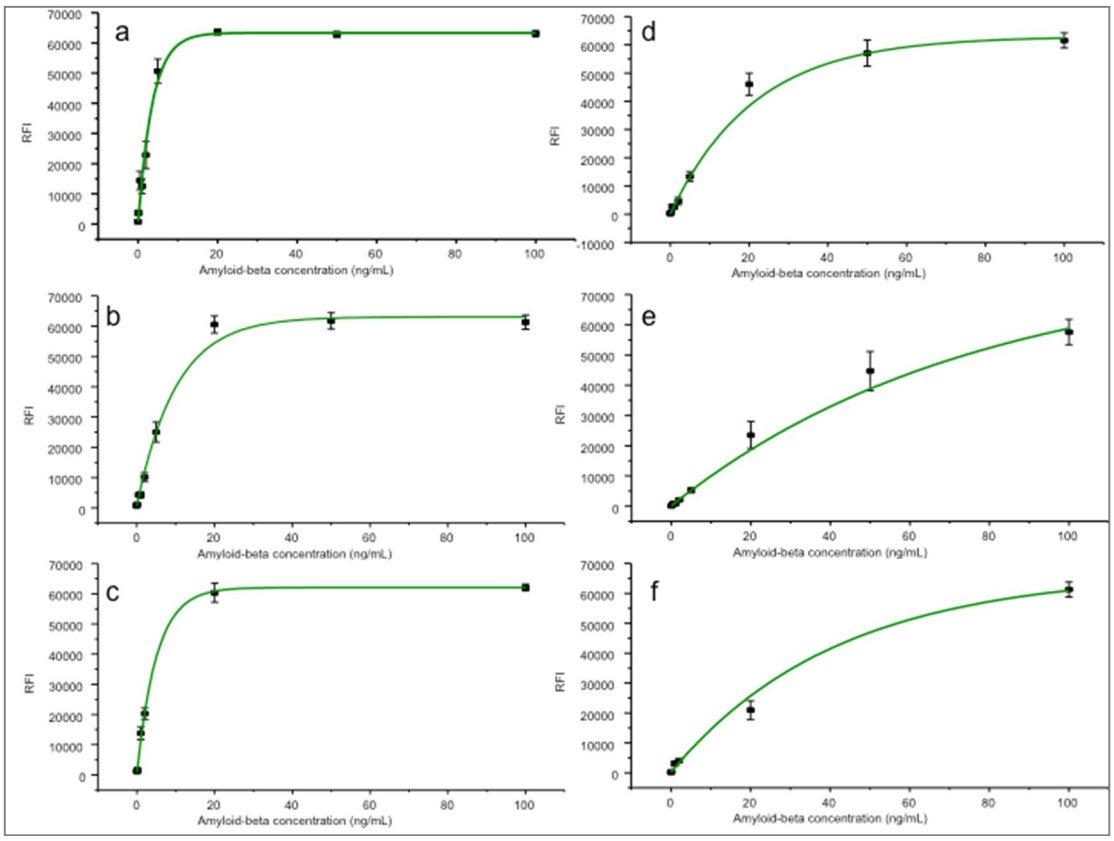

Figure 6.7 - Calibration curves obtained for all tested conditions. The left panel shows the calibration obtained curves using COV-12F4 as the capture antibody for Aβ(1-42) detection when incubation was performed under dynamic conditions for 2 h (*a*), static conditions for 2 h (*b*) and static conditions overnight (*c*). The right panel shows calibration curves obtained using SC-D17 as the capture antibody for Aβ(1-42) detection when incubation was performed under dynamic conditions for 2 h (*d*), static conditions for 2 h (*e*) and static conditions overnight (*f*).

Figure 6.8 shows the fitted dose–response curves obtained using a 2 h dynamic incubation with matched antibody pairs Cov-12F4/Cov-6E10 at 90% laser power and PMT gain. Panel *b* focuses on the linear range of the curve, which yielded a limit of detection of 73.07 pg/mL.

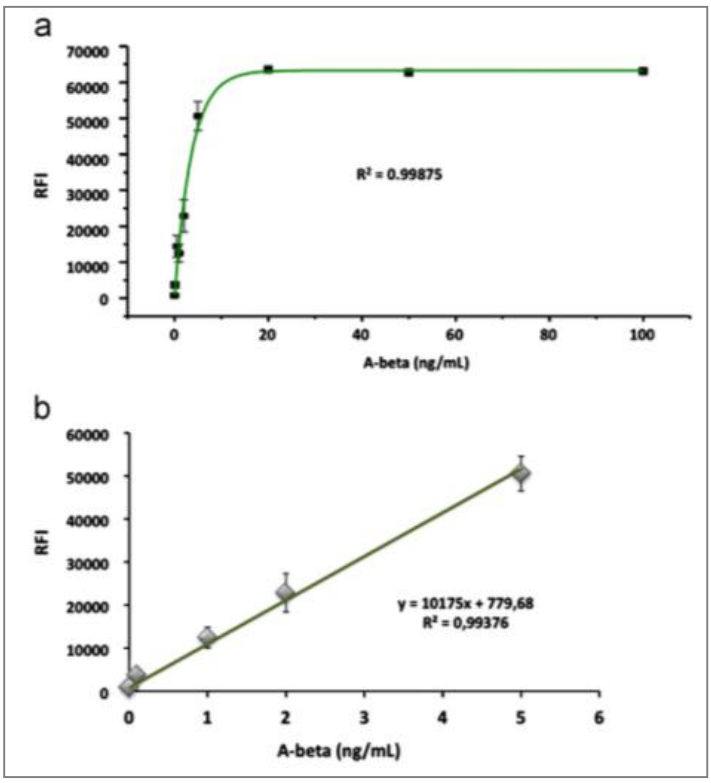

Figure 6.8- *a*) Calibration curvefor Aβ(1-42) detection in ACSF with Cov-12F4 as the capture antibody and Cov-6E10 as the detection antibody and 90% laser power and PMT gain. Aβ(1-42) was incubated under dynamic conditions for 2h. *b*) Close-up of the liner range of the curve, which yielded a LOD of 73.07 pg/mL.

Limits of detection (LODs) were extrapolated from the average fluorescent value of the blank samples plus three standard deviations (3s) using the linear range of the calibration curves [Wild, 1998]. Among the multiple factors that affect detection sensitivity in fluorescent microarrays, optimal assay design to compensate for kinetic limitations [Kusnezow et al., 2006] is of high importance.

Table 6.4T shows that the LODs obtained using either 2 h of dynamic and static incubation or overnight static incubation with SC-D17 as the capture antibody are all in

the ng/mL range. With Cov-12F4 as the capture antibody, the LODs were in the pg/mL range (**Table 6.5T**) [Gagni et al., 2013].

Table 6.4T – LODs for Aβ42 using SC-D17/Cov-6E10 matched antibody pair.

Incubation conditions:	**Static, 2h**	**Dynamic, 2h**	**Static, overnight**
Aβ(1-42) LOD (**ng/mL**)	6.76	1.13	7.76

Table 6.5T - LODs for Aβ42 using Cov-12F4/Cov-6E10 matched antibody pair

Incubation conditions:	**Static, 2h**	**Dynamic, 2h**	**Static, overnight**
Aβ(1-42) LOD (**pg/mL**)	148.36	73.07	94.15

As expected, for both antibodies, incubation under dynamic conditions was more sensitive compared with the static one. However, overnight incubation did not provide a significant improvement in the LODs, probably due to the ongoing aggregation of Aβ(1-42) in solution which was previously observed in CD analysis. Although the mouse monoclonal antibody Cov-12F4 had a lower binding yield on poly(DMA-NAS-MAPS)-coated silicon compared with the goat polyclonal antibody SC-D17 (resectively, 1.52 vs. 2.89 ng/mm^2 as reported in **Table 6.3T**), it allowed detection limits approximately one order of magnitude lower in all tested conditions, most likely due to its higher affinity towards Aβ(1-42). **Figure 6.9** shows the fluorescence results from arrays after 2 h of dynamic incubation with 0, 0.1, 0.5, 1, 2, 5, 20, 50 and 100 ng/mL of Aβ(1-42) in ACSF using the two tested capture antibodies, SC-D17 and Cov-12F4 [Gagni et al., 2013].

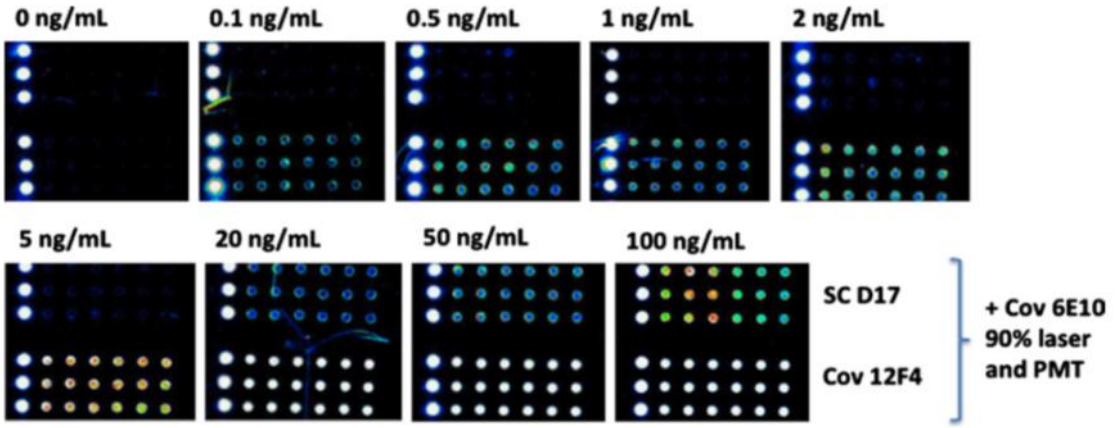

Figure 6.9 - Fluorescence images (at 90% laser power and PMT gain) of Aβ(1-42) detection using SC-D17 (upper array) or Cov-12F4 (lower array) as the capture antibody and Cov-6E10 as the detection antibody. Samples with concentrations ranging from 0 to 100 ng/mL were analysed.

Cov-12F4 gave a clear fluorescence response even at the lowest concentration tested, whereas SC-D17 yielded detectable signals only for concentrations higher than 5 ng/mL. These data indicate that Cov-12F4 allows to achieve a detection limit one order of magnitude lower [Gagni et al., 2013].

In summary, the best conditions developed for Aβ(1-42) detection consisted of the use of Cov-12F4/Cov-6E10 matched antibody pair and 2 h of dynamic incubation and resulted in the unprecedented microarray LOD of Aβ(1-42) in ACSF of 73.07 pg/mL [Gagni et al., 2013]. This value is compatible with the use of the proposed assay in diagnostics, where controls show a concentration of Aβ(1-42) in CSF of 794 ± 20 pg/mL and AD patients show a concentration lower than 500 pg/mL [Humpel, 2011].

6.2.4 - Aβ(1-42) detection in human CSF

Reagents and protocols developed in this study were tested with real human samples of CSF (kindly provided by Prof. Markus Otto, University of Ulm).

Figure 6.10 shows the typical results for the detection of Aβ(1-42) in CSF using Cov-12F4/Cov-6E10 matched antibody pair and four different incubation conditions, including both static incubation for 2 h or overnight and dynamic incubation for 2 h or overnight. In contrast to the use of standard Aβ(1-42) in ACSF, either in static or dynamic conditions an overnight incubation resulted in an increased signal to noise ratio. This event is most likely because in real human samples, the aggregation phenomenon observed in artificial CSF does not occur or rarely occurs, and a longer incubation time allows the analyte to reach the equilibrium. However, a further validation of the proposed assay using clinical samples is currently underway in our laboratory [Gagni et al., 2013].

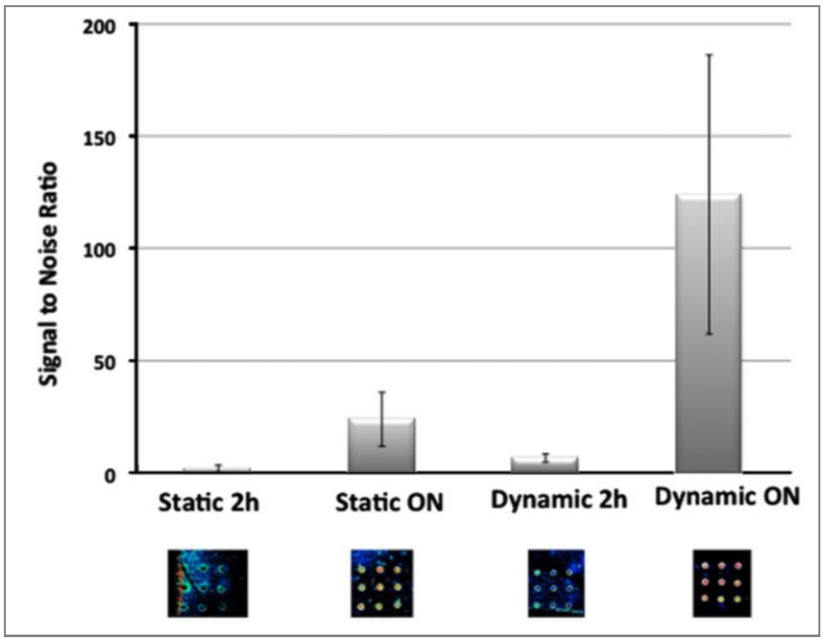

Figure 6.10 - Representative image of Aβ42 detection in a human CSF sample using Cov12F4 as capture antibody and Cov-6E10 as detection antibody. For both static and dynamic incubation, a longer incubation time yielded higher signal-to-noise responses.

6.2.5 - Detection of Aβ(1-40) in ACSF

Three antibodies were tested as capture probes against the carboxy terminus of the Amyloid-β (1-40) peptide, while the selected Cov-6E10 biotin-labeled antibody was used for detection as it recognizes the ammino terminus of the same target.

Static incubations were performed with 50 ng/mL of Aβ(1-40) in ACSF in comparison with the same concentration of Aβ(1-42) and the blank sample. As reported in **Figure 6.11**, the capture probes for the Aβ(1-42) isoform (SC-D17 and Cov-12F4 antibodies) do not recognize the Aβ(1-40), while a high interaction is provided by the Millipore G2-10 and the Cov11A50-B10 antibodies, which were selected for further investigation concerning their specificity. The best antibody pair is the Millipore G2-10/Cov6E10 as the blank sample does not display any fluorescence. The Cov 29-6 slightly interacts with the target and thus it was not used further.

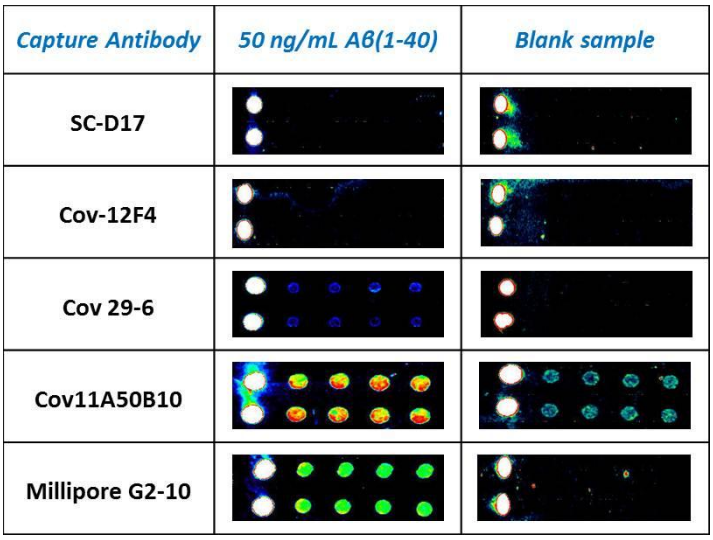

Figure 6.11 – Fluorescence signals (at 90% laser power and PMT gain) from arrays incubated with 50 ng/mL Aβ(1-40) in ACSF (left column) or blank sample (right column) and detected with biotin-labeled Cov-6E10 antibody, coupled with SA-Cy3. Each line corresponds to a different capture antibody, spotted on the surface: two antibodies specific for Aβ(1-42) as control of specificity (SC-D17 and Cov-12F4) and three antibodies for Aβ(1-40) to be tested (Cov 29-6, Cov11A50-B10 and Millipore G2-10).

In order to validate the specificity of Aβ(1-40) detection, the same antibody pairs (Millipore G2-10/Cov-6E10 and Cov11A50-B10/Cov-6E10) were incubated in dynamic conditions with 50 ng/mL of Aβ(1-42) peptide. As shown in **Figure 6.12**, no signals were detectable on the interested spot.

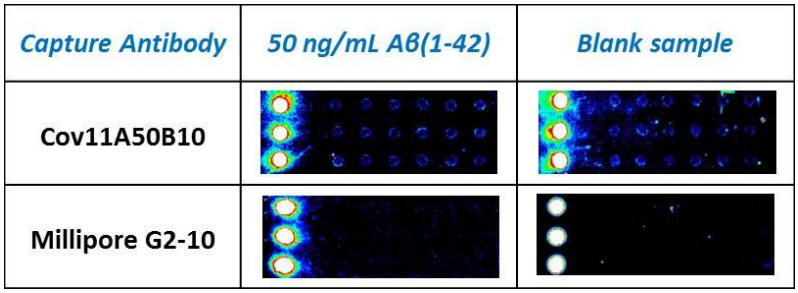

Figure 6.12 – Fluorescence signals (at 90% laser power and PMT gain) from arrays incubated with 50 ng/mL Aβ(1-42) in ACSF (left column) or blank sample (right column) and detected with biotin-labeled Cov-6E10 antibody, coupled with SA-Cy3. Each line corresponds to a different capture antibody against Aβ(1-40) carboxy terminus: Cov11A50-B10 and Millipore G2-10.

By incubating with several concentration of Aβ(1-40) peptide, limits of detection (LODs) of this peptide were extrapolated when using both matched antibody pairs: Millipore G2-10/Cov-6E10 and Cov11A50-B10/Cov-6E10. The incubation protocols were the same performed for the Aβ(1-42) peptide, using both static and dynamic incubations.

As reported in **Table 6.6T**, the Cov11A50-B10 provided a LOD of 2.05 ng/mL in static conditions, but no gain in detection limits was achieved when incubationg in dynamic conditions as a value of 2.14 ng/mL was obtained. On the contrary, the capture

antibody Millipore G2-10 provided a LOD of 0.35 ng/mL in dynamic incubations, much lower than the 2.15 ng/mL value obtained in static ones.

Table 6.6T – LODs (ng/mL) for Aβ(1-40) using two selected matched antibody pairs.

Capture antibody	**Static, 2h**	**Dynamic, 2h**
Cov11A50-B10	2.05 ng/mL	2.14 ng/mL
Millipore G2-10	2.15 ng/mL	0.35 ng/mL

The possibility to capture the Amyloid peptideS through their carboxy terminus and to detect them using a common antibody against the ammino terminus enabled the development of a microarray-based immunoassay able to detect at the same time, on a single device, both Aβ(1-40) and Aβ(1-42) present in a given sample.The obtained results are compatible with the use of the proposed assay in diagnostics, where CSF controls show a concentration of about 800 pg/mL for Aβ(1-42) and 7 ng/mL for Aβ(1-40) [Humpel et al., 2011].

6.2.6 - Contemporary detection of Aβ(1-40) and Aβ(1-42) in human CSF

The fluorescence-based microarray immunoassay developed in this thesiswas applied to the simultanoeus detection of both Amyloid-β peptides (1-40) and (1-42) on a single device in human CSF samples. To reach this goal, two subarrays were patterned on each chip, corresponding to the capture antibodies selected for each target analyte: Cov11A50-B10 and Cov-12F4, respectively. Four CSF samples were kindly provided by Dr. Roberta Ghidoni from IRCSS Fatebenefratelli (Brescia, Italy). Due to the low amount of human CSF available, it was not possible to perform dynamic incubations, which

require more than 1 mL of sample. Thus, as outlined in **Figure 6.13**, 20 uL of each solution was assayed using static conditions. The two peptides were captured on each subarray with antibodies specific for their C-termini, while the detection by Cov-6E10 biotin-labeled antibody occured through the recognition of the common N-terminus of both analytes.

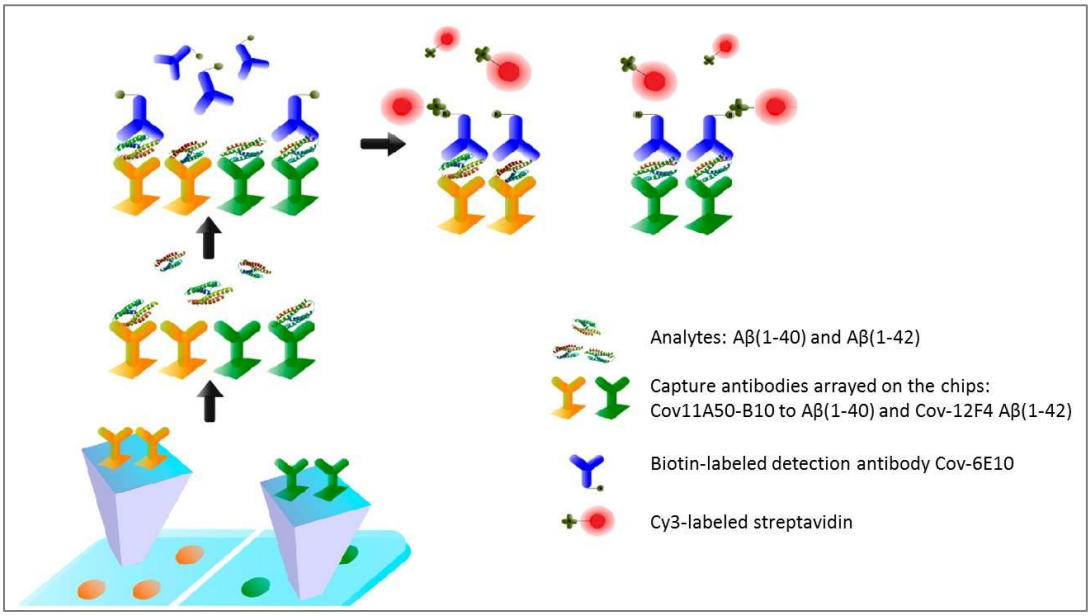

Figure 6.13 – Assay scheme for the contemporary detection of both Aβ(1-40) and Aβ(1-42) in human CSF samples on a single device. Two capture antibodies are arrayed on the same chip: Cov11A50-B10 was selected as being specific for Aβ(1-40), while Cov-14F4 for Aβ(1-42). 20uL of CSF samples were incubated for 2h in static conditions and then detected by the common biotin-labeled Cov6E10 antibody, followed by incubation with Cy3-labeled streptavidin.

The fluorescence signals shown in **Figure 6.14**, demonstrate the capability of this microarray to detect at the same time both analytes in CSF in a specific manner, although possible physiological variations of peptides in real samples may occur.

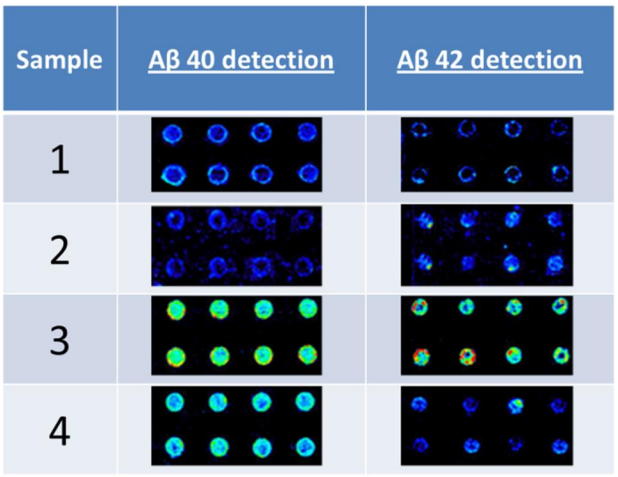

Figure 6.14 – Fluorescence detection (at 90% laser power and PMT gain) from arrays incubated for 2 hours in static conditions with four human CSF samples. Per each sample, both Aβ(1-40) (left column) and Aβ(1-42) (right column) were detectable.

6.3 - CONCLUSIONS

Alzheimer Disease (AD) is a Neurodegenerative disorder, characterized by abnormal extracellular accumulation of β-Amyloid peptide in the brains of patients. The pathological isoform Aβ(1-42) agregates order of magnitudesfaster than Aβ(1-40) or Aβ(1-39) [Silheimer et al., 1997]. However the analysis of the sole Aβ(1-42) concencentration is not specific enough for the discrimination of AD from other kinds

of Dementia in subjects with constitutively high or low levels of total Aβ peptides. Thus, it may be better to consider the ratio between Aβ(1-42)/Aβ(1-40) for higher reliability [Wiltfang et al., 2007]. Therefore, a method to detect simoultanously both analytes in cerebrospinal fluids is needed. Because of their multiplexing capability, low sample volume consumption and sample-to-result time, microarrays are ideal tools for the identification of individuals with preclinical AD who are still cognitively healthy in population-wide screenings.

In this work, a highly sensitive fluorescence immunoassay that utilizes silicon/silicon oxide substrates for the detection of the AD biomarkers Aβ(1-40) and Aβ(1-42) in artificial cerebrospinal fluid (ACSF) has been developed [Gagni et al., 2013].

In preliminary tests, the commercial peptides Aβ(1-42) and Aβ(1-39) aggregation status were assessed by Circular Dicroism, demonstrating the stability of Aβ(1-42) structure for at least 2 hours, while Aβ(1-39) does not show any conformational changes, even in 24 hours. Thereafter, an optimal antibody matched pair for Aβ(1-42) detection was selected with a label and label-free microarray platform, using the Interfermometric Reflectance Imaging Sensor (IRIS), to determine binding yield on the silicon surface and the spot morphology. The selected antibodies were tested on poly(DMA–NAS–MAPS)-coated silicon chips for Cy3-label microarray analysis [Cretich et al., 2009b]. Two antibody-matched pairs resulted specific and sensitive for Aβ(1-42). To selectively detect Aβ(1-40), different capture antibodies were selected based on their specificity for the C-terminus of the peptide. In this way, both Aβ(1-42) and Aβ(1-40) were simultaneously detected on a multiplexed fluorescence microarray using the same biotin-labeled antibody against the common N-terminus sequence of the peptides and the respective LODs were extrapolated. The best condition developed for Aβ(1-42) detection in ACSF requires 2 hours of dynamic incubation, resulting in a LOD of 73 pg/mL [Gagni et al., 2013]. In the same conditions the LOD for Aβ(1-40) was 350 pg/mL. The obtained results are compatible for the use of the proposed assay in

diagnostics, where CSF controls show a concentration of about 800 pg/mL for Aβ42 and 7 ng/mL for Aβ40 [Humpel, 2011]. As a proof of concept, thefluorescence-based tool was applied to simultaneouslydetect on single chipthese two biomarkers in real human CSF samples [Gagni et al., 2013].

Chapter 7 - Direct and Indirect Detection of intact Exosomes on dual Fluorescence-based and Label-free Microarray Platform

Dual fluorescence and label-free microarray platform has been further extended to the detection of extracellular vesicles, such as exosomes, through surface antigen-antibodies recognition.

Exosomes and microvesicles (MVs) belong to the bigger family of extracellular vesicles (EVs) as they both are submicron-sized spheric containers made of phospholipidic bilayer membrane, released by any kind of cells and characterized by an aqueous cargo-containing core. Although structurally similar, they differ in cellular origin, lipid composition, and size [Kastelowitz et al., 2014]. In general, MVs are big particles (100-1000 nm of diameter), that bear by outward budding and fission of the plasma membrane [Al-Nedawi et al., 2009]. Their surface composition is similar to that of the cell membrane but lacks the asymmetric distribution of lipids normally seen across the two leaflets of the plasma membrane [Scott et al., 1984; Hugel, 2005]. On the contrary, exosomes are smaller vesicles, defined on the base of size (40–100 nm) and density (1.12-1.19 g/ml). They originate intracellularly by inward budding of the limiting membrane of endocytic compartments, leading to vesicle-containing endosomes, called multivesicular bodies (MVBs). MVBs eventually fuse with the plasma membrane, thus releasing their internal vesicles (i.e., exosomes) into the extracellular medium [Théry et al., 2006] through an exocytosis event. Exosomes appear to have a similar lipid composition between the two membrane leaflets, consistent with the presence of a phospholipid-scramblase [Record et al., 2011].

The physiological function of exosomes still remains a matter of debate. Two secretion mechanism routes have been described: secretion of exosomes can be constitutive or inducible, depending on the cell type and on the activation state of the cell [Théry et al., 2009]. In the first way, exosomes secretion is a function *per se* as vesicles are routed through an anterograde pathway from the Trans Golgi Network (TGN) by an ubiquitary constitutive pathway that does not require any specific stimulus or any transit via MVBs, and thus they are secreted into the extracellular medium [Record et al., 2011]. For example, exosome secretion by reticulocytes allows the elimination of proteins such as transferrin receptor or integrins, which are useless in differentiated red blood cells [Pan et al., 1985; Vidal et al., 1997]. Differently, basing on a regulated mechanism, the second secretion route of exosome release takes advantage from MVBs pathway. Depending on the cell type and its activation state many cellular stimuli (e.g., calcium-dependent release [Savina et al., 2003], cellular depolarization induced by K^+ [Record et al., 2011], receptor-mediated release [Qu et al., 2009]) can induce MVBs fusion with plasma membrane. However, irrespective to the stimulus, this kind of exosome production results involved in intercellular communication, allowing exchange of proteins and lipids between the exosome-producing cell and the target one [Wolfers et al., 2001; Andre et al., 2002; Théry et al., 2002].

In addition to a number of proteins being involved in intercellular signalling, exosomes have been found to exhibit a specific content of proteins, lipids and transported micro as well as messenger RNAs [Valadi et al., 2007]. As they contain specific signatures from producing-cells, analyses of exosomes may be used for diagnostic purposes, e.g. for melanoma [Logozzi et al., 2009] or ovarian cancer diagnosis [Taylor et al., 2008]. Universal markers commonly used to identify exosomes include transmembrane proteins (like tetraspanins CD9, CD63, CD81, and CD82), major histocompatibility complexes (MHC, class-I and -II) and cytosolic proteins (like heat shock proteins, Hsp70 and Hsp90) [Heijnen et al., 1999; Caby et al., 2005; Lee et al., 2011]. Exosomes protein

composition analyses have revealed both an ubiquitary and a cell type-specific protein composition.

As reported in **Figure 7.1**, Record and colleagues listed many types of molecules tipically found on exosomes [Record et al., 2011]:

- antigen-presentation (MHC-I, MHC-II) and co-presentation molecules (CD86),
- cell adhesion (Integrins, MFGE8, etc.),
- cell structure and motility (actins, myosin, tubulin, etc.),
- Heat shock proteins and chaperones (Hsp70, Hsp90, Hsc70),
- metabolic enzymes (β-enolase, fatty acid synthase, glyceraldehyde-3-phosphate dehydrogenase, peroxidases, pyruvate kinase),
- proteins referring to exosomes or MVBs biogenesis (e.g. Tsg101, lyso-bis-phosphatidic acid, Alix),
- lysosomal markers (LAMP-1/2),
- signalling proteins (kinases 143-3, GTPase Hras, RhoA, RAP1B, Guanine nucleotide-binding protein subunits, Gproteins, etc.),
- tetraspanins (CD9, CD63, CD81, CD82),
- proteins involved in transcription and protein synthesis (histones, ribosomal proteins, ubiquitin, etc.),
- proteins involved in trafficking and membrane fusion (Annexins, Rab protein family, ARF).

However, the functional significance of certain proteins is not completely understood. It is worth noting that markers commonly used to characterize a composition of exosomes may have varying distribution between cell types. For instance, the Transferring Receptor (TfR) is absent in exosomes derived from B-cells whereas it is present in erythrocyte derived exosomes [Record et al., 2011].

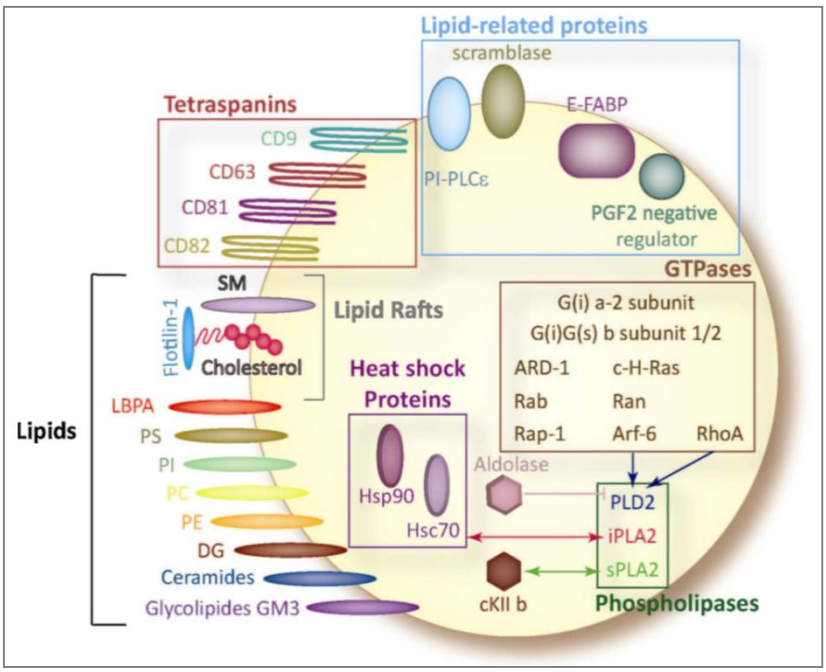

Figure 7.1 - Main typical proteins and lipids present in exosomes. About a hundred fold enrichment of tetraspanins (CD9, CD63, CD81, CD82) in exosomes comparatively to parent cells is a hallmark of exosomes. Heat shock proteins (Hsp90, Hsp70, Hsc70) also are enriched. Activation of phospholipases by GTPases (Rab, Rap, ran, RhoA, Arf) and their regulation by aldolase, casein kinase II and Hsp/Hsc70 has been reported in literature. The major phospholipids are present in exosomes but in distinct proportions as compared to parent cells. The specific MVB lyso-lipid LBPA (BMP) is also found in exosomes [Record et al., 2011].

In this third study, exosomes have been investigated for their role as biomarkers or carriers of biomarkers for Neurodegenerative Disorders (NDs). In fact, many cells of the nervous system have been shown to release extra-cellular vesicles (EVs), implicating their active roles in growth, function, and pathologies of this system. Exosomes and microvesicles are capable of transferring DNAs, mRNAs, microRNAs, non-coding RNAs, proteins and lipids among cells without direct cell-to-cell contact [Fauré et al., 2006]. Moreover, they have recently been proposed to participate in myelin formation as well as in neurite outgrowth and neuronal survival [Wang et al.,

2011]. For these reasons, exosomes from cerebrospinal fluid (CSF) can be considered as carriers of biomarkers for neurological disorders [Lachenal et al., 2011]. Exosomes are reported to be involved in pathological pathways, such as tumor pathogenesis or transmission of viruses, prions and Amyloid-β peptide precipitation in AD [Wolfers et al., 2001; Rajendran et al., 2006].

In particular, the finding that proteins and peptides associated with AD (i.e. APP - Amyloid Precursor Protein-, APP C-terminal fragments, APP intracellular domain, Amyloid-beta, tau, presenilins) are released in association with exosomes has shed light on previously unidentified pathways in the processing of APP and provided potential explanation for extracellular amyloid deposition in the brain [Sharples et al., 2008; Vingtdeux et al., 2007; Ghidoni et al., 2011; Saman et al., 2012; An et al., 2013; Saman et al., 2014]. In support to this hypothesis, other exosomal proteins (such as alix and flotillin) have been found to accumulate in the plaques of AD brains.

However it is still a matter of debate if in some pathologies (such as NDs) differences in exosome pathways lead to a different content of proteins or to variations in quantity of vesicle production, respectively making exosomes carriers of biomarkers or biomarkers themselves. For this reason an hot topic of recent researches focused on the isolation, detection and characterization of exosomes from different sources in order to discover any correlation between their production and content with the interested pathology.

Any cell of animal beings can be an exosome-producing cell, both *in vivo* and *in vitro*. For example, exosomes have been isolated from different body fluids, such as blood, urine, saliva, amniotic fluid, CSF, bile, broncho-alveolar lavage and tumor ascites,through a simple collection by the usual means [Théry et al., 2006]. Similarly exosomes have also been found in many cell culture supernatants with an average level of production of about 0.1 μg/10^6 cells as a rough general estimate [Théry et al., 2006]. However, irrespective to their source, the purification of exosomes from cell

culture supernatants or other biological fluids is not trivial and follows the same principle. In particular, when dealing with cell lines, in order to avoid contamination by exosomes from serum present in the culture medium, it becomes necessary to grow cells in serum-free conditions, to ensure that all vesicles present in the supernatant derive from cellular production [Théry et al., 2006]. In order to purify and concentrate vesicles from collected samples, the original and most widespread protocol involves several centrifugation and ultracentrifugation steps [Raposo et al.,1996]. Nevertheless, purification of vesicles from body fluids is usually less efficient due to the high complexity of the matrix and the viscosity of the samples themselves. For these reasons, it is recommended to dilute them and to increase the speed and lengths of centrifugations [Caby et al., 2005]. An alternative new method for purifying exosomes is by ultrafiltration instead of ultracentrifugation, employing cartridges and pumps in a way useful when dealing with large volumes (>1 L) of conditioned medium, but it is not the easiest option for laboratory applications [Théry et al., 2006]. However, Lamparski and colleagues have compared the two preparation methods for the same dendritic cell supernatants side by side, using biochemical, morphological, and functional assays for exosomes, founding no significant differences [Lamparski et al., 2002].

The general flowchart of exosome purification by ultracentrifugation is depicted in **Figure 7.2**. The first steps are designed to eliminate large dead cells and large cell debris by successive centrifugations at increasing times and speeds. The first pellet contains cellular debris, the second is enriched in MVBs, while only through the third centrifugation, ectosomes and exosomes can be separated. Ectosomes are slightly bigger vesicles, released from cells upon plasma membrane shedding and bearing distinct protein markers, such as CD41 or CD45 [Record et al. 2011]. In order to purify exosomes, at each of these centrifugation steps the pellet is thrown away and the supernatant is used for the following steps. The final supernatant is then ultracentrifuged at 110000 × *g* to pellet the small vesicles that correspond to exosomes

(Pellet #4, often indicated as *P4*). This pellet is then resuspended in an appropriate volume of PBS. This preparation is usually stored at 4° C and tests should be set up in the immediate following days. Sokolovaa and colleagues characterized exosomes by scanning electron microscopy (SEM), dynamic light scattering (DLS) and nanoparticle tracking analysis (NTA), measuring a diameter around 110 nm and observing that multiple ultracentrifugations do not affect the exosome size [Sokolovaa et al., 2011].

Although centrifugation protocols reasonably provide pure exosomes, for some applications it may be advisable to include an extra purification step using a sucrose cushion or by immunoisolation. This further step eliminates more contaminants, such as proteins non specifically associated with exosomes, or large protein aggregates, which are sedimented by centrifugation but do not float on a sucrose gradient. Hence, exosomes from pellet P4, resuspended in PBS, can be loaded on a sucrose gradient column (ranging fron 1.125 to 1.186 g/mL) to be fractioned according to their density. After 16 hours centrifugation at 200000 x *g*, each fraction is isolated and furthermore centrifuged at 110000 x *g* for 1 hour. Empty supernatants are discharged while pellets are resuspended in an appropriate volume of PBS. These preparations can be stored, as well, at 4° C and tests should be set up in the immediate following days.

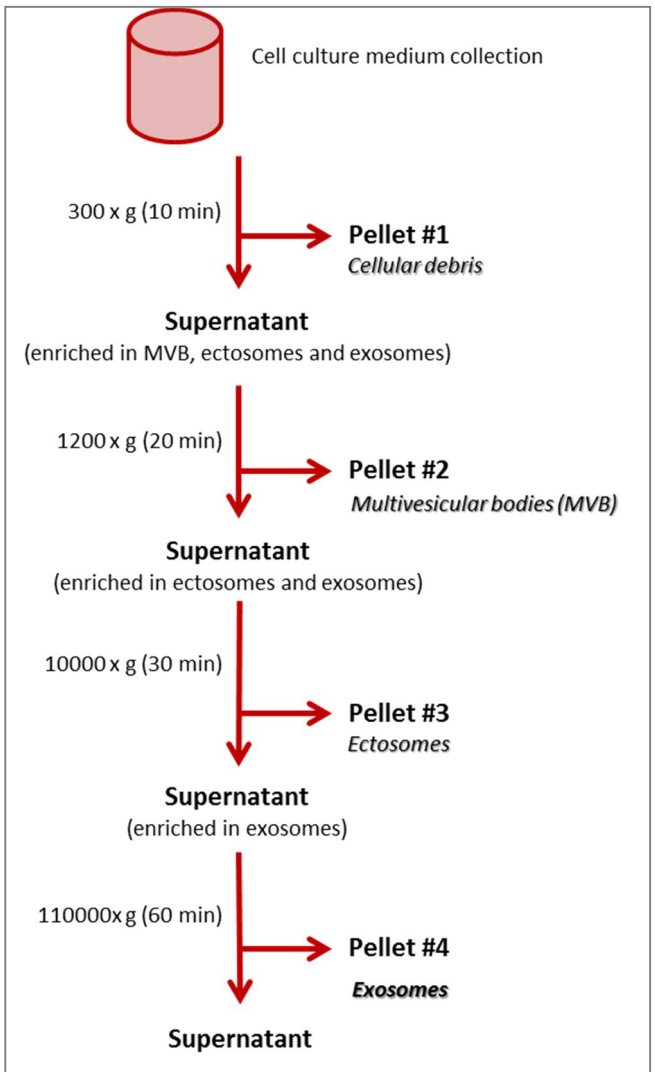

Figure 7.2 - Flowchart of exosomes purification protocol based on differential ultracentrifugation. The speed and length of each centrifugation are indicated to the left of the arrows. After each of the first three centrifugations, pellets are discarded, and the supernatant is kept for the next step. In contrast, after the final centrifugation, the pellet enriched in exosomes is kept and the empty supernatant is discarded.

Purified vesicles need to be detected and characterized. Up to now, due to their physical properties, it is very difficult to distinguish and characterize exosomes among all extra-cellular vesicles (EVs) in biological samples and for these reasons a major

ongoing challenge is to establish methods to discriminate between exosomes and other types of vesicles [Bobrie et al., 2011]. Since they are too small for direct analysis by flow cytometry or other conventional techniques for the analysis of nanoparticles, new methods are required to successfully quantify exosomes and to identify their cellular origin. Widely applied technologies used for a *qualitative*detection of exosomes consider them as ultramicroscopic particles. Among all the techniques, the most commonly used include electron microscopy (EM), dynamic light scattering (DLS), and nanoparticle tracking analysis (NTA).

EM provides an appropriate evaluation of both the purity of exosome preparations as well as their characterization [Théry et al., 2006]. In **Figure 7.3**, negatively stained exosomes reveal cup-shaped membrane vesicles of 50 to 100 nm [Théry et al., 2006]. In the extracellular space, highly curved membranes are less common; as most cells have higher diameters, nano-sized exosomes represent uniquely curved lipid surfaces [Gyorgy et al., 2011]. However it is possible that the morphological appearance of exosomes may be influenced by chemical fixation, used in EM detection protocols [Théry et al., 2006]. The “contrasting and embedding” procedure (“positive-negative” contrast) was originally developed for ultrathin cryosections, in order to provide a reproducible method and to combine both increase in contrast and stabilization of the membranes [Théry et al., 2006], as it takes advantage of fixing membranes with 2% or 4% (w/v) of paraformaldehyde.

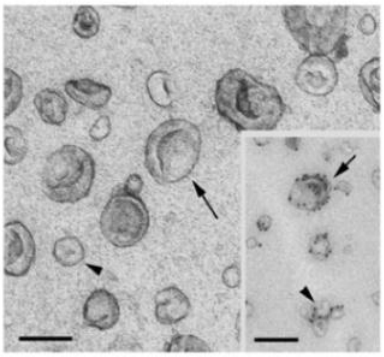

Figure 7.3 - Electron-microscopic observation of whole-mounted exosomes purified from mouse dendritic cells. Arrows indicate exosomes while arrowheads point to smaller non-exosomal vesicles. The insert emphasizes immunogold labelling of MHC class II molecules, with 10 nm gold particles. Scale bar corresponds to 100 nm [Théry et al., 2006].

Dynamic light scattering (DLS) is a useful technique which tries to detect exosomes based on their low refractive index [Dragovic et al., 2011]. However the actual instrumentationsare not able to distinguish between microvesicles (>100 nm) and exosomes (<100 nm) in a mixed solution [Lawrie et al., 2009]. On the contrary, nanoparticle tracking analysis (NTA) is perhaps the most promising method to detect smaller nanoparticles, because it can identify both microvesicles and exosomes and is not dependent on their refractive index [Kastelowitz et al., 2014]. However, without a fluorescently labeled antibody directed towards a vesicle surface marker or without the use of a vesicle isolation method to reduce polydispersity of the sample, there can be considerable intra-assay count variability [Dragovic et al., 2011; Oosthuyzen et al., 2013].

Nevertheless, depending on the method used, the reported absolute number of extracellular vesicles in a liter of blood can vary by as much as five orders of magnitude

[van der Pol et al., 2010]. Moreover, all these techniques share the limit of not being applicable in clinical diagnostic tools.

On the other side, irrespective to a quality control of purified samples, two bioanalytical approaches are widely used for a *quantitative* analysis of exosome content: immunoblotting (e.g., ELISA), which quantifies the amount of a given exosomal protein, and the Bradford assay, able to measure the total protein concentration in the exosome preparations [Théry et al., 2006]. Both these analysis often require the disruption of vesicles and the release of proteins in solution for the quantification of the target analyte.

To overcome the lack of tools suitable for both quantitative and qualitative analysis of EVs, this study focused on the development of fluorescence-based and label-free microarray platforms able to assess at the same time concentration, size distribution and phenotype of intact exosomes.

Exosomes purified from human fibroblast cell culture were chosen as a standard model to set assay conditions, in order to develop a tool available for human plasma samples of clinical interest. Prior, direct immunoassay tests were performed to select the best antibody against the human tetraspanin CD63 (hCD63), chosen as a typical biomarker of exosomes. In the following step, sandwich immunoassays were carried out by combining fluorescence-based and label-free detection technologies. In particular, conventional IRIS provided quantitative measurements of biomaterial immobilized on the surface, while SP-IRIS was useful in defining the size distribution of vesicles in a given sample whereas fluorescence was used in their phenotyping. The integration of all these type of information, allowed the development of an innovative tool able to detect, count and characterize intact exosomes.

7.1- MATERIALS AND METHODS

7.1.1 - Materials

Phosphate buffered saline (PBS), Trizma base (Tris), HCl, ethanolamine, Bovine Serum Albumin (BSA), Tween-20, ammonium sulphate, N,N'-dymethylacrylamide (DMA), 3-(trimethoxysilyl)propylmethacrilate (MAPS) and paraformaldehyde (PFA)were purchased from Sigma-Aldrich (St. Louis, MO, USA).

Mouse biotin-labeled antibodies against human tetraspanin CD63 (hCD63) were purchased from different suppliers: clone 215-030fromAncell (Bayport, MN, USA), clone H5C6 from BioLegend (San Diego, CA, USA) andclone MEM-259from ExBio (Praha, Czech Republic). Rabbit IgG anti-hCD63, clone EXOEL-CD63A-1, was bought from System Biosciences (SBI - Mountain View, CA, USA). Capture IgG against hCD63, clone H5C6 was obtained from BioLegend (San Diego, CA, USA). Cy3-labeled streptavidin (SA-Cy3), Cy3-labeled Goat anti-Rabbit IgG and Goat anti-Rabbit IgG *whole molecule* were obtained from Jackson Immunoresearch (West Grove, PA, USA). Mouse IgG against hCD63 clone H5C6 labeled with 40nm gold nanoparticled (NP-Au) were a gift from Prof. Selim M. Unlu from Boston University, MA (USA).

Silicon chips with a 100 nm thermal oxide layer were bought from Silicon Valley Microelectronics (Santa Clara, CA , USA); Single Particle (SP) chips with 100 nm thermal oxide layer and IRIS chips with a 500 nm thermal oxide layer were a kind gift from Prof. Selim M. Unlu from Boston University, MA (USA).

Exosomes were purified from human fibroblast cell culture according to the protocol reported in the introductive paragraph (**Figure 7.2**) by Dr. Roberta Ghidoni team from IRCSS – Fatebenefratelli (Brescia, Italy). Pellet ***P4*** samples were diluted into a volume of 5uL PBS per starting Petri dishes and delivered the same day experiments took place.

Human plasma samples of clinical interest were a gift from Dr. Roberta Ghidoni (IRCSS – Fatebenefratelli, Brescia, Italy), obtained from hospital sample bank, tawed and simply centrifuged at 3000*g* before delivery.

7.1.2- NanoSight measurements

Suspensions containing vesicles were analysed using a Nano-Sight LM10 instrument (NanoSight, Amesbury, UK) by the laboratory of Prof. Prosperi at Bicocca University (Milan, Italy). For this analysis, a monochromatic laser beam at 405 nm was applied to thedilute suspension of vesicles. A video of 60 seconds duration was taken with a mean frame rate of 30 frames/s, and particle movement was analysed by NTA software (version 2.2, NanoSight). The NTA software is optimized to first identify and then track each particle ona frame-by-frame basis, and its Brownian movement is trackedand measured from frame to frame. The velocity of particlemovement is used to calculate particle size by applying the two-dimensional Stokes–Einstein equation. The range of sizes thatcan be analysed by NTA depends on the particle type: metal NPs, such as colloidal gold, have a highrefractive index while for cell-derived vesicles, like exosomes and microvesicles, the refractive index is very low and their smallest detectable size using theNTA system is approximately 50 nm [Gercel-Taylor et al., 2012]. NTA post-acquisition settingswere optimized and kept constant between samples, and eachvideo was then analysed to give the mean, mode, and median vesicle size together with an estimate of the concentration.

7.1.3 - Coating of microarray silicon chips with poly(DMA-NAS-MAPS)

Poly(DMA-NAS-MAPS)-coated silicon microarrays were fabricated according to the protocol described in ***paragraph 5.1.2***. Briefly, silicon chips were immersed in a poly(DMA-NAS-MAPS) solution (1% w/v in 0.9 M $(NH_4)_2SO_4$) for 30 min. The chips were

then rinsed with water, dried under nitrogen and cured for 15 min under vacuum at 80° C [Cretich et al., 2009b].

7.1.4 - Direct immunoassays using IRIS and fluorescence-based detection platforms

Purified standard exosomes peraprations were provided by collaborators from IRCSS – Fatebenefratelli (Brescia, Itay) as described in ***paragraph 7.1.1***.

Samples were at first diluted four times in pure PBS or in 2% paraformaldehyde (PFA) in PBS and printed on both uncoated and poly(DMA-NAS-MAPS)-coated silicon chips, with 100 and 500 nm oxide layer thickness, using a SciFlexArrayer S5 spotter from Scienion (Berlin, Germany). On the same chips, also a Goat anti-Rabbit IgG whole molecule was printed as reference together with the empty printing buffers as negative controls. Four replicate spots were patterned on each surface; in the experimental conditions used, the volume of the spotted drops was 400 pL. Printed chips were placed in a humid chamber and incubated overnight at room temperature. The copolymer-coated chips were then blocked with 50 mM ethanolamine solution in 1 M TRIS/HCl pH 9 for 1 h. Both uncoated and coated chips were subsequently washed with water and dried under a stream of nitrogen. IRIS images were acquired and fitted with Zoiray Acquire software. For each protein, signals from 4 replicate spots were averaged.

Further uncoated and poly(DMA-NAS-MAPS)-coated silicon chips were arrayed with several dilutions (i.e. 1:2, 1:4, 1:8, 1:16, 1:32) of the same exosome samples in 2% PFA in PBS as printing buffer. Empty printing buffer was spotted as negative control while Cy3-labeled steptavidin (SA-Cy3) was used as reference for fluorescence acquisitions. Seven replicate spots were patterned according to the same spotting protocol described above. Also in this assay, printed chips were placed in a humid chamber and incubated overnight at room temperature. The copolymer-coated chips were then

blocked with **50 mM ethanolamine solution in 1 M TRIS/HCl pH 9** for 1 h. Both uncoated and coated chips were subsequently washed with water and dried under a stream of nitrogen. Chips were then incubated in static conditions for 2 hours with detection antibodies against the human tetraspanin CD63 (hCD63): Rabbit IgG from SBI (clone EXOEL-CD63A-1) or biotin-labeled Mouse IgG from Ancell (clone 215-030), BioLegend (clone H5C6) or ExBio (clone MEM-259). All detection antibodies were diluted to a final concentration of 1 ug/mL in **incubation buffer (50 mM Tris/HCl, 150 mM NaCl, 0.02% Tween-20 and 1% BSA)**. Chips were then washed with PBS for 10 min with stirring, rinsed with water and incubated in static conditions, for 1 hour, respectively with Cy3-labeled Goat anti-Rabbit IgG (GaR-Cy3) at 1 µg/mL or with Cy3-labeled streptavidin (SA-Cy3) at 2 mg/mL in PBS. Chips were washed again with PBS and water for 10 min each, rinsed with water and dried under nitrogen stream. Fluorescence was determined by a ProScanArray scanner (PerkinElmer, Boston, MA), and silicon chips were analysed using 90% Photomultiplier (PMT) gain and laser power. The fluorescence intensities of 7 replicate spots were averaged.

7.1.5 - Sandwich immunoassays using IRIS and fluorescence-based detection platforms

Capture IgG against hCD63, clone H5C6 (from BioLegend) and Cy3-labeled streptavidin (as reference) were arrayed on poly(DMA-NAS-MAPS)-coated silicon chips, with 100 and 500 nm oxide layer thickness, using a SciFlexArrayer S5 spotter from Scienion (Berlin, Germany). Antibodies were printed at 1 mg/mL in 25 replicates; the volume of spotted drops was 400 pL. Printed chips were placed in a humid chamber and incubated overnight at room temperature. Then they were blocked with 50 mM ethanolamine solution in 1 M TRIS/HCl pH 9 for 1 h, washed with water and dried under a stream of nitrogen. IRIS images of printed capture antibodies were acquired with Zoiray Acquire software, before any incubation with exosome samples.

Purified exosomes standard samples were provided by collaborators from IRCCS-Fatebenefratelli (Brescia, Italy) as described in ***paragraph 7.1.1***, and quantified using NanoSight measurements by partners from Prosperi's laboratory at Bicocca Unuversity (Milan, Italy). Accordig to NTA quantification, exosomes were diluted in PBS to a concentration of 16, 4, 2, 1.6, 0.6, 0.4 and 0 E+10 particles/mL and then 20 uL of each suspension was incubated in static conditions for 2 hours on printed chips. After that, chips were washed with PBS with stirring, rinsed in water and dried under nitrogen stream. Further label-free IRIS images were acquired with Zoiray Acquire software, after the incubation with exosome samples. All IRIS files were fitted and processed using Zoyray Process software.The effective mass increase from captured exosomes on printed antibodies was obtained subtracting the signals measured before and after sample incubation. Net values from 25 spots were averaged to design a calibration curve.

Chips were furthermore incubated in static conditions, for 1 hour, with 1 μg/mL (in incubation buffer, 1% BSA) of the selected biotin-labeled detection antibody against hCD63, clone H5C6 (from BioLegend). As vesicles display several tetraspanins on their membrane, a sandwich immunoassay is possible even when using the same monoclonal antibody for both capture and detection purposes. Chips were then washed with PBS for 10 min with stirring, rinsed with water and incubated in static conditions, for 1 hour, with Cy3-labeled streptavidin (SA-Cy3) at 2 mg/mL in PBS. Chips were washed again with PBS and water for 10 min each, rinsed with water and dried under nitrogen stream. Fluorescence was determined by a ProScanArray scanner (PerkinElmer, Boston, MA), and silicon chips were analysed using 70% or 80% Photomultiplier (PMT) gain and laser power. The fluorescence intensities of 25replicate spots were averaged to define a calibration curve.

7.1.6 - Indirect immunoassays using SP-IRIS detection platform

Capture IgG against hCD63, clone H5C6 (from BioLegend) was arrayed, using a SciFlexArrayer S5 spotter from Scienion (Berlin, Germany), on poly(DMA-NAS-MAPS)-coated silicon chips for SP-IRIS detector, characterized by 100 nm silicon oxide layer thickness on top and patterned with silicon references. The antibody was printed at 0.5 mg/mL in 12 replicates; the volume of spotted drops was 400 pL. Printed chips were placed in a humid chamber and incubated overnight at room temperature. Then they were blocked with 50 mM ethanolamine solution in 1 M TRIS/HCl pH 9 for 1 h, washed with water and dried under a stream of nitrogen. IRIS images of printed capture antibodies were acquired with Zoiray Acquire software, before any incubation with exosome samples, in order to check spot morphology and quality. Then SP-IRIS images were acquired using a custom-made *MGrid* software running on MatLab. The instrument records the position of each spot of interest leading to quantification of single particles at the same positions before and after any incubation step.

Afterwards, purified exosomes standard samples, provided by collaborators from IRCCS- Fatebenefratelli (Brescia, Italy) as described in ***paragraph 7.1.1***, and quantified using NanoSight measurements by partners from Prosperi's laboratory at Bicocca Unuversity (Milan, Italy), were diluted in PBS to a final concentration of 1.5 E+10 particles/mL and 20 uL of this preparation were incubated on printed chips, overnight in static conditions. After that, chips were washed with PBS with stirring, rinsed in water and dried under nitrogen stream. Further label-free SP-IRIS images were acquired with the same procedure described above. Chips were furthermore incubated in static conditions, for 1 hour, with 40 nm gold nanoparticle-labeled detection antibody (NP(Au)-IgG) against hCD63, clone H5C6 (from BioLegend), at 1 µg/mL, kindly provided by collaborators at Boston University. As vesicles display several tetraspanins on their membrane, a sandwich immnoassay is possible even when using the same monoclonal antibody for both capture and detection purposes. Chips were then washed again with PBS and water for 10 min each, rinsed with water

and dried under nitrogen stream. Final SP-IRIS measurements were acquired with the same instrumentation and protocol described above. Signals from 12 replicate spots were analysed and averaged. In order to measure the net single particle counts due to exosomes accumulation on each spot, the *MGrid process* software subtracted counts before from after exosomes incubation. Differently, in order to measure the the effect caused by the adding of nanoparticles, the software was set for gold scattering and subtracted counts before from after incubating with NP(Au)-IgG.

7.1.7 - Indirect fluorescence detection of exosomes from human plasma samples

Capture IgG against hCD63, clone H5C6 (from BioLegend) and Cy3-labeled streptavidin (as reference) were arrayed on a poly(DMA-NAS-MAPS)-coated silicon chip, with 100 nm oxide layer thickness, using a SciFlexArrayer S5 spotter from Scienion (Berlin, Germany). The antibody was printed at 1 mg/mL in 80 replicates; the volume of spotted drops was 400 pL. Printed chip was placed in a humid chamber and incubated overnight at room temperature. Then it was blocked with 50 mM ethanolamine solution in 1 M TRIS/HCl pH 9 for 1 h, washed with water and dried under a stream of nitrogen.

Human plasma from IRCSS Fatebenefratelli hospital (Brescia, Italy) bio-bank was thawed and simply centrifuged at 3000*g*. Part of the sample was characterized using NanoSight measurements by partners from laboratory of Prof. Prosperi at Bicocca University (Milan, Italy), while, as delivered, 20 uL of this plasma were incubated overnight at room temperature on the chip. After that, the chip was washed with PBS with stirring, rinsed in water and dried under nitrogen stream. The chip was furthermore incubated in static conditions, for 2 h, with 1 µg/mL (in incubation buffer, 1% BSA) of the selected biotin-labeled detection antibody against hCD63, clone H5C6 (from BioLegend). The chip was then washed with PBS for 10 min with stirring, rinsed with water and incubated in static conditions, for 1 hour, with Cy3-labeled streptavidin

(SA-Cy3) at 2 mg/mL in PBS. The chip was washed again with PBS and water for 10 min each, rinsed with water and dried under nitrogen stream. Fluorescence was determined by a ProScanArray scanner (PerkinElmer, Boston, MA), and silicon chips were analysed using 90% Photomultiplier (PMT) gain and laser power. The fluorescence intensities of 80 replicate spots were averaged to define a calibration curve.

7.2 - RESULTS AND DISCUSSION

7.2.1 - Direct immunoassays for IRIS and fluorescence-based exosomes detection

The firs step to set a feasible immunoassay able to detect exosomes as intact vesicles consisted in chosing the best experimental parameters and the best conditions to handle samples preserving their integrity during tests. For these reasons, in preliminary experiments, exosomes purified from human fibroblast cell culture were chosen as standard model.

Direct immunoassays require the target biomolecules to be printed on the a proper surface and subsequently assayed by labelled detection antibodies. Thus, first of all, exosomes were diluted in two different printing buffers, respectively PBS and 2% paraformaldehyde (PFA), and arrayed on both uncoated and poly(DMA-NAS-MAPS)-coated silicon chips with 100 or 500 nm silicon oxide layer thickness. IRIS acquisitions of the printed material did not show any spot when using PBS as printing buffer, while the fixation of membranes by PFA increased vesicles capability to bind the surface, thus providing the visible spots reported the central line of **Figure 7.4**. In the same picture, the first line corresponds to the printing buffer only (2% PFA in PBS), demonstrating that there are no artifacts in the biomass measurements due to the printing solution. On the contrary, the third line shows highly contrasting spots

corresponding to 1 mg/mL IgG (goat anti-rabbit IgG), that has been used as internal reference for focusing during acquisitions.

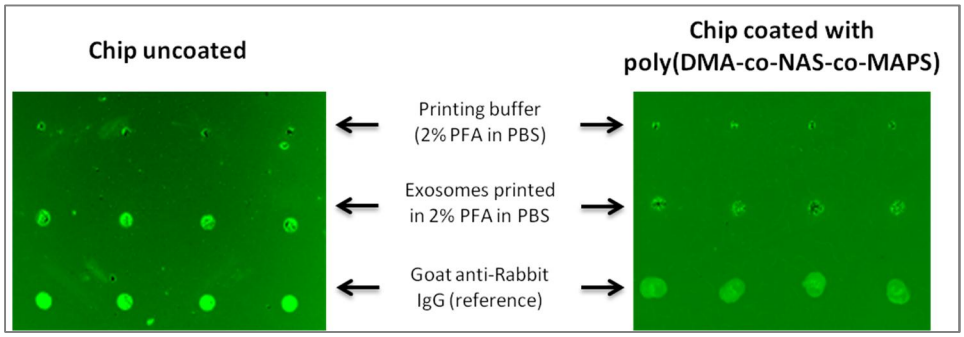

Figure 7.4 - LowMag-IRIS images of uncoated and poly(DMA-NAS-MAPS)-coated silicon chips, spotted in 2% PFA in PBS (central line); printing buffer was spotted as blank control (first line) and Goat anti-Rabbit IgG was spotted as reference.

Figure 7.5 reports the quantification of IRIS signals in terms of thickness increase on each spot of interest from the first and second line, on both surfaces. Confirming what discussed above, the printing buffer itself does not provide any signal, while a significative increase is measured on printed exosomes. Moreover, higher values were detected on the uncoated surface rather than on the poly(DMA-NAS-MAPS)-coated one, likely due to hydrophobic interactions between the lipidic vesicles and bare silicon which facilitate vesicle binding on the surface.

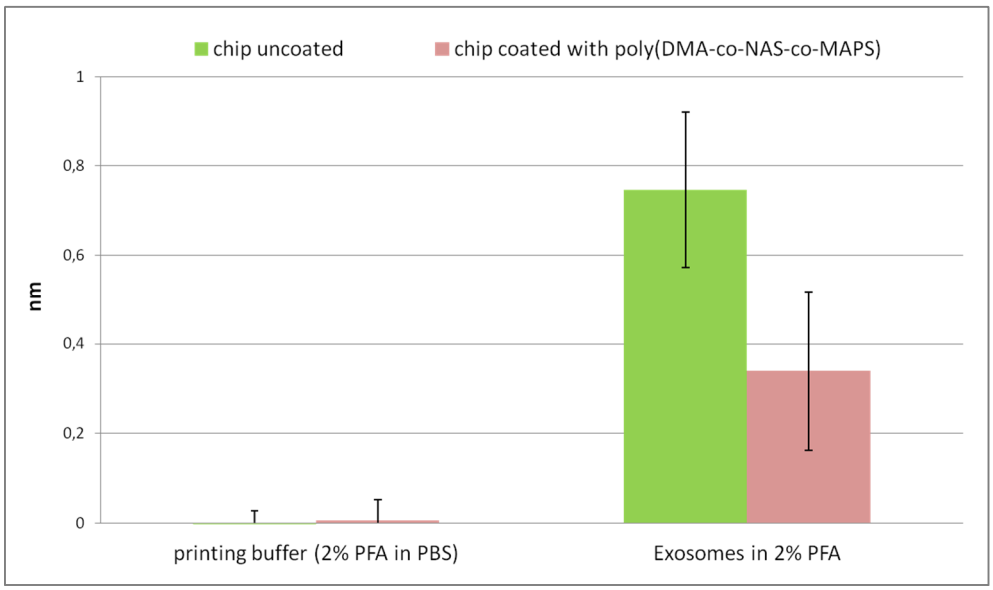

Figure 7.5 - Quantification of LowMag-IRIS signals, measured in terms of thickness increase (nm) on the silicon surfaces due to biomass accumulation. Green bars refers to signals on uncoated chip; pink bars represent signals fron poly(DMA-NAS-MAPS)-coated chip.

Figure 7.6 summarizes the workflow of the direct assay development. As outlined, after IRIS measurements, chips printed with several exosomes dilutions, in 2% PFA, were further incubated with labeled antibodies for fluorescence detection. In order to detect whole vesicles through fluorescence detection, antibodies against membrane proteins are required. Among all proteins known as EV markers, the human tetraspanin CD63 (hCD63) was selected. Four different antibodies were tested in a two-step incubation assay. First the antibody (Rabbit IgG from SBI or biotin-labeled Mouse IgG from Ancell, BioLegend and ExBio) were incubated, then a secondary reporter was added (respectively, a secondary Goat anti-Rabbit IgG-Cy3 or streptavidin-labeled Cy3).

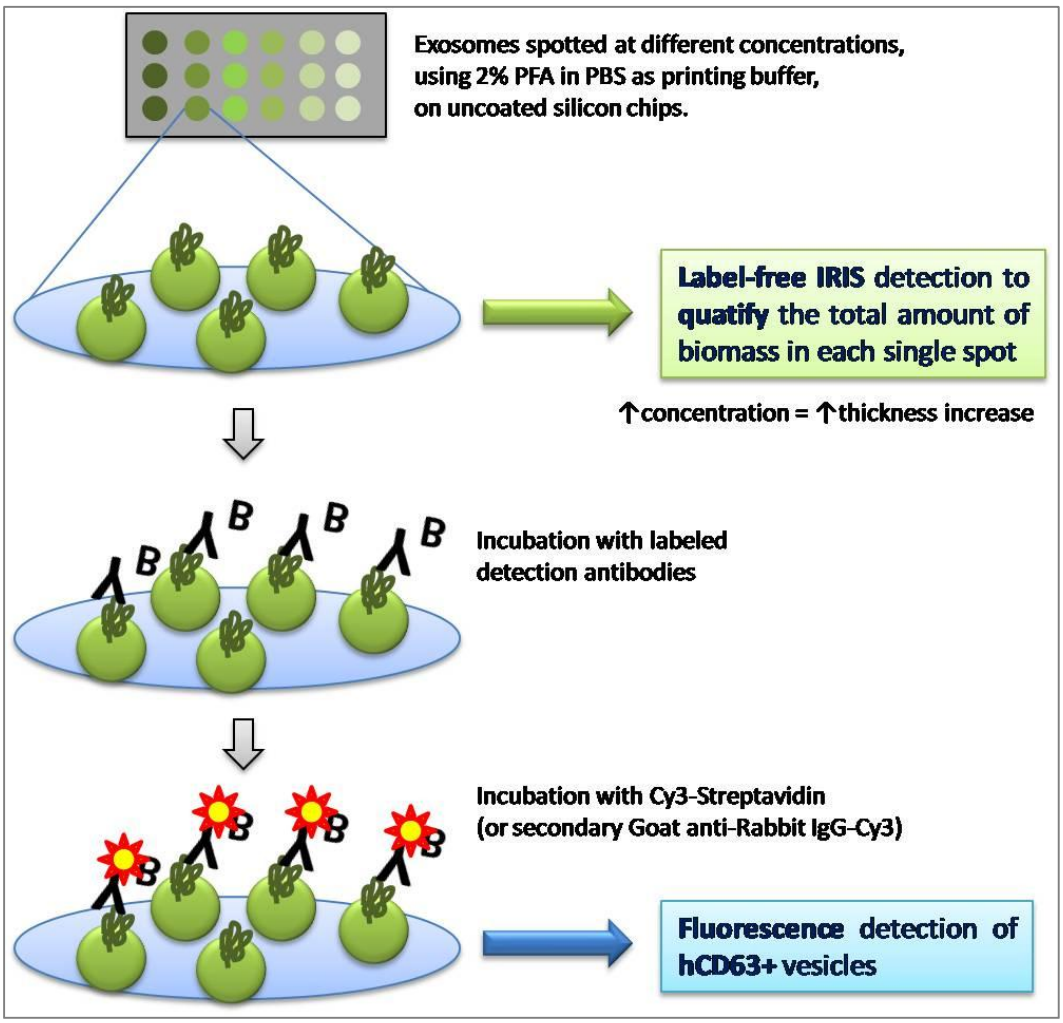

Figure 7.6 – Direct immunoassay workflow. First, exosomes were spotted on uncoated silicon chips, using 2% PFA in PBS as printing buffer and label-free IRIS detection was used to quantify the total amount of printed biomaterial per spot. Later, chips were further incubated with antibodies against hCD63 and detected using a fluorescent reporter (SA-Cy3 or Goat anti-Rabbit IgG-Cy3). Fluorescence detection revealed hCD63-positiveprinted vesicles.

Images from each tested condition are reported in **Figure 7.7**. It is clearly evident that also fluorescence detection provides higher signals on uncoated chips (right column of *panel b*) as compared to poly(DMA-NAS-MAPS)-coated ones (left column of *panel b*), corroborating the idea of a higher binding capability on hydrophobic surfaces.

Among all tested antibodies, only signals from antibodies from SBI and BioLegend were detectable. However, the first one was not specific as higher fluorescence was detected on negative control and lower vesicle concentration rather then higher. On the opposite, the Mouse biotin-labed IgG to hCD63 from BioLegend (clone H5C6) was the only one able to provide linear and specific signals on printed exosomes, expecially on uncoated silicon chips. Thanks to its performances this clone was chosen for further investigations. The combination of information provided by direct detection is still not sufficient to provide phenotiping and size distribution of this kind of vesicles. Thus, once a protocol to handle exosomes was established and based on the selected antibody clone, indirect sandwich immunoassays were developed.

a)

SA-Cy3	Exosomes diluted 1:2 in 2% PFA/PBS (7 spots)
SA-Cy3	Exosomes diluted 1:4 in 2% PFA/PBS (7 spots)
SA-Cy3	Exosomes diluted 1:8 in 2% PFA/PBS (7 spots)
SA-Cy3	Exosomes diluted 1:16 in 2% PFA/PBS (7 spots)
SA-Cy3	Exosomes diluted 1:32 in 2% PFA/PBS (7 spots)
SA-Cy3	[Negative control] 2% PFA/PBS (7 spots)

b)

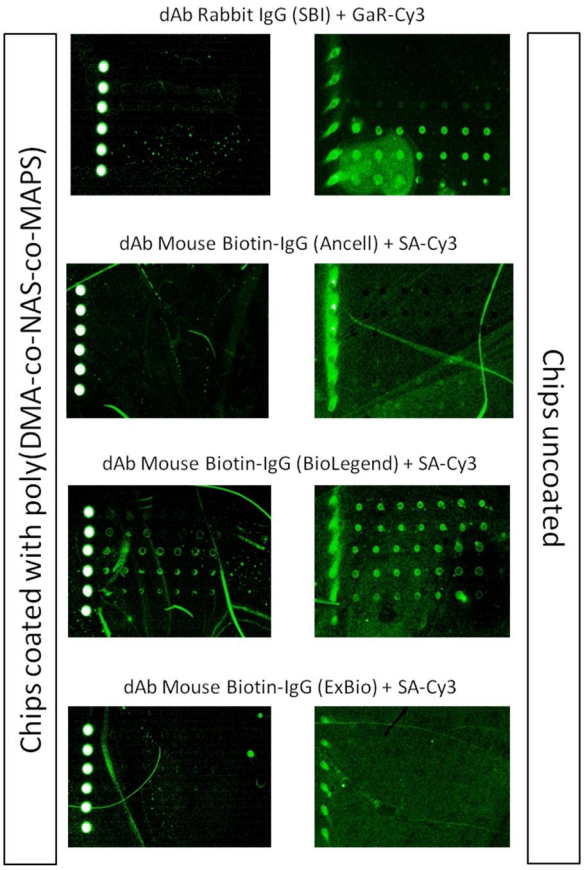

Figure 7.7 - Selection of anti-hCD63 detection antibody on fluorescence microarrays. a) Spotting scheme. b) fluorescence images (90% laser power and PMT gain) on poly(DMA-NAS-MAPS)-coated and uncoated chips, respectively on the left and right column. Per each line detection with four diffeernt antibodies are reported. The best performances are given by the biotinylated Mouse anti-hCD63 IgG from BioLegend, coupled with Cyanine 3 labeled with streptavidin (SA-Cy3).

7.2.2 - Sandwich immunoassays forIRIS and fluorescence-based exosomes detection

After establishing a protocol for exosomes purified from human fibroblast cell culture and following the selection of an antibody with high sensitivity and specificity (clone H5C6 from BioLegend), a sandwich immunoassay was developed. As reported in **Figure 7.8**, exosomes were captured by antibodies printed on the poly(DMA-NAS-MAPS)-coated silicon chips and then detected using the conventional label-free IRIS platform.

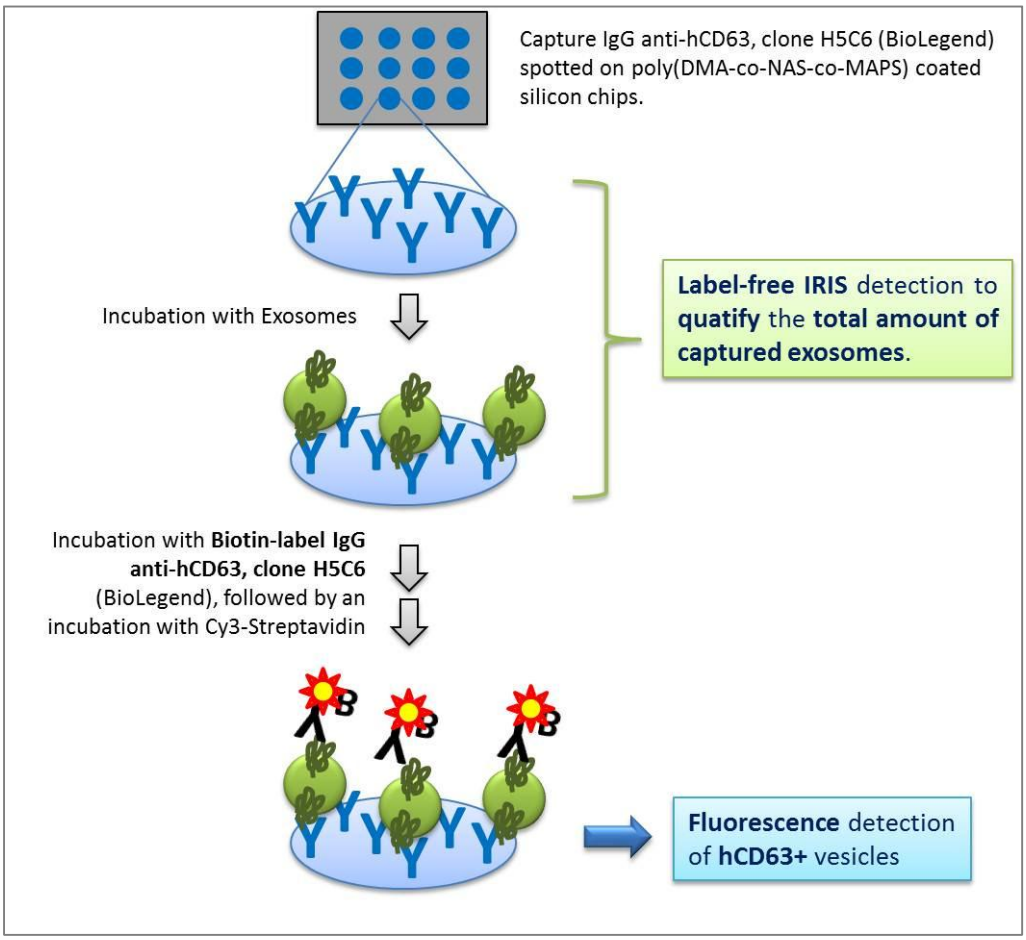

Figure 7.8 – Sandwich immunoassay workflow. First, capture antibodies were printed on poly(DMA-NAS-MAPS)-coated silicon chips and IRIS measurements of background signals were acquired before any incubation. Then several sample dilutions were incubated in static conditions for 2 h and further IRIS images were acquired in order to detect the net signal increase due to exosomes bound to their capture antibodies. Later, the same chips were incubated with biotin-labeled antibody against hCD63 (clone H5C6, from BioLegend) and detected using Cy3-labeled streptavidin as fluorescence reporter.

The net signal from exosomes bound to their specific antibodies was obtained subtracting the measurements after the sample incubation from the one before it. According to the NanoSight quantifications, several sample dilutions were tested to obtain the curve reported in **Figure 7.9**.

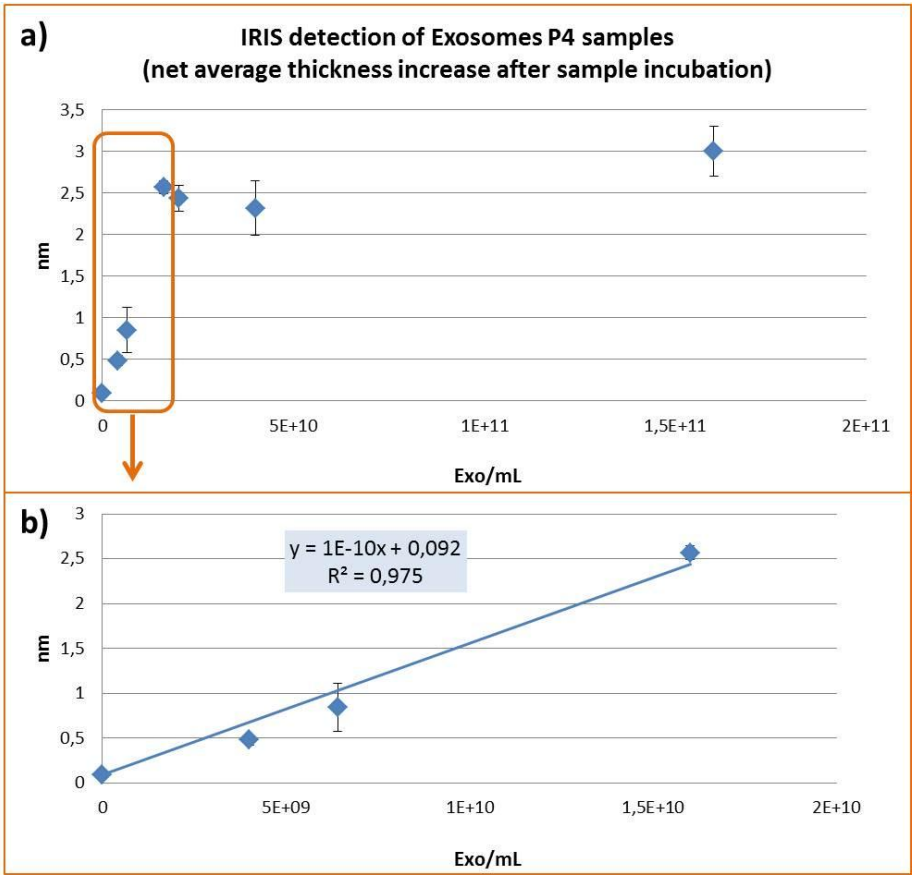

Figure 7.9 – Conventional IRIS measurements of exosomes bound to capture antibodies (against hCD63, clone H5C6, from BioLegend) printed on the poly(DMA-NAS-MAPS)-coated silicon chips. ***a)*** Signals from samples with more than 1.6 E+10 exosomes/mL reach the plateau as a consequence of saturation of binding sites on each spot of interest. ***b)***Close-up of the linear range from 0 to 1.6 E+10 exosomes/mL.

Samples from 0 to 1.6 E+10 particles/mL shows a linear correlation between the incubated vesicles and the biomass measured on the capture antibodies, demonstrating the capability to capture and quantify exosomes in a label-free fashion. On the contrary, samples with more than 1.6 E+10 exosomes/mL do not provide any thickness increase on the spots. This is likely due to the saturation of printed capture antibodies, as a consequence of steric hindrance or depletion of available binding sites.

Moreover, as vesicles display several hCD63 tetraspanins on their membrane, a sandwich immunoassay is possible even when using the same monoclonal antibody for both capture and detection purposes. Thus, as reported in **Figure 7.8**, chips were further incubated with the selected biotin-labeled antibody to hCD63, clone H5C6 (from BioLegend) and subsequently detected using Cy3-labeled streptavidin as fluorescence reporter. Signals were revealed and quantified using 70% laser power and PMT gain. A calibration curve was obtained in a linear range from 0 to 4.0 E+10 particles/mL (**Figure 7.10**).

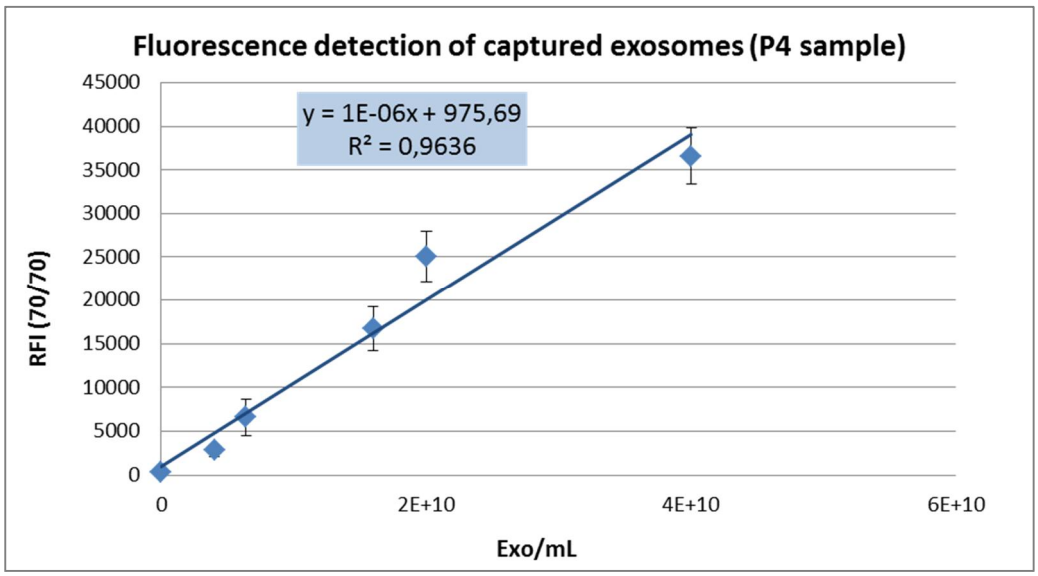

Figure 7.10 – Fluorescence signals (70% laser power and PMT gain) from exosomes captured and detected using antibodies against hCD63 (clone H5C6, from BioLegend) in a sandwich immunoassay format.

Label-free IRIS and Fluorescence detection provided complementary information: the first reports the total amount of biomass bound to the spots of interest while the latter provides biological data. For instance, in the proposed assay, hCD63-positive exosomes were detected leading to the possibility of phenotyping vesicles in a given sample. In order to corroborate the feasibility of this tool, the signals from both measurements, in the common range from 0 to 1.6 E+10 exosomes/mL, were plot on a single graph (**Figure 7.11**), demonstrating a good correlation factor between the two analytical platforms.

It would be of great interest to improve this tool printing a cocktail of capture antibodies against several exosome biomarkers. This would enhance the vesicle capturing yield in a given sample, allowing the detection of the total amount of bound biomaterial as well as to phenotype it by incubating with differential detection antibodies, specific for a given tissue or pathology biomarker.

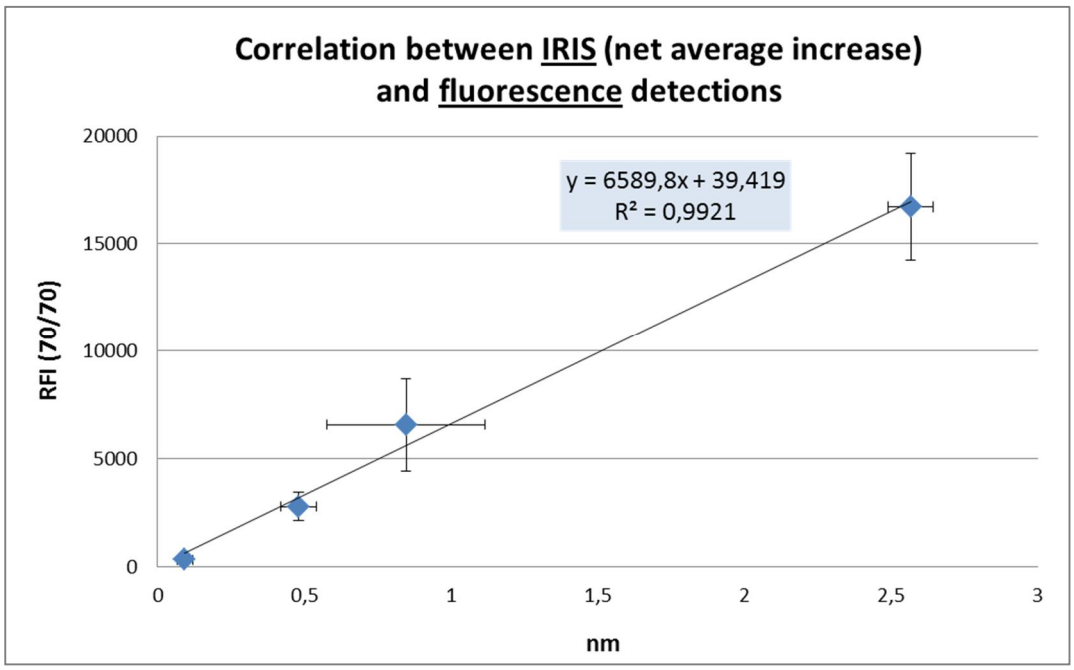

Figure 7.11 – Correlation between IRIS (*x axis*) and fluorescence (at 70% laser power and PMT gain, *y axis*) detection platforms.

7.2.3 - Indirect detection of intact exosomes as singleparticles using SP-IRIS platform

Although the integration of data collected from IRIS and fluorescence detection platforms provided an innovative tool for detection and characterization of exosomes, still they do not characterize the size distribution of vesicles in a given sample, which is an information of paramount importance as exosomes are not defined only based on biomarkers expressed on their surface, but also on their size. For this reason, further investigations were performed at the *Electrical and Computer Engineering Department* at Boston University (MA, USA), where the team of Prof. S. Unlu had developed a label-free detection platform called Single particle IRIS (SP-IRIS), which is a recent evolution of the conventional IRIS to enable digital detection of nanoparticles (NPs) on surface

with unique orthogonal verification via size/shape discrimination and minimal sample preparation.

As described in the ***Chapter 3*** (***paragraph 3.2.2***), the detection principle of SP-IRIS is based on the enhanced contrast in the scattering signal from particles on a layered substrate. To detect and size nanoparticles (NPs), IRIS shines light from visible LED sources on NPs bound to the sensor surface, which consists of 100 nm silicon dioxide layer on top of a silicon substrate. Interference of light reflected from the sensor surface is modified by the presence of particles producing a distinct signal that reveals the size of the particle itself. In this approach the dielectric layered structure acts as an optical antenna optimizing the elastic scattering characteristics of NPs for sensitive detection and analysis. The instrument is set for low-index dielectric particles with diameters of 60 to 200nm and metallic (Au and Ag) NPs with diameters ranging from 20 to 100nm [Yurt et al., 2012].

Originally, Daaboul and colleagues applied this platform to detect virus particles in complex samples. Considering the virions as NPs allowed the size discriminations and differentiation between wild-type and modified particles, demonstrating also the simultaneous detection of multiple viruses in serum or whole blood as well as in samples contaminated with high levels of bacteria [Daaboul et al., 2014]. By employing affinity-based capture, size discrimination and a “digital” detection scheme to count single virus particles, they showed that a robust and sensitive virus/NP sensing assay could be established for targets in complex samples.Based on their physical properties, exosomes do not exhibit distinct spectral resonances in the visible spectral region and have low refractive index contrast with respect to the background, making their detection difficult comparing to similar size metallic nanoparticles under resonance. However, exosome samples were analysed using SP-IRIS in a fashion similar to the one described for viruses. As depicted in **Figure 7.12**, individual exosomes were captured using a commecial antibody against the tetraspanin hCD63, arrayed on the surface of

silicon chips. Spot quality and antibody density was characterized using the total biomass measurement modality of conventional IRIS. The chips were then incubated with samples and the surface accumulation of exosomes was observed in dry conditions. The advantage of the dry measurements is the improved visibility; the refractive index of exosomes is low and their contrast (visibility) in liquid would have been further reduced.

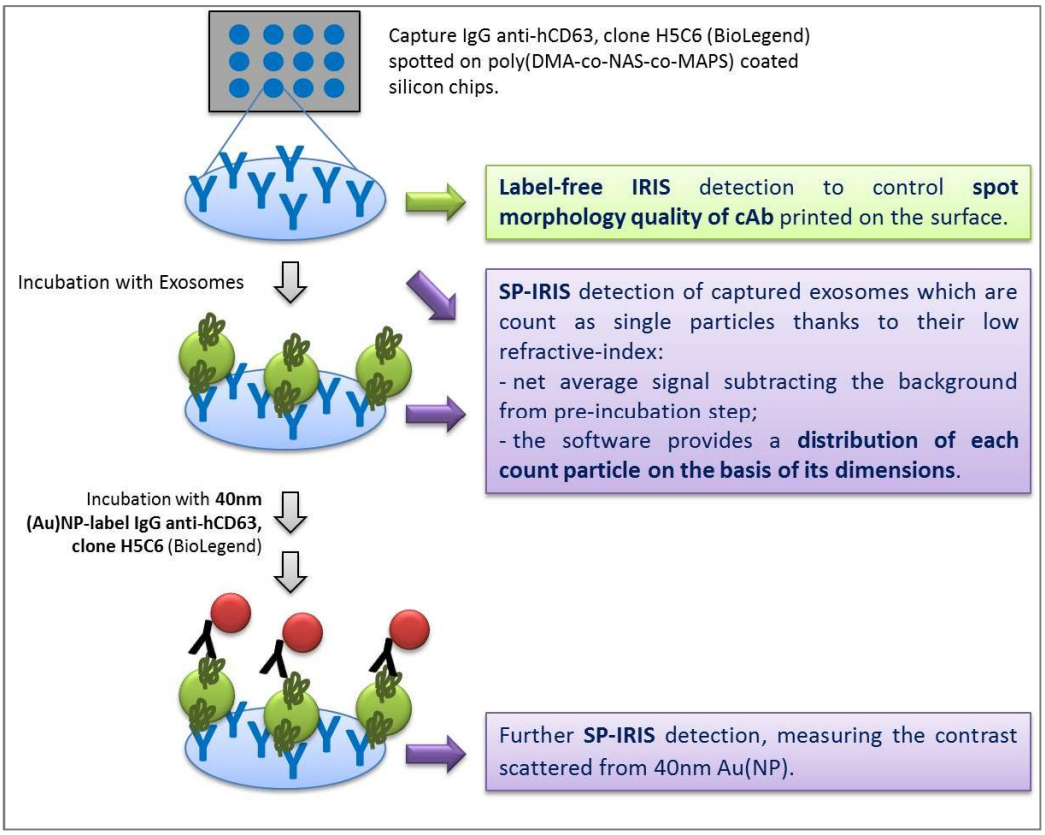

Figure 7.12 - Indirect immunoassay workflow using SP-IRIS detection platform. First, capture antibodies were printed on poly(DMA-NAS-MAPS)-coated silicon chips and IRIS analysis of spot quality was performed before any incubation. Then SP-IRIS images were acquired to measure background particle counts and to record spot positions on the chip. Afterwards, exosomes were incubated in static conditions overnight and further SP-IRIS images were acquired in order to detect the net signal increase due to exosomes bound to their capture antibodies. Later, the same chips were incubated again with gold nanoparticle-labeled antibody ((Au)NP-IgG) against hCD63 (clone H5C6, from BioLegend) and final SP-IRIS measurements were performed in order to evaluate the binding of labeled antibodies to capture exosomes.

Data collected in dry conditions at end-point, as shown in **Figure 7.13**, demonstrate the capability of the technology to detect exosome particles. Exosomes from a population with size distribution of 60-100nm in diameter are already distinguishable from the background, however for their accurate quantification and size discrimination, further system improvements need to be implemented. Later, the same chips were further incubated with secondary antibodies (still against hCD63) labelled with 40nm gold nanoparticles (Au-NP) and imaged again under dry conditions. A significant shift in the size distribution shows that many of the previously captured, detected and sized exosomes are decorated with Au-NP indicating their affinity to the particular antibody.

Further experiments will aim at multiplexing array formats to provide incubations with different secondary antibodies labeled with Au-NP, for phenotyping exosomes based on the presence of specific surface antigens.

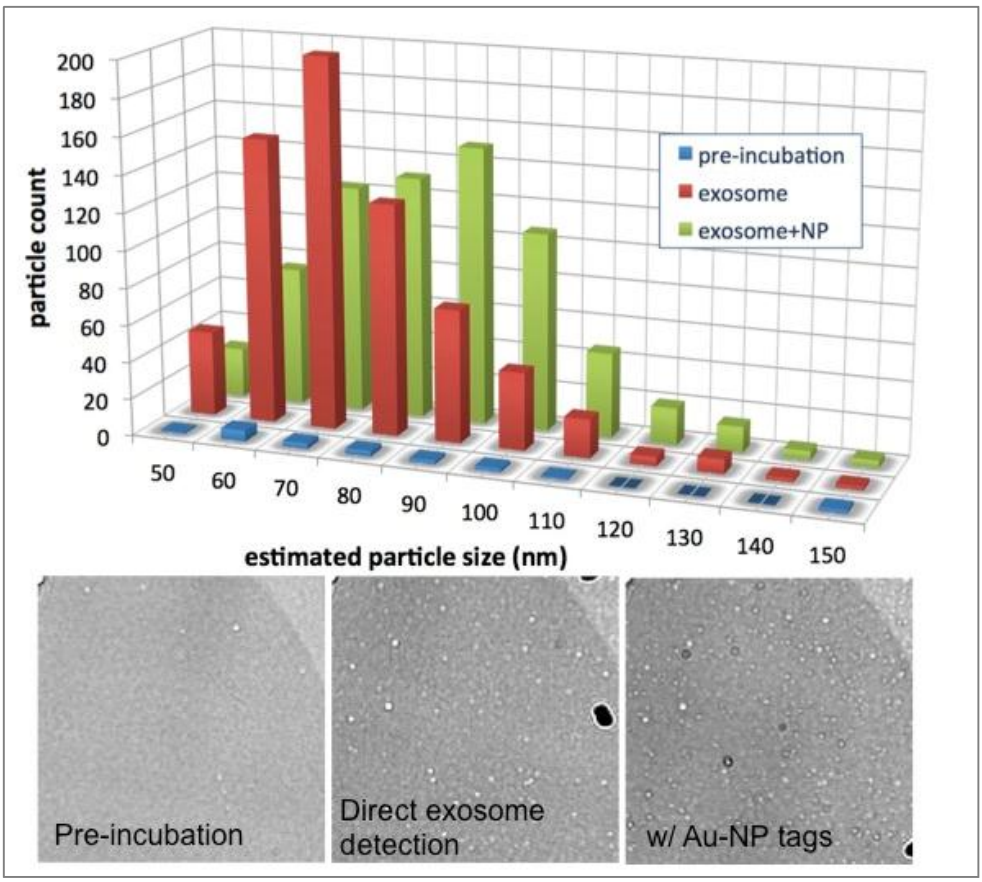

Figure 7.13 - SP-IRIS detection of whole exosomes as single particles. The graph at the top reports the size distribution of particles count on each spot of interest. The blu bars correspond to counts on printed antibodies, as a pre-incubation background. The red bars indicate the total counts on spots after sample incubation, due to exosomes captured on their specific antibodies; it is clearly evident that vesicles under study are exosomes as their size distribution stands within 50 and 100 nm of diameter. Moreover, green bars correspond to measurements after incubation with gold nanoparticles-labeled antibodies, leading to a shift in the size distribution as a consequence of exosomes decorated by detection IgG. Pictures under the graph are example of images acquired by SP-IRIS detector: printed capture antibodies (pre-incubation), after exosomes incubation (Direct exosomes detection), and after incubation with gold nanoparticles-labeled IgG. NP, both vesicles and gold, are visible as white dots, thanks to their contrast during scattering of incident light.

7.2.4 - Indirect fluorescence detection of intact exosomes from human plasma samples

The sandwich immunoassay developed as described above, was validated using real samples of clinical interest in order to detect exosomes in biological fluids without the need of time-consuming purification protocols.

For this reason, a human plasma sample form the IRCSS Fatebenefratelli hospital bio-bank (Brescia, Italy) was assayed. Frozen plasma was thawed and simply centrifuged at 3000*g*, then NanoSight measurements estimated the exosomes content in 1.31 E+10 particles/mL. Microarray experiment required the overnight incubation of 20 uL of plasma in static condition. Exosomes captured on spotted antibodies were then detected by fluorescence using the anti hCD63 selected biotin-labeled antibody, coupled with Cy3-labeled streptavidin. **Figure 7.14** shows fluorescence (at 90% laser power and PMT gain) from hCD63-positive vesicles in the tested sample. Signals from 80 spots were averaged, as reported in the graph below.

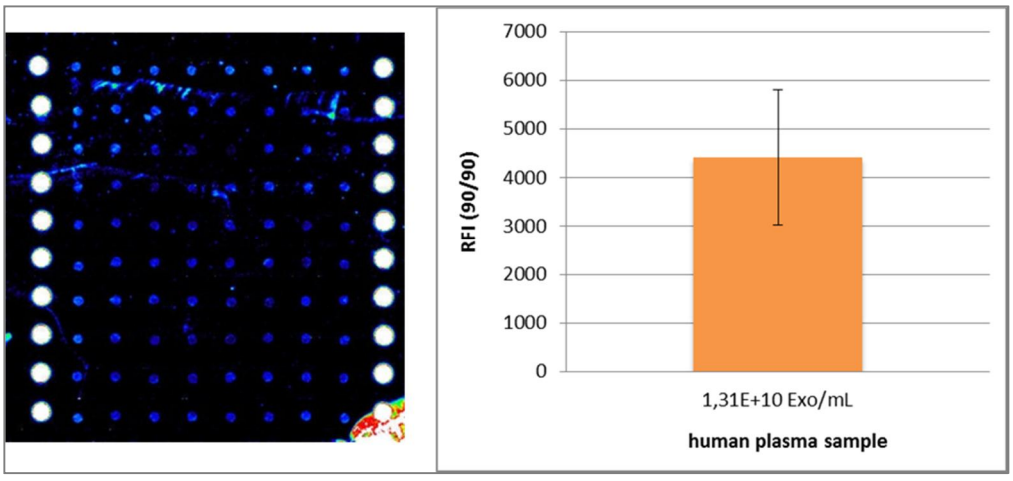

Figure 7.14 – Fluorescence detection (at 90% laser power and PMT gain) and quantification of corresponding signals from hCD63-expressing exosomes in human plasma sample.

It is noticeable how, at comparable exosomes concentration of about E+10 particles/mL, the signals from exosomes in plasma are lower than the signals detected for samples purified from cell culture and resuspended in PBS. In the case of plasma samples it was necessary to increase the laser power in order to improve the signal-to-noise ratio. **Figure 7.15** reports the comparison of fluorescence detection when using 90% laser power and PMT gain for both plasma and standard exosome preparations. In this latter case signals are more than ten times higher, most likely due to the presence of many proteins and factors in the unpurified plasmawhich prevent the efficient binding of hCD63-positive vesicles, making it a very complex buffer.

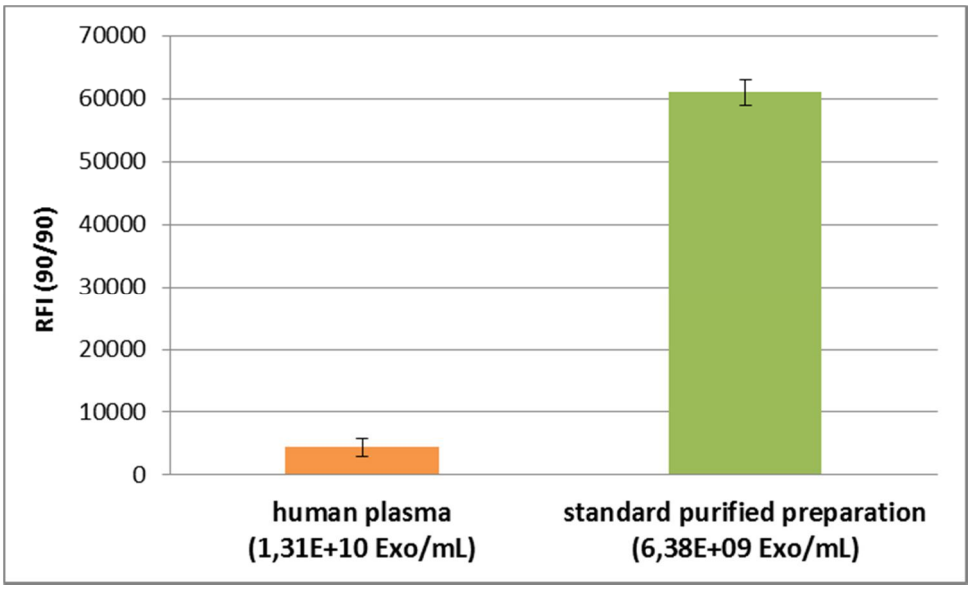

Figure 7.15 - Fluorescence detedction (at 90% laser power and PMT gain) of exosomes incubated overnight in static conditions at comparable concentration, as estimated by NanoSight measurements, respectively 1,31E+10 particles/mL in human plasma and 6,38E+09 particles/mL in the standard purified preparation. Orange bar corresponds to signals from exosomes in human plasma sample, while the green bar shows the intensity of signals from the standard purified exosome preparation. It is evident that purification removes many proteins and factors which may interact with printed antibodies, preventing the capture of target vesicles.

7.3 - CONCLUSIONS

Exosomes are small vesicles, defined based on their size (40–100 nm) and density (1.12-1.19 g/ml), released during cell differentiation as a consequence of multivesicular endosome fusion with the plasma membrane. These vesicles, enriched in several cell-derived factors such as proteins like the tetraspanin CD63 [Record et al., 2011], have been isolated from different body fluids. In particular, many cells of the nervous system have been shown to release extra-cellular vesicles (EVs), implicating their active roles in development, function, and pathologies of this system and, more specifically, exosomes from CSF can be considered as carriers of biomarkers for neurological disorders [Lachenal et al., 2011].

Up to now, due to their physical properties, it is very difficult to distinguish and characterize exosomes among all EVs in biological samples and for these reasons a major ongoing challenge is to establish methods to discriminate between exosomes and other types of vesicles [Bobrie et al., 2011]. As a consequence, a method to simultaneously detect, size and phenotype intact EVs is needed, by combining both accurate qualitative and quantitative analysis. The present study shows an innovative microarray platform which combines the information from label-free conventional and Single Particle IRIS with the fluorescence-based detection in order to analyse exosomes without disrupting their membranes.

Exosomes from standard preparations of purified vesicles from human fibroblast cell culture were at first analyzed by NTA; then vesicles have been characterized through both direct and sandwich immunoassay formats. The monoclonal antibody against the biomarker hCD63, clone H5C6 from BioLegend, was chosen for its specificity and affinity to the target and was then used for both capture and detection of hCD63-positive vesicles. Conventional IRIS measurements allowed to quantify the total amount of biomaterial on each spot of interest, which means the amount of vesicles captured by the printed antibodies. Moreover, these vesicles were also detected as

single nanoparticles using SP-IRIS, showing a size distribution between 60 and 100 nm which confirmed their being exosomes. Further SP-IRIS and fluorescence detection of hCD63 biomarker proved their identity and the vesicle integrity.

Tests were performed on human plasma samples, in order to validate the detection tool also when exosomes are in a more complex matrix. Sandwich fluorescence-based immunoassays allowed the detection of hCD63-expressing nano-vesicles. However, further studies will aim at multiplexing the assay, searching at the same time for different biomarkers expressed on the surface of exosomes while characterizing them by the size distribution of bound particles.

APPENDIX

Research paper publications regarding the development of protein microarrays for diagnostics applications are here reported:

- Cretich M., Torrisi M., Daminelli S., **Gagni P.**, Plavisch L. and Chiari M., *Flow-through, viral co-infection assay for resource-limited settings*. Talanta (2014), *in press*.

- Cretich M., Galati C., Renna L., Condorelli G.G., **Gagni P.** and Chiari M., *Characterization of a new fluorescence-enhancing substrate for microarrays with femtomolar sensitivity*. Sensors and Actuators B Chemical (2014), 192, 15–22.

- Cretich M., Sola L., **Gagni P.** and Chiari M., *Novel fluorescent microarray platforms: a case study in neurodegenerative disorders*. Expert Review of Molecular Diagnostics (2013), 13(8), 863-73.

- **Gagni P.**, Sola L., Cretich M. and Chiari M., *Development of a high-sensitivity immunoassay for amyloid-beta 1-42 using a silicon microarray platform*. Biosensors & bioelectronics (2013), 47C, 490-495.

- Sola L., **Gagni P.**, Cretich M. and Chiari M., *Surface immobilized hydrogels as versatile reagent reservoirs for microarrays*. Journal of immunological methods (2013), 391(1-2), 95-102.

- Peri C., **Gagni P.**, Combi F., Gori A., Chiari M., Longhi R., Cretich M. and Colombo G., *Rational Epitope Design for Protein Targeting*. ACS Chemical Biology (2012); 8(2), 397-404.

REFERENCES

Al-Nedawi K., Meehan B. and Rak J.,*Microvesicles: messengers and mediators of tumor progression*. Cell Cycle (**2009**), 8, 2014–2018.

Alonso R., Rodriguez M.C., Pindado J., Merino E., Merida I. and Izquierdo M.,*Diacylglycerol kinase alpha regulates the secretion of lethal exosomes bearing Fas ligand during activation-induced cell death of T lymphocytes*. J Biol Chem (**2005**), 280, 28439–28450.

Amzallag N., Passer B.J., Allanic D., Segura E., Théry C., Goud B., Amson R. and Telerman A.,*TSAP6 facilitates the secretion of translationally controlled tumor protein/histamine-releasing factor via a nonclassical pathway*. J. Biol. Chem. (**2004**), 279, 46104-46112.

An K., Klyubin I., Kim Y., Jung J.H., Mably A.J., O'Dowd S.T., Lynch T., Kanmert D., Lemere C.A., Finan G.M., Park J.W., Kim T.-W., Walsh D.M., Rowan M.J. and Kim J.-H., *Exosomes neutralize synaptic-plasticity-disrupting activity of Aβ assemblies in vivo*. Mol. Brain. (**2013**), 6, 47. DOI: 10.1186/1756-6606-6-47.

Andre F., Schartz N.E., Movassagh M., Flament C., Pautier P., Morice P., Pomel C., Lhomme C., Escudier B., Le Chevalier T., Tursz T., Amigorena S., Raposo G., Angevin E. and Zitvogel L.,*Malignant effusions and immunogenic tumour-derived exosomes*. Lancet (**2002**), 360, 295-305.

Angenendt P., *Progress in protein and antibody microarray technology*. Drug Discov.Today(**2005**), 10, 503-511.

Ammar M., Smadja C., Giang Thi Phuong L., Azzouz M., Vigneron J., Etcheberry A., Taverna M. and Dufour-Gergam E.,*A new controlled concept of immune-sensing platform for specific detection of Alzheimer's biomarkers*. Biosensors & bioelectronics (**2013**), 40, 329-325.

Balboni I., Chan S.M., Kattah M., Tenenbaum J.D., Butte A.J. and Utz P.J., *Multiplexed protein array platforms for analysis of autoimmune diseases*.Annual Review of Immunology (**2006**), 24, 391-418.

Bard M.P., Hegmans J.P., Hemmes A., Luider T.M., Willemsen R., Severijnen L.A., van Meerbeeck J.P., Burgers S.A., Hoogsteden H.C. and Lambrecht B.N.,*Proteomic analysis of*

exosomes isolated from human malignant pleural effusions. Am. J. Respir. Cell Mol. Biol. (**2004**), 31, 114-121.

Batra D., Vogt S., Laible P.D. and Firestone M.A., *Self-assembled, mesoporous polymeric networks for patterned protein arrays*. Langmuir (**2005**), 21, 10301–10306.

Bauer D.C., Hunter D.J., Abramson S.B., Attur M., Corr M., Felson D., Heinegard D., Jordan J.M., Kepler T.B., Lane N.E., Saxne T, Tyree B. and Kraus V.B.,*Classification of osteoarthritis biomarkers: a proposed approach*. Osteoarthritis Cartilage (**2006**), 14, 723–727.

BierF.F. and Schumacher S., *Integration in Bioanalysis: Technologies for Point-of-Care Testing.*Adv Biochem Eng Biotechnol (**2013**), 133, 1–14. DOI: 10.1007/10_2012_164.

BiswasA., Wang T. and Biris A.S.,*Single metal nanoparticle spectroscopy: optical characterization of individual nanosystems for biomedical applications*. Nanoscale (**2010**), 2, 1560–1572.

Blackburn J.M. and Hart D.J.,*Fabrication of protein function microarrays for systems-oriented proteomic analysis.* Methods in Molecular Biology (**2005**), 310, 197–216.

Blanchard N., Lankar D., Faure F., Regnault A., Dumont C., Raposo G. and Hivroz C.,*TCR activation of human T cells induces the production of exosomes bearing the TCR/CD3/zeta complex*. J. Immunol. (**2002**), 168, 3235-3241.

Blennow K, Hampel H, Weiner M and Zetterberg H., *Cerebrospinal fluid and plasma biomarkers in Alzheimer disease*.Nat. Rev. Neurol. (**2010**), 6, 131–144.

Bobrie A., Colombo M., Raposo G. and Théry C., *Exosome secretion: molecular mechanism and roles in immune response*. Traffic (**2011**), 12, 1659-1668. DOI: 10.1111/j.1600-0854.2011.01225.x

Bohm D., Keller K., Boehm N., Lebrecht A., Schmidt M., Kolbl H. and Grus F.H., *Antibody microarray analysis of the serum proteome in primary breast cancer patients*. Cancer Biol. Ther. (**2011**), 12, 772.

Boyer D., Tamarat P., Maali A., Lounis B. and Orrit M., *Photothermal imaging of nanometer-sized metal particles among scatterers.* Science(**2002**), 297, 1160.

Brandenburg A., Curdt F., Sulz G., Ebling F., Nestler J., Wunderlich K. and Michel D.,*Biochip readout system for point-of-care applications.* Sens Actuators B (**2009**), 139, 245–251.

Buchhave P., Minthon L., Zetterberg H., Wallin A.K., Blennow K. and Hansson O., *Cerebrospinal fluid levels of β-amyloid 1-42, but not of tau, are fully changed already 5 to 10 years before the onset of Alzheimer dementia*. Arch. Gen. Psychiatry (**2012**), 69, 98–106.

Caby M.P., Lankar D., Vincendeau-Scherrer C., Raposo G. and Bonnerot C., *Exosomal like vesicles are present in human blood plasma*. Int. Immunol. (**2005**), 17, 8.

CamussiG., Deregibus M.C., Bruno S., Cantaluppi V., Biancone L., *Exosomes/microvesicles as a mechanism of cell-to-cell communication*. Kidney Int. (**2010**), 78, 838–848.

Carlsson A., Wingren C., Kristensson M., Rose C., Ferno M., Olsson H., Jernstrom H., Ek S., Gustavsson E., Ingvar C., Ohlsson M., Peterson C., Borrebaeck C.A.K., *Molecular serum portraits in patients with primary breast cancer predict the development of distant metastases*. PNAS (**2011**), 108, 14252.

Carter S. B., *Principles of cell motility: the direction of cell movement and cancer invasion*. Nature (**1965**), 208, 1183–1187.

Cedazo-Minguez A. and Winblad B.,*Biomarkers of Alzheimer's disease and other forms of dementia: clinical needs, limitations and future aspects*. Exp. Gerontol. (**2010**), 45, 5–14.

Chaput N., Taieb J., Andre F. and Zitvogel L., *The potential of exosomes in immunotherapy*, Exp. Opin. Biol. Ther. (**2005**), 5, 737–747.

Charles P.T., Goldman E.R., Rangasammy J.G., Schauer C.L., Chen M.S. and Taitt C.R., *Fabrication and characterization of 3D hydrogel microarrays to measure antigenicity and antibody functionality for biosensor applications*. Biosens. Bioelectron. (**2004**), 20, 753.

Chen S., Zheng J., Li L. and Jiang S., *Strong resistance of phosphorylcholine self-assembled monolayers to protein adsorption: insights into nonfouling properties of zwitterionic materials*. J. Am. Chem. Soc. (**2005**), 127, 14473–14478.

Chiari M., Cretich M., Corti A., Damin F., Pirri G. and Longhi R.,*Peptide microarrays for the characterization of antigenic regions of human chromogranin A*. Proteomics (**2005**), 5 , 3600–3603.

Clark C.M., Pontecorvo M.J., Beach T.G., Bedell B.J., Coleman R.E., Doraiswamy P.M., Fleisher A.S., Reiman E.M., Sabbagh M.N., Sadowsky C.H., Schneider J.A., Arora A., Carpenter A.P., Flitter M.L., Joshi A.D., Krautkramer M.J., Lu M., Mintun M.A. and Skovronsky D.M., *Cerebral PET with florbetapir compared with neuropathology at autopsy for detection of neuritic amyloid beta plaques: a prospective cohort study*. Lancet Neurol (**2012**), 11, 669–78.

Clayton A., Court J., Navabi H., Adams M., Mason M.D., Hobot J.A., Newman G.R. and Jasani B.,*Analysis of antigen presenting cell derived exosomes, based on immunomagnetic isolation and flow cytometry*. J. Immunol. Methods (**2001**), 247, 163-174.

Collins F.S.,*Medical and societal consequences of the human genome project*. New England J Med (**1999**), 341, 28–37.

Collins F.S. and McKusik V.A.,*Implications of the human genome project for medical sciences, Opportunities for medical research*. JAMA (**2001**), 285(5), 540–544.

Cretich M., Pirri G., Damin F., Solinas I. and Chiari M., *A new polymeric coating for protein microarrays*. Analytical Biochemistry(**2004**), 332, 67–74.

Cretich M., Damin F., Pirri G. and Chiari M.,*Protein and peptide arrays: recent trends and new directions*. Biomolecular Engineering (**2006**), 23, 77–88.

Cretich M., Sedini V., Damin F., Di Carlo G., Oldani C. and Chiari M., *Functionalization of poly(dimethylsiloxane) by chemisorption of copolymers: DNA microarrays for pathogen detection*. Sensors and Actuators B (**2008**), 132, 258–264.

Cretich M., Di Carlo G., Giudici C., Pokoj S., Lauer I., Scheurer S. and Chiari M., *Detection of allergen specific immunoglobulins by microarrays coupled to microfluidics*. Proteomics (**2009**), 9, 2098–2107.

Cretich M., Di Carlo G., Longhi R., Gotti C., Spinella N., Coffa S., Galati C., Renna L. and Chiari M., *High Sensitivity Protein Assays on Microarray Silicon Slides*.Analytical Chemistry (**2009b**), 81, 5197–5203.

CretichM., BredaD., Damin F., BorghiM., Sola L., Unlu S.M., BurasteroS.E. and Chiari M., *Allergen microarrays on high-sensitivity silicon slides*. Analytical and Bioanalytical Chemistry (**2010**), 398, 1723–1733.

Cretich M., Sedini V., Damin F., Pelliccia M., Sola L. and Chiari M., *Coating of nitrocellulose for colorimetric DNA microarrays.* Anal. Biochem. (**2010b**), 397, 84-88.

CretichM., Bagnati M., Damin F., Sola L. and Chiari M.,*Overcoming mass transport limitations to achieve femtomolar detection limits on silicon protein microarrays*.Analytical Biochemistry (**2011**), 418,164–166.

CretichM., Reddington A., Monroe M., Bagnati M., Damin F., Sola L., Unlu S.M. and Chiari M.,*Silicon biochips for dual label-free and fluorescence detection: Application to protein microarray development*.Biosensors and Bioelectronics (**2011b**), 26, 3938-3943.

Cretich M., Monroe M.R., Reddington A., Zhang X.R., Daaboul G.G., Damin F., Sola L., Unlu M.S. and Chiari M.,*Interferometric silicon biochips for label and label-free DNA and protein microarrays*. Proteomics (**2012**), 12, 2963-2977.

Cretich M., Sola L.,Gagni P. and Chiari M., *Novel fluorescent microarray platforms: a case study in neurodegenerative disorders*. Expert review of molecular diagnostics (**2013**), 13(8), 863-873. DOI: 10.1586/14737159.2013.849574.

Cretich M., Galati C., Renna L., Condorelli G.G., Gagni P. and Chiari M., Characterization of a new fluorescence-enhancing substrate for microarrays with femtomolar sensitivity. Sensors and Actuators B (**2014**), 192, 15– 22.

Crowther J. R.,*ELISA: Theory and Practice*. Humana press (**1995**), New Jersey.

Cullen V.C., Fredenburg R.A., Evans C., Conliffe P.R. and Solomon M.E.,*Development and advanced validation of an optimized method for the quantitation of Aβ42 in human cerebrospinal fluid*. AAPS Journal (**2012**), 14, 510-518.

Cummings J.L.,*Biomarkers in Alzheimer's disease drug development*. Alzheimers Dement (**2011**), 7, e13–44.

DaaboulG.G., Yurt A., Zhang X., Hwang G.M., Goldbergand B.B. and Unlu M.S.,*High-throughput detection and sizing of individual low-index nanoparticles and viruses for pathogen identification*. Nano Lett.(**2010**), 10, 4727–4731.

Daaboul G.G., Vedula R.S., Ahn S., Lopez C.A., Reddington A., Ozkumur E. and Unlu M.S., LED-based Interferometric Reflectance Imaging Sensor for quantitative dynamicmonitoring of biomolecular interactions. Biosensors and Bioelectronics (**2010**), 4962-4969.

Daaboul G.G., Lopez C.A., Chinnala J., Goldberg B.B., Connor J.H. and Unlu M.S., *Digital sensing and sizing of Vesicular Stomatitis Virus Pseudotypes in complex media: a model for Ebola and Marburg detection*. ACS nano (**2014**), 8(6), 6047-6055.

de Almeida S.M., Shumaker S.D., LeBlanc S.K., Delaney P., MarquieBeck J., Ueland S., Alexander T. and Ellis R.J., *Incidence of post-dural puncture headache in research volunteers.* Headache (**2011**), 51, 1503–1510.

de Gassart A., Geminard C., Fevrier B., Raposo G. and Vidal M.,*Lipid raft-associated protein sorting in exosomes*. Blood (**2003**), 102, 4336-4344.

de JesusA.J., Kastelowitz N. and Yin H.,*Changes in lipid density induce membrane curvature.* RSC Adv. (**2013**), 3, 13622.

Denzer K., Kleijmeer M.J., Heijnen H.F., Stoorvogel W. and Geuze H.J., *Exosome: from internal vesicle of the multivesicular body to intercellular signaling device*.J. Cell Sci. (**2000**), 113(19), 3365–3374.

Desai A.K. and Grossberg G.T., *Diagnosis and treatment of Alzheimer's disease*. Neurology (**2005**), 64, S34–S39.

Diamandis E.P. and Christopoulos T.K. (Editors.), *Immunoassays*. Academic Press (**1996**).

Dilly S.J., Beecham M.P., Brown S.P., Griffin J.M., Clark A.J., Griffin C.D., Marshall J., Napier R.M., Taylor P.C. and Marsh A., *Novel tertiary amine oxide surfaces that resist nonspecific protein adsorption*. Langmuir (**2006**), 22, 8144–8150.

Djoba Siawaya J.F., Roberts T., Babb C., Black G., Golakai H.J., Stanley K., Bapela N.B., Hoal E., Parida S., van Helden P. and Walzl G., *An evaluation of commercial fluorescent bead-based luminex cytokine assays*. PLoS One (**2008**), 3, e2535.

DragovicR.A., Gardiner C., Brooks A.S., Tannetta D.S., Ferguson D.J.P., Hole P., Carr B., Redman C.W.G., Harris A.L., Dobson P.J., Harrison P. and Sargent I.L.,*Sizing and phenotyping of cellular vesicles using Nanoparticle Tracking Analysis*. Nanomedicine (**2011**), 7, 780–788.

Ellington A.A., Kullo I.J., Bailey K.R. and Klee G.G., *Antibody-based protein multiplex platforms: technical and operational challenges*. Clin. Chem. (**2010**), 56, 186-193.

Espina V., Woodhouse E.C., Wulfkuhle J., Asmussen H.D., Petricoin E.F. and Liotta L.A., *Protein microarray detection strategies: focus on direct detection technologies.* J. Immunol. Methods (**2004**), 290, 121-133.

Ewis A.A., Zhelev Z., Bakalova R., Fukuoka S., Shinohara Y., Ishikawa M. and Baba Y., *A history of microarrays in biomedicine*. Expert. Rev. Mol. Diagn. (**2005**), 5, 315.

Fagan A.E. and Perrin R.J., Upcoming candidate cerebrospinal fluid biomarkers of Alzheimer's disease. Biomarkers Med (**2012**), 6, 455-476.

Failla A.V., Qian H., Qian H., Hartschuh A. and Meixner A.J., *Orientational imaging of subwavelength Au particles with higher order laser modes*. Nano Lett.(**2006**), 6, 1374–1381.

Fall B.I. and Niessner R., Detection of known allergen-specific IgE antibodies by immunological methods, Methods Mol Biol. (**2009**), 509, 107-22.

Fauré J., Lachenal G., Court M., Hirrlinger J., Chatellard-Causse C., Blot B., Grange J., Schoehn G., Goldberg Y., Boyer V., Kirchhoff F., Raposo G., Garin J. and Sadoul R.,Exosomes are released by cultured cortical neurons. Mol. Cell. Neurosci. (**2006**), 31, 642-648.

Fevrier B., Vilette D., Archer F., Loew D., Faigle W., Vidal M., LaudeH. and Raposo G., Cells release prions in association with exosomes. Proc. Natl. Acad. Sci. U.S.A. (**2004**), 101, 9683-9688.

Forsberg A., Engler H., Almkvist O., Blomquist G., Hagman G., Wall A., Ringheim A., Langstrom B. and Nordberg A., PET imaging of amyloid deposition in patients with mild cognitive impairment. Neurobiol Aging (**2008**), 29, 1456–1465.

Fouqué B., Schaack B., Obeïd P., Combe S., Getin S., Barritault P., Chanton P. and Chatelain F., Multiple wavelength fluorescence enhancement on glass substrates for biochip and cell analyses. Biosens. Bioelectron. (**2005**), 20, 2335-2340.

Fung E.T., Protein Arrays: Methods and Protocols. Methods in Molecular Biology, Vol. 264(**2004**), Humana Press, Totowa.

Frey H.J., Mattila K.M., Korolainen M.A. and Pirttila T., Problems associated with biological markers of Alzheimer's disease. Neurochemical Res. (**2005**), 30, 1501–1510.

GagniP., Sola L., Cretich M. and Chiari M., Development of a high-sensitivity immunoassay for amyloid-beta 1–42 using a silicon microarray platform. Biosensors and Bioelectronics (**2013**), 47, 490–495.

Gaster R.S., Hall D.A. and Wang S.X., Autoassembly protein arrays for analyzing antibody cross-reactivity. Nano Lett. (**2011**), 11, 2579.

Genius J., Klafki H., Benninghoff J., Esselmann H. and Wiltfang J., Current application of neurochemical biomarkers in the prediction and differential diagnosis of Alzheimer's disease and other neurodegenerative dementias. Eur Arch Psychiatry Clin Neurosci (**2012**), 262(2), S71-77. DOI:10.1007/s00406-012-0362-3.

Gercel-Taylor C., Atay S., Tullis R.H., Kesimer M. and Taylor D.D., *Nanoparticle analysis of circulating cell-derived vesicles in ovarian cancer patients*. Analytical Biochemistry (**2012**), 428, 44-53.

Ghidoni R., Paterlini A., Albertini V., Glionna M., Monti E., Schiaffonati L., Benussi L., Levy E. and Binetti G.,*Cystatin C is released in association with exosomes: a new tool of neuronal communication which is unbalanced in Alzheimer's disease*. Neurobiol. Aging (**2011**), 32, 1435-1442.

Gonzalez R.M., Seurynck-Servoss S.L., Crowley S.A., Brown M., Omenn G.S., Hayes D.F. and Zangar R.C., Development and validation of sandwich ELISA microarrays with minimal assay interference. J. Proteome Res. (**2008**), 7, 2406.

Groll J., Amirgoulova E.V., Ameringer T., Heyes C.D., Röcker C., Nienhaus G.U. and Möller M.,*Biofunctionalized, ultrathin coatings of cross-linked star-shaped poly(ethylene oxide) allow reversible folding of immobilized proteins*. Journal of the American Chemical Society (**2004**), 126, 4234 – 4239.

GyorgyB., Szabó T.G., Pásztói M., Pál Z., Misják P., Aradi B., László V., Pállinger É., Pap E., Kittel Á., Nagy G., Falus A. andBuzàs E.I., Membrane vesicles, current state-of-the-art: emerging role of extracellular vesicles. Cell. Mol. Life Sci. (**2011**), 68, 2667–2688.

Hampel H., Burger K., Teipel S.J., Bokde A.L., Zetterberg H. and Blennow K.,*Core candidate neurochemical and imaging biomarkers of Alzheimer's disease*. Alzheimers Dement (**2007**), 4, 38–48.

Hampel H., Frank R., Broich K., Teipel S.J. Katz R.G., Hardy J., Herholz K., Bokde A.L., Jessen F., Hoessler Y.C., Sanhai W.R., Zetterberg H., Woodcock J. and Blennow K., *Biomarkers for Alzheimer's disease: academic, industry and regulatory perspectives*. Nat. Rev. Drug Discov. (**2010**), 9, 560–574.

Hampel H., Lista S. and Khachaturian Z.S.,*Development of biomarkers to chart all Alzheimer's disease stages: the royal road to cutting the therapeutic Gordian Knot*. Alzheimers Dement (**2012**), 8, 312–336.

Harding C., Heuser J. and Stahl P., *Receptor-mediated endocytosis of transferrin and recycling of the transferrin receptor in rat reticulocytes.* J. Cell Biol. (**1983**), 97, 329–339.

Harding C., Heuser J. and Stahl P., *Endocytosis and intracellular processing of transferrin and colloidal gold-transferrin in rat reticulocytes: demonstration of a pathway for receptor shedding.* Eur. J. Cell Biol. (**1984**), 35, 256–263.

Hatzakis N.S., Bhatia V.K., Larsen J., Madsen K.L., Bolinger P.-Y., Kunding A.H., Castillo J., Gether U., Hedegàrd P. and Stamou D.,*How curved membranes recruit amphipathic helices and protein anchoring motifs*. Nat. Chem. Biol. (**2009**), 5, 835–841.

Hegmans J.P., Bard M.P., Hemmes A., Luider T.M., Kleijmeer M.J., Prins J.B., Zitvogel L., Burgers S.A., Hoogsteden H.C. and Lambrecht B.N.,*Proteomic analysis of exosomes secreted by human mesothelioma cells*. Am. J. Pathol. (**2004**), 164, 1807-1815.

Heijnen H.F., Schiel A.E., Fijnheer R., Geuze H.J. and Sixma J.J.,*Activated platelets release two types of membrane vesicles: Microvesicles by surface shedding and exosomes derived from exocytosis of multivesicular bodies and alpha-granules*. Blood (**1999**), 94, 3791-3799.

Henley S.M.D., Bates G.P. and Tabrizi S.J., *Biomarkers for neurodegenerative diseases*. Curr. Opin. Neurol. (**2005**), 18, 698–705.

Henriksen K., Wang Y., Sorensen M.G., Barascuk N., Suhy J., Pedersen J.T., Duffin K.L., Dean R.A., Pajak M., Christiansen C., Zheng Q. and Karsdal M.A.,*An enzyme-generated fragment of tau measured in serum shows aninverse-correlation to cognitive function.* PLoS One (**2013**), 8(5), e64990.

Henriksen K., O'Bryant S.E., Hampel H., Trojanowskid J.Q., Montine T.J., Jeromin A., Blennowg K., Lönneborgh A., Wyss-Coray T., Soares H., Bazenet C., Sjögren M., Hu W., Lovestone S., Karsdal M.A. and Weiner M.W., *The future of blood-based biomarkers for Alzheimer's disease - Review Article*. Alzheimer's & Dementia (**2014**), 10, 115–131.

Ho L., Fivecoat H., Wang J. and Pasinetti G.M., *Alzheimer's disease biomarker discovery in symptomatic and asymptomatic patients: Experimental approaches and future clinical applications*. Exp. Gerontol. (**2010**), 45, 15–22.

Hoffmann J., Groll J., Heuts J., Rong H., Klee D., Ziemer G., Möller M. and Wendel H.P., *Blood cell and plasma protein repellent properties of star-PEG-modified surfaces*.Journal of Biomaterial Science, Polymer(**2006**), 17, 985 – 996.

Holloway A.J., van Laar R.K., Tothill R.W. and Bowtell D.D., *Options available--from start to finish--for obtaining data from DNA microarrays II*. Nature Genetics (**2002**), 32, 481–489.

Holmes D.L. and Stellwagen N.C., *Estimation of polyacrylamide-gel pore size from Ferguson plots of linear DNA fragments 2. Comparison of gels with different cross-linker concentrations, added agarose and added linear polyacrylamide*. Electrophoresis (**1991**), 12, 612.

Hugel B., Martinez M.C., Kunzelmann C. and Freyssinet J.M.,*Membrane microparticles: two sides of the coin*. Physiology (**2005**), 20, 22–27.

Humpel C., *Identifying and validating biomarkers for Alzheimer's disease*. Trends in Biotechnology (**2011**),29(1), 26-32.

HuntH.K. and Armani A.M., *Label-free biological and chemical sensors*.Nanoscale (**2010**), 2, 1544–1559.

IgnatovichF.V. and Novotny L., *Real-time and background-free detection of nanoscale particles*. Phys. Rev. Lett. (**2006**), 96, 013901.

Jacobsen V., Stoller P., Brunner C., Vogel V. and Sandoghdar V., *Interferometric optical detection and tracking of very small gold nanoparticles at a water-glass interface*. Opt. Express, (**2006**), 14, 405–414.

Jeter C.B., Hergenroeder G.W., Hylin M.J., Redell J.B., Moore A.N. and Dash P.K., *Biomarkers for the diagnosis and prognosis of mild traumatic brain injury/concussion*. J Neurotrauma (**2013**), 30(8), 657–670.

Jørgensen M., Bæk R., Pedersen S., Søndergaard E.K.L., Kristensen S.R. and Varming K., *Extracellular Vesicle (EV) Array: microarray capturing of exosomes and other extracellular vesicles for multiplexed phenotyping*. J. Extracell. Vesicles (**2013**), 2, 20920.

Kambhampati D., *Protein Microarray Technology.* Wiley-VCH(**2003**), Weinheim.

Kane R.S., Deschatelets P. and Whitesides G.M., *Kosmotropes Form the Basis of Protein-Resistant Surfaces*. Langmuir (**2003**), 19, 2388–2391.

Kang J.H., Vanderstichele H., Trojanowski J.Q. and Shaw L.M., *Simultaneous analysis of cerebrospinal fluid biomarkers using microsphere-based xMAP multiplex technology for early detection of Alzheimer's disease*. Methods (**2012**), 56, 484-493.

Karsdal M.A., Henriksen K., Leeming D.J., Mitchell P., Duffin K., Barascuk N., Klickstein L., Aggarwal P., Nemirovskiy O., Byrjalsen I., Qvist P., Bay-Jensen A.C., Dam E.B., Madsen S.H. and Christiansen C.,*Biochemical markers and the FDA Critical Path: how biomarkers may contribute to the understanding of pathophysiology and provide unique and necessary tools for drug development*. Biomarkers (**2009**), 14(3), 181–202.

Kastelowitz N. and Yin H., *Exosomes and Microvesicles: Identification and Targeting By Particle Size and Lipid Chemical Probes.* ChemBioChem (**2014**), 15, 923–928.

Kaufmann H., Bailey J.E. and Fussenegger M., *Use of antibodies for detection of phosphorylated proteins separated by two-dimensional gel electrophoresis.*Proteomics (**2001**), 1, 194 –199.

Kim S.H., Tamrazi A., Carlson K.E., Katzenellenbogen J.A., *A proteomic microarray approach for exploring ligand-initiated nuclear hormone receptor pharmacology, receptor selectivity, and heterodimer functionality*. Molecular and Cellular Proteomics (**2005**), 4(3), 267–277.

Klafki H.W., Staufenbiel M., Kornhuber J. and Wiltfang J., *Therapeutic approaches to Alzheimer's disease*. Brain (**2006**), 129, 2840-2855.

Klunk W.E. and Mathis C.A., *The future of amyloid-beta imaging: a tale of radionuclides and tracer proliferation.* Curr Opin Neurol (**2008**), 21, 683–687.

Knezevic V., Leethanakul C., Bichsel V.E., Worth J.M., Prabhu V.V., Gutkind J.S., Liotta L.A., Munson P.J., Petricoin E.F. and Krizman D.B., *Proteomic profiling of the cancer microenvironment by antibody arrays.* Proteomics (**2001**), 1, 1271-1278.

Ko K.S., Jaipuri F.A. and Pohl N.L., *Fluorous-based carbohydrate microarrays*. Journal of the American Chemical Society(**2005**), 127, 13162–13163.

Koyama A., Okereke O.I., Yang T., Blacker D., Selkoe D.J. and Grodstein F., *Plasma amyloid-beta as a predictor of dementia and cognitive decline: a systematic review and meta-analysis*. Arch Neurol (**2012**), 69, 824–831.

Kukar T., Eckenrode S., Gu Y., Lian W., Megginson M., She J.X. and Wu D., *Protein microarrays to detect protein-protein interactions using red and green fluorescent proteins*. Anal. Biochem. (**2002**), 306, 50-54.

Kung L.A., Tao S.C., Qian J., Smith M.G., Snyder M. and Zhu H., *Global analysis of the glycoproteome in Saccharomyces cerevisiae reveals new roles for protein glycosylation in eukaryotes*. Mol. Syst. Biol. (**2009**), 5, 308.

Kusnezow W., Syagailo Y.V., Ruffer S., Baudenstiel N., Gauer C., Hoheisel J.D., Wild D. and Goychuk I., *Optimal design of microarray immunoassays to compensate for kinetic limitations: theory and experiment*. Molecular & Cellular Proteomics (**2006**), 5, 1681-1696.

Lachenal G., Pernet-Gallay K., Chivet M., Hemming F.J., Belly A., Bodon G., Blot B., Haase G., Goldberg Y. and Sadoul R., *Release of exosomes drom differentiated neurons and its regulation by synaptic glutamatergic activity*. Mol. Cell. Neurosci. (**2011**), 46(2), 409-418. DOI: 10.1016/j.mcn.2010.11.004.

Lai R.C., Arslan F., Lee M.M., Sze N.S., Choo A., Chen T.S., Salto-Tellez M., Timmers L., Lee C.N., El Oakley R.M., Pasterkamp G., de Kleijn D.P. and Lim S.K., *Exosome secreted by MSC reduces myocardial ischemia/reperfusion injury*, Stem Cell Res. (**2010**), 4, 214–222.

Lamparski H.G., Metha-Damani A., Yao J.Y., Patel S., Hsu D.H., Ruegg C. and Le Pecq J.B*., Production and characterization of clinical grade exosomes derived from dendritic cells.* J. Immunol. Methods (**2002**), 270, 211-226.

Laske C., *Clinical and biomarker changes in Alzheimer's disease*. New Eng J Med (**2012**), 367, 2050.

Laulagnier K., Motta C., Hamdi S., Roy S., Fauvelle F., Pageaux J. F., Kobayashi T., Salles J. P., Perret B. and Bonnerot C., *Mast cell- and dendritic cell-derived exosomes display a specific lipid composition and an unusual membrane organization*. Biochem. J. (**2004**), 380, 161–171.

Laulagnier K., Vincent-Schneider H., Hamdi S., Subra C., Lankar D. and Record M., *Characterization of exosome subpopulations from RBL-2H3 cells using fluorescent lipids*. Blood Cells Mol Dis (**2005**), 35, 116–121.

Lawrie A.S., Albanyan A., Cardigan R.A., Mackie I.J. and Harrison P., *Microparticle sizing by dynamic light scattering in fresh-frozen plasma*. Vox Sang. (**2009**), 96, 206–212.

Lee H.J., Yan Y., Marriott G. and Corn R.M., *Quantitative functional analysis of protein complexes on surfaces*. Journal of Physiology (**2005**), 563, 61–71.

Lee T.H., D'Asti E., Magnus N., Al-Nedawi K., Meehan B. and Rak J., *Microvesicles as mediators of intercellular communication in cancer--the emerging science of cellular 'debris'.* Semin. Immunopathol. (**2011**), 33, 455–467.

Lespagnol A., Duflaut D., Beekman C., Blanc L., Fiucci G., Marine J.C., Vidal M., Amson R. and Telerman A., *Exosome secretion, including the DNA damage-induced p53-dependent secretory pathway, is severely compromised in TSAP6/Steap3-null mice*. Cell Death Differ (**2008**), 15, 1723–1733.

Lewczuk P., Esselmann H., Otto M., Maler J.M., Henkel A.W., Henkel M.K., Eikenberg O., Antz C., Krause W.-R., Reulbache U., Kornhuber J. and J. Wiltfang, *Neurochemical diagnosis of Alzheimer's dementia by CSF Aβ42, Aβ42/Aβ40 ratio and total tau*. Neurobiology of Aging (**2004**), 25, 273–281.

Li Y., Zhang Y., Qiu F. and Qiu Z., *Proteomic identification of exosomal LRG1: a potential urinary biomarker for detecting NSCLC*. Electrophoresis (**2011**), 32, 1976–1983.

Li H., Bergeron S. and Junncker D., *Microarray-to-microarray transfer of reagents by snapping of two chips for cross-reactivity-free multiplex immunoassays*. Anal. Chem. (**2012**), 84, 4776.

Li J., Llano D.A., Ellis T., LeBlond D., Bhathena A., Jhee S.S., Ereshefsky L., Lenz R. and Waring J.F., *Effect of human cerebrospinal fluid sampling frequency on amyloid-beta levels*. Alzheimers Dement (**2012**), 8, 295–303.

Lindfors K., Kalkbrenner T., Stoller P. and Sandoghdar V., *Detection and spectroscopy of gold nanoparticles using supercontinuum white light confocal microscopy*. Phys. Rev. Lett. (**2004**), 93, 037401.

Logozzi M., De Milito A., Lugini L., Borghi M., Calabro L., Spada M., Perdicchio M., Marino M.L., Federici C., Iessi E., Brambilla D., Venturi G., Lozupone F., Santinami M., Huber V., Maio M., Rivoltini L. and Fais S., *High levels of exosomes expressing CD63 and caveolin-1 in plasma of melanoma patients*. PLoS ONE (**2009**), 4, e5219.

Luk Y.Y., Kato M. and Mrksich M., *TI Self-assembled monolayers of alkanethiolates presenting mannitol groups are inert to protein adsorption and cell attachment*. Langmuir (**2000**), 16, 9604–9608.

Lyman E., Cui H., Voth G.A., *Water under the BAR*. Biophys. J. (**2010**), 99, 1783–1790.

Marquette C.A., Cretich M., Blum L.J. and Chiari M., *Protein microarrays enhanced performance using nanobeads arraying and polymer coating*. Talanta (**2007**), 71, 1312-1318.

Mattsson N., Blennow K. and Zetterberg H., *CSF biomarkers: pinpointing Alzheimer pathogenesis*. Ann NYAcad Sci (**2009**), 1180, 28–35.

Mears R., Craven R.A., Hanrahan S., Totty N., Upton C., Young S.L., Patel P., Selby P.J. and Banks R.E., *Proteomic analysis of melanoma-derived exosomes by twodimensional polyacrylamide gel electrophoresis and mass spectrometry*. Proteomics (**2004**), 4, 4019-4031.

Mendelsohn J.D., Yang S.Y., Hiller J.A., Hochbaum A.I. and Rubner M.F., *Rational design of cytophilic and cytophobic polyelectrolyte multilayer thin films*. Biomacromolecules (**2003**), 4, 96–106.

Michel R., Pasche S., Textor M. and Castner D.G., *Influence of PEG architecture on protein adsorption and conformation*. Langmuir (**2005**), 21, 12327–12332.

Molloy M.P., Phadke N.D., Chen H., Tyldesley R., Garfin D.E., Maddock J.R. and Andrews P.C., *Profiling the alkaline membrane proteome of Caulobacter crescentus with two-dimensional electrophoresis and mass spectrometry*.Proteomics (**2002**), 2, 899–910.

Monroe M., Reddington A., Collins A.D., LaBoda C., Cretich M., Chiari M., Little F.F. and Unlu M.S., *Multiplexed method to calibrate and quantitate fluorescence signal for allergen-specific IgE*. Analytical Chemistry (**2011**), 83, 9485-9491.

Montelione G.T. and Anderson S., *Structural genomics: keystone for a human proteome project*. Nat Struct Biol (**1999**), 6(1), 11–12.

Moorthy J., Burgess R., Yethiraj A., Beebe D., *Microfluidic based platform for characterization of protein interactions in hydrogel nano-environments*. Anal. Chem. (**2007**), 79, 5322.

Morales-Narvaez E., Monton H., Fomicheva A. and Merkoçi A., *Signal enhancement in antibody microarrays using quantum dots nanocrystals: application to potential Alzheimer's disease biomarker screening*. Anal Chem (**2012**), 84, 6821-6827.

Morris J.C., Roe C.M., Grant E.A., Head D., Storandt M., Goate A.M., Fagan A.M., Holtzman D.M. and Mintun M.A., *Pittsburgh compound B imaging and prediction of progression from cognitive normality to symptomatic Alzheimer disease*. Arch Neurol (**2009**), 66, 1469–1475.

Mrksich M., Sigal G.B. and Whitesides G.M., *Surface Plasmon Resonance Permits in Situ Measurement of Protein Adsorption on Self-Assembled Monolayers of Alkanethiolates on Gold*. Langmuir (**1995**), 11, 4383–4385.

Mucke L., *Alzheimer's disease*. Nature (**2009**), 461, 895-897.

Nath N., Hyun J., Ma H. and Chilkoti A., *Surface engineering strategies for control of protein and cell interactions*. Surface Science (**2004**), 570, 98–110.

Noguchi M., Yoshita M., Matsumoto Y., Ono K., Iwasa K. and Yamada M.,*Decreased beta-amyloid peptide42 in cerebrospinal fluid of patients with progressive supranuclear palsy and corticobasal degeneration*. Neurol. Sci. (**2005**), 237, 61–65.

Oh E.S., Mielke M.M., Rosenberg P.B., Jain A., Fedarko N.S., Lyketsos C.G. and Metha P.D., *Comparison of conventional ELISA with electrochemiluminescence technology for detection of amyloid-beta in plasma*. J Alzheimers Dis (**2010**), 21, 769–773.

Oosthuyzen W., Sime N.E.L., Ivy J.R., Turtle E.J., Street J.M., Pound J., Bath L.E., Webb D.J., Gregory C.D., Bailey M.A., Dear J.W., *Quantification of human urinary exosomes by nanoparticle tracking analysis*. J. Physiol. (**2013**), 591, 5833–5842.

Ostuni E., Chapman R.G., Holmlin R.E., Takayama S. and Whitesides G.M., *A survey of structure-property relationships of surfaces that resist the adsorption of protein*. Langmuir (**2001**), 17, 5605–5620.

Özkumur E., Yalçın A., Cretich M., Lopez C.A., Bergstein D.A., Goldberg B.B., Chiari M. and Ünlü M.S., *Quantification of DNA and protein adsorption by optical phase shift.* Biosensors and Bioelectronics (**2009**), 25, 167–172.

Pan B.T., Teng K., Wu C., Adam M. and Johnstone R.M., *Electron microscopic evidence for externalization of the transferrin receptor in vesicular for min sheep reticulocytes*. J. Cell Biol. (**1985**), 101, 942-948.

Patton W. F., *Proteome analysis. II. Protein subcellular redistribution: linking physiology to genomics via the proteome and separation technologies involved*. Journal of Chromatography B (**1999**), 722, 203– 223.

PerezG.V., Pesini P., Allué J.A., Sarasa L., Montanés M., Lacosta A.M., Casabona D., San-José I., Boada M., Tarraga L., Ruiz A and Sarasa M., *Beta-amyloid-17 is a major beta-amyloid fragment isoform in cerebrospinal fluid and blood that shows diagnostic value*. Alzheimers Dement (**2012**), 8(4suppl), P2–40.

Perez-Grijalba V., Pesini P., Monleon I., Boada M., Tarraga L., Ruiz-Laza A., Martinez-Lage P., San-José I. and Sarasa M., *Biomarkers from the amyloid-beta pool in blood are associated with an increased likelihood of suffering from mild cognitive impairment*. J Alzheimers Dis (**2013**), 36, 211–219.

Perez-Pujol S., Marker P.H. and Key N.S., *Platelet microparticles are heterogeneous and highly dependent on the activation mechanism: studies using a new digital flow cytometer*. Cytometry A (**2007**), 71A, 38–45.

Perrin R.J., Fagan A.M. and Holtzman D.M., *Multimodal techniques for diagnosis and prognosis of Alzheimer's disease*.Nature (**2009**), 461, 916-922.

Phizicky E., Bastiaens P.I.H., Zhu H., Snyder M. and Fields S., *Protein analysis on a proteomic scale*. Nature (**2003**), 422, 208-2015.

Pirri G., Damin F., Chiari M., Bontempi E. and Depero L.E., *Characterization of a polymeric adsorbed coating for DNA microarray glass slides*. Analytical Chemistry (**2004**), 76, 1352–1358.

Pisitkun T., Shen R.F. and Knepper M.A., *Identification and proteomic profiling of exosomes in human urine*. Proc. Natl. Acad. Sci. U.S.A. (**2004**), 101, 13368-13373.

Plakhotnik T. and Palm V., *Interferometric signatures of single molecules*. Phys. Rev. Lett. (**2001**), 87, 183602.

Pla-Roca M., Leulmi R.F., Tourekhanova S., Bergeron S., Laforte V., Moreau E., Gosline S.J.C., Bertos N., Hallett M., Park M. and Juncker D., *Antibody colocalization microarray: a scalable technology for multiplex protein analysis in complex samples*. Mol. Cell. Proteomics (**2012**), 4, 11.

Ponnambalam S. and Baldwin S.A., *Constitutive protein secretion from the trans Golgi network to the plasma membrane*. Mol Membr Biol (**2003**), 20, 129–139.

Ponten J. and Stolt L., *Proliferation control in cloned normal and malignant human cells*. Experimental Cell Research (**1980**), 129, 367–375.

Prime K.L. and Whitesides G.M., *Adsorption of proteins onto surfaces containing end-attached oligo(ethylene oxide): A model system using self-assembled monolayers*. Journal of the American Chemical Society, (**1993**), 115, 10714–10721.

Qu Y. and Dubyak G.R., *P2X7 receptors regulate multiple types of membrane trafficking responses and non-classical secretion pathways*. Purinergic Signal (**2009**), 5, 163–173.

Rajendran L., Honsho M., Zahn T.R., Keller P., Geiger K.D., Verkade P. and Simons K.,*Alzheimer's disease beta-amyloid peptides are released in association with exosomes*. PNAS (**2006**), 30, 11172-11177.

Randall C., Mosconi L., de Leon M. and Glodzik L., *Cerebrospinal fluid biomarkers of Alzheimer's disease in cognitively healthy elderly*. Front Biosci (**2013**), 18, 1150–1173.

Raposo G., Nijman H.W., Stoorvogel W., Liejendekker R., Harding C.V., Melief C.J. and Geuze H.J., *B lymphocytes secrete antigen-presenting vesicles*. J. Exp. Med. (**1996**), 183, 1161-1172.

Record M., Subra C., Silvente-Poirot S., Poirot M., *Exosomes as intercellular signalosomes and pharmacological effectors*. Biochemical Pharmacology (**2011**), 81, 1171-1182.

Ringman J.M., Coppola G., Elashoff D., Rodriguez-Agudelo Y., Medina L.D., Gylys K., Cummings J.L. and Cole G.M.,*Cerebrospinal fluid biomarkers and proximity to diagnosis in preclinical familial Alzheimer's disease*. Dement. Geriatr. Cogn. Disord. (**2012**), 33, 1–5.

Robinson W.H., Fontoura P., Lee B.J., Neuman de Vegvar H.E., Tom J., Pedotti R., Di Gennaro C.D., Mitchell D.J.,Fong D., Ho P.P-K., Ruiz P.J., Maverakis E., Stevens D.B., Bernard C.C.A., Martin R., Kuchroo V.K., van Noort J.M.,Genain C.P., Amor S., Olsson T., Utz P.J., Garren H. and Steinman L., *Protein microarrays guide tolerizing DNA vaccine treatment of autoimmune encephalomyelitis*.Nature Biotechnology (**2003**), 21, 1033 - 1039.

Rubina A.Y., Dementieva E.I., Stomakhin A.A., Darii E.L., Pankov S.V., Barsky V.E., Ivanov S.M., Konovalova E.V. and Mirzabekov A.D., *Hydrogelbased protein microchips: manufacturing, properties and applications*. Biotechniques (**2003**), 34, 1008.

Rubina A.Y., Pankov S.V., Dementieva E.I., Penkov D.N., Butygin A.V., Vasiliskov V.A., Chudinov A.V., Mikheikin A.L., Mikhailovich V.M. and Mirzabekov A.D., *Hydrogel drop microchips with immobilized DNA: properties and methods for large-scale production*. Anal. Biochem. (**2004**), 325, 92.

Saman S., Kim W., Raya M., Visnick Y., Miro S., Saman S., Jackson B., McKee A.C., Alvarez V.E., Lee N.C. and Hall G.F., Exosome-associated tau is secreted in tauopathy models and is selectively phosphorylated in cerebrospinal fluis in early Alzheimer disease. J. Biol. Chem. (**2012**), 287, 3842-3849.

Saman S., Lee N.C., Inoyo I., Jin J., Li Z., Doyle T., McKee A.C. and Hall G.F., Proteins recruited to exosomes by tau overexpression implicate novel cellular mechanisms linking tau secretion with Alzheimer's disease. J. Alzheimers Dis. (**2014**), 40, S47-S70.

Santoni V., Kieffer S., Desclaux D., Masson F. and Rabilloud T., *Membrane proteomics: use of additive main effects with multiplicative interaction model to classify plasma membrane proteins according to their solubility and electrophoretic properties.* Electrophoresis (**2000**), 21, 3329 –3344.

Sarioglu H., Lottspeich F., Walk T., Jung G. and Eckerskorn C., *Deamidation as a widespread phenomenon in two-dimensional polyacrylamide gel electrophoresis of human blood plasma proteins.*Electrophoresis (**2000**), 21, 2209–2218.

Savina A., Furlán M., Vidal M. and Colombo M.I., *Exosome release is regulated by a calcium-dependent mechanism in K562 cells*. J. Biol. Chem. (**2003**), 278, 20083–20090.

Sawicki M.P., Samara G., Hurwitz M. and Passaro E., Human genome project. The Am J Surg (**1993**), 165, 258–264.

Sharples R.A., Vella L.J., Nisbet R.M., Naylor R., Perez K., Barnham K.J., Masters C.L. and Hill A.F.,Inhibition of gamma-secretase causes increased secretion of amyloid precursor protein C-terminal fragments in association with exosomes. Faseb. J.(**2008**), 22, 1469-1478.

Schneider P., Hampel H. and Buerger K., *Biological marker candidates of Alzheimer's disease in blood, plasma, and serum*. CNS Neurosci Ther (**2009**), 15, 358–374.

Schneiderhan-Marra N., Sauer G., Kazmaier C., Hsu H.Y., Koretz K., Deissler H. and Joos T.O., *Multiplexed immunoassays for the analysis of breast cancer biopsies*. Anal. Bioanal. Chem. (**2010**), 397, 3329.

Schoonenboom N.S., Mulder C., van Kamp G.J., Mehta S.P., Scheltens P., Blankenstein M.A. and Mehta P.D., *Amyloid beta 38,40 and 42 species in cerebrospinal fluid: More of the same?* Ann. Neurol. (**2005**), 58, 139–142.

Schumacher S., Lüdecke C., Ehrentreich-Förster E. and Bier F.F., *Platform Technologies for Molecular Diagnostics Near the Patient's Bedside*. Adv Biochem Eng Biotechnol (**2013**), 133, 75–87. DOI: 10.1007/10_2012_165.

Scott S., Pendlebury S.A. and Green C., *Lipid organization in erythrocyte membrane microvesicles*. Biochem. J. (**1984**), 224, 285–290.

Segura E., Nicco C., Lombard B., Véron P., Raposo G., Batteux F., Amigorena S. and Théry C., *ICAM-1 on exosomes from mature dendritic cells is critical for efficient naive T cell priming*. Blood (**2005**), 106, 216-223.

Seilheimer B., Bohrmann B., Bondolfi L., Muller F., Stuber D. and Dobeli H., *The toxicity of the Alzheimer's beta-amyloid peptide correlates with a distinct fiber morphology*. J Structural Biol (**1997**), 119, 59-71.

Shaw L.M., Korecka M., Clark C.M., Lee V.M.Y. and Trojanowski J.Q., *Biomarkers of neurodegeneration for diagnosis and monitoring therapeutics*. Nat. Rev. Drug Discov. (**2007**), 6, 295-303.

Schweitzer B., Predki P. and Snyder M., *Microarrays to characterize protein interactions on a whole-proteome scale*. Proteomics (**2003**), 3, 2190-2199.

SjögrenM., Andreasen N. and Blennow K., *Advances in the detection of Alzheimer's disease use of cerebrospinal fluid biomarkers*. Clin. Chim. Acta (**2003**), 332, 1–10.

Skokos D., Le Panse S., Villa I., Rousselle J.C., Peronet R., David B., Namane A. and Mecheri S., *Mast cell-dependent B and T lymphocyte activation is mediated by the secretion of immunologically active exosomes*. J. Immunol. (**2001**), 166, 868-876.

Snyder H.M., Carrillo M.C., Grodstein F., Henriksen K., Jeromin A., Lovestone S., Mielke M.M., O'Bryant S., Sarasa M., Sjøgren M., Soares H., Teeling J., Trushina E., Ward M., West T., Bain L.J., Shineman D.W., Weiner M. and Fillit H.M., *Developing novel blood-based biomarkers for Alzheimer's disease*. Alzheimer's & Dementia (**2014**), 10, 109–114.

Sokolovaa V., Ludwigb A.-K., Hornungb S., Rotana O., Hornb P.A., Epplea M., Giebelb M., *Characterisation of exosomes derived from human cells by nanoparticle tracking analysis and scanning electron microscopy*. Colloids and Surfaces B: Biointerfaces (**2011**), 87, 146– 150.

Sola L., *Design, synthesis and characterization of new polymers for bioanalytical applications*. PhD thesis in "Chimica del Farmaco" XXIV cycle, Università degli Studi di Milano (**2012**).

Sola L., Gagni P., Cretich M. and Chiari M., *Surface immobilized hydrogels as versatile reagent reservoirs for microarrays.*Journal of Immunological Methods (**2013**), 391, 95–102.

Sprott R.L., *Biomarkers of aging and disease: introduction and definitions.*Exp. Gerontol. (**2010**), 45, 2–4.

Stefani A., Bernardini S., Panella M., Pierantozzi M., Nuccetelli M., Koch G., Urbani A., Giordano A., Martorana A., Orlacchio A. Federici G. and Bernardi G., *AD with subcortical white matter lesions and vascular dementia: CSF markers for differential diagnosis*. J. Neurol. Sci. (**2005**), 237, 83–88.

Stevens D.Y., Petri C.R., Osborn J.L., Spicar-Mihalic P., McKenzie K.G. and Yager P., *Enabling a microfluidic immunoassay for the developing world by integration of on-card dry reagent storage*. Lab Chip (**2008**), 8, 2038.

Stoorvogel W., Kleijmeer M.J., Geuze H.J. and Raposo G., *The Biogenesis and Functions of Exosomes*. Traffic (**2002**), 3, 321–330.

Sugawara T. and Matsuda T., *Photochemical surface derivatization of a peptide containing Arg-Gly-Asp (RGD)*. Journal of Biomedical Materials Research (**1995**), 29, 1047–1052.

Sunderland T., Mirza N. Putnam K.T., Linker G., Bhupali D., Durham R., Soares H., Kimmel L., Friedman D., Bergeson J., Csako G., Levy J.A., Bartko J.J. and Cohen R.M., *Cerebrospinal fluid beta-amyloid1-42 and tua in control subjects at risk for Alzheimer´s disease: the effect of APOEe4 allele*. Biol. Psychiatry (**2004**), 56, 670–676.

Taniguchi N., Ekuni A., Ko J.H., Miyoshi E., Ikeda Y., Ihara Y., Nishikawa A., Honke K. and Takahashi M., *A glycomic approach to the identification and characterization of glycoprotein function in cells transfected with glycosyltransferase genes*. Proteomics (**2001**), 1, 239– 247.

Taylor D.D. and Gercel-Taylor C., *MicroRNA signatures of tumor-derived exosomes as diagnostic biomarkers of ovarian cancer*. Gynecol. Oncol. (**2008**), 110, 13–21.

Théry C., Regnault A., Garin J., Wolfers J., Zitvogel L., Ricciardi-Castagnoli P., Raposo G. and Amigorena S., *Molecular characterization of dendritic cell-derived exosomes. Selective accumulation of the heat shock protein hsc73*. J Cell Biol (**1999**), 147, 599–610.

Théry C., Duban L., Segura E., Veron P., Lantz O. and Amigorena S., *Indirect activation of naïve CD4+ T cells by dendritic cell-derived exosomes*. Nat. Immunol. (**2002**), 3, 1156-1162.

Théry C., Clayton A., Amigorena S. and Raposo G., *Current Protocols in Cell Biology.* Copyright © (**2006**) by John Wiley & Sons, Inc. – Unit 3.22: *Isolation and Characterization of Exosomes from Cell Culture Supernatants and Biological Fluids*.

Théry C., Ostrowski M. and Segura E., *Membrane vesicles as conveyors of immune responses*. Nat Rev Immunol (**2009**), 9, 581–93.

Trajkovic K., Hsu C., Chiantia S., Rajendran L., Wenzel D., Wieland F., Schwille P., Brügger B. and Simons M., *Ceramide triggers budding of exosome vesicles into multivesicular endosomes*. Science (**2008**), 319, 1244–1247.

Valadi H., Ekstrom K., Bossios A., Sjostrand M., Lee J.J. and Lotvall J.O., *Exosome mediated transfer of mRNAs and microRNAs is a novel mechanism of genetic exchange between cells.* Nat. Cell Biol. (**2007**), 9, 654–659.

van de Hulst H. C., *Light Scattering by Small Particles*. Dover Publications (**1981**).

van der Pol E., Hoekstra A.G., Sturk A., Otto C., van Leeuwen T.G., Nieuwland R. and Thromb J., *Optical and non-optical methods for detection and characterization of microparticles and exosomes*. J Thromb Haemost. (**2010**), 8, 2596–2607.

van der Vlist E. J., Nolte-'t Hoen E.N.M., Stoorvogel W., Arkesteijn G.J.A. and Wauben M.H.M., *Fluorescent labeling of nano-sized vesicles released by cells and subsequent quantitative and qualitative analysis by high-resolution flow cytometry*. Nat. Protoc. (**2012**), 7, 1311–1326.

van Dijk M.A., Tchebotareva A.L., Orrit M., Lippitz M., Berciaud S., Lasne D., Cognet L. and Lounis B., *Absorption and scattering microscopy of single metal nanoparticles*. Phys. Chem. Chem. Phys. (**2006**), 8, 3486–3495.

van Niel G., Mallegol J., Bevilacqua C., Candalh C., Brugiere S., Tomaskovic-Crook E., Heath J.K., Cerf-Bensussan N. and Heyman M., *Intestinal epithelial exosomes carry MHC class II/peptides able to inform the immune system in mice*. Gut (**2003**), 52, 1690-1697.

Vargo T.G., Bekos E.J., Kim Y.S., Ranieri J.P., Bellamkonda R., Aebischer P., Margevich D.E., Thompson P.M., Bright F.V. and Gardella J.A.Jr., *Synthesis and characterization of fluoropolymeric substrata with immobilized minimal peptide sequences for cell adhesion studies. I*. Journal of Biomedical Materials Research (**1995**), 29, 767–778.

Vedula R., Daaboul G., Reddington A., Ozkumur E., Bergstein D.A. and Unlu M.S., *Self-referencing substrates for optical interferometric biosensors*. J. Mod. Opt. (**2010**), 57, 1564–1569.

Vidal M., Mangeat P. and Hoekstra D., *Aggregation reroutes molecules from a recycling to a vesicle-mediated secretion pathway during reticulocyte maturation*. J. Cell Sci. (**1997**),110, 1867-1877.

Vingtdeux V., Hamdane M., Loyens A., Gelé P., Drobeck H., Bégard S., Galas M.C., Delacourte A., Beauvillain J.C., Buée L and Sergeant N., *Alkalizing drugs induce accumulation of amyloid precursor protein by-products in luminal vesicles of multivesicular bodies*. J. Biol. Chem (**2007**), 282, 18197-18205.

Wang S., Cesca F., Loers G., Schweizer M., Buck F., Benfenati F., Schachner M. and Kleene R., *Synapsin I is an oligomannose-carrying glycoprotein, acts as an oligomannose-binding lectin, and promotes neurite outgrowth and neuronal survival when released via glia-derived exosomes.* J. Neurosci. (2011), 31, 7275-7290.

WildD. Editor, *The Immunoassy Handbook*. (**1998**), Elsevier.

WiltfangJ.,Esselmann H., Bibl M., Hüll M., Hampel H., Kessler H., Frölich L., Schröder J., Peters O., Jessen F., Luckhaus C., Perneczky R., Jahn H., Fiszer M., Maler J.M., Zimmermann R., Bruckmoser R., Kornhuber J. and Lewczuk P.,*Amyloid-beta peptide ratio 42/40 but not A beta 42 correlates with phosphor-Tau in patients with low- and high-CSF A beta 40 load*. J. Neurochem. (**2007**), 101, 1053–1059.

Wolfers J., Lozier A., Raposo G., Regnault A., Théry C., Masurier C., Flament C., Pouzieux S., Faure F., Tursz T., Angevin E., Amigorena S. and Zitvogel L., *Tumor-derived exosomes are a source of shared tumor rejection antigens for CTL cross-priming*. Nat. Med. (**2001**), 7, 297-303.

Wong E.L.S., Chow E. and Gooding J.J., *DNA recognition interfaces: the influence of interfacial design on the efficiency and kinetics of hybridization*.Langmuir(**2005**), 21, 6957-6965.

Wubbolts R., Leckie R.S., Veenhuizen P.T., Schwarzmann G., Mobius W., Hoernschemeyer J., Slot J.W., Geuze H.J. and Stoorvogel W., *Proteomic and biochemical analyses of human B cell-derived exosomes. Potential implications for their function and multivesicular body formation*. J. Biol.Chem. (**2003**), 278, 10963-10972.

Xiao, Z., Prieto D., Conrads T.P., Veenstra T.D. and Issaq H.J., *Proteomic patterns: their potential for disease diagnosis*. Mol. Cell Endocrinol. (**2005**), 230, 95–106.

Yager P., Domingo G.J. and Gerdes J., *Point-of-care diagnostics for global health*. Annu. Rev. Biomed. Eng. (**2008**), 10, 107–144.

Yalcin A., Cretich M., DiCarlo G., Sola L., Monroe M., Unlu S. and Chiari M., *Fluorescence enhancement on reflecting substrates for microarray applications*. IEEE LEOS Annual Meeting Conference Proceedings (2009), 465-466.

Yam C.M., Deluge M., Tang D., Kumar A. and Cai C., *Preparation, characterization, resistance to protein adsorption, and specific avidin-biotin binding of poly(amidoamine) dendrimers functionalized with oligo(ethylene glycol) on gold*. Journal of Colloid Interface Science (**2006**), 296, 118–130.

Yurt A., Daaboul G.G., Connor J.H., Goldberg B.B. and Unlu M.S., *Single nanoparticle detectors for biological applications*. Nanoscale (**2012**), 4, 715.

Zetterberg H., WahlundL.O. and Blennow K., *Cerebrospinal fluid markers for prediction of Alzheimer's disease*. Neurosci. Lett. (**2003**), 352, 67–69.

Zetterberg H., Blennow K. and Hanse E., *Amyloid beta and APP as biomarkers for Alzheimer's disease*. Exp. Gerontol. (**2010**), 45, 23–29.

Zhu H. and Snyder M., *Protein chip technology*. Current Opinion in Chemical Biology(**2003**), 7, 55-63.

Zhu Q., Uttamchandani M., Li D., Lesaicherre M.L. and Yao S.Q., *Enzymatic profiling system in a small-molecule microarray*.Organic Letters (**2003**), 5, 1257–1260.

Zimmerberg J. and Kozlov M.M., *How proteins produce cellular membrane curvature*. Nat. Rev. Mol. Cell Biol. (**2006**), 7, 9–19.

Zuchner T., Failla A.V., Steiner M. and Meixner A.J., *Probing dielectric interfaces on the nanoscale with elastic scattering patterns of single gold nanorods*. Opt. Express (**2008**), 16, 14635–14644.

ACKNOWLEDGEMENTS

I wish to offer a due homage to people who shared their knowledge, making their time and talent available, and to everyone who supported me during this PhD research.

First of all, I have to thank my special supervisors: Dr. Marcella Chiari and Dr. Marina Cretich, for having accepted me in their team and for giving me so many opportunities to meet people and learn something new every day!

I thank Prof. Carlo De Micheli, my tutor, for having let me attend this PhD School in *Chimica del Farmaco* at *Università degli Studi di Milano*; and I thank, also, Prof. Paola Conti, who introduced me to ICRM-CNR, where I actually spent my time.

Thus, my thanks go to lab-mates who shared with me their days, abilities and coffees: Dr. Francesco Damin, Dr. Laura Sola, Dr. Caterina Zilio, Dr. Finetti Chiara and Dr. Marcello Torrisi, Lauren Plavisch, Dr. Margherita Pezzullo and all students who spent their thesis period with us during these years.

I would thank also collaborators: Prof. Selim Unlu and his team, from *Electrical and Computer Engineering department at Boston University* (MA, USA); Prof. Davide Prosperi and Dr. Elisabetta Galbiati, from *Bicocca* University (Milan); Dr. Roberta Ghidoni, Dr. Luisa Benussi and Dr. Elisa Tonoli, from *IRCSS – Fatebenefratelli* (Brescia).

And finally, I thank my parents Isa and Lino, my sister Silvia and my dear Andrea for being my family and for having thought me that "*On ne voit bien qu'avec le Cœur. L'essentiel est invisible pour les yeux*" (Antoin de Saint-Exupéry).